DEVELOPMENT OF NOVEL INTEGRATED BEAD AND FIBER ANTIBODY FILTERS FOR SPECIFIC REMOVAL OF ANTI-A ANTIBODIES FROM BLOOD

by

Azadeh Hajy Alikhani

B.S., Sharif University of Technology, 2001

Submitted to the Graduate Faculty of

Swanson School of Engineering in partial fulfillment

of the requirements for the degree of

Doctor of Philosophy

University of Pittsburgh

2010

UNIVERSITY OF PITTSBURGH

SWANSON SCHOOL OF ENGINEERING

This dissertation was presented

by

Azadeh Hajy Alikhani

It was defended on

March 17, 2010

and approved by

David K.C. Cooper, M.D., Ph.D., Professor, Department of Surgery, University of Pittsburgh Medical Center

Steven Little, Ph.D., Assistant Professor and Bicentennial Faculty Fellow, Departments of Chemical Engineering, Bioengineering, Immunology and the McGowan Institute for Regenerative Medicine

Alan J. Russell, Ph.D., University Distinguished Professor, Departments of Surgery, Bioengineering and Chemical Engineering, Director, McGowan Institute for Regenerative Medicine

Dissertation Director: William J. Federspiel, Ph.D., William Kepler Whiteford Professor, Departments of Bioengineering, Chemical Engineering and Critical Care Medicine, McGowan Institute for Regenerative Medicine, Director, Medical Devices Laboratory

DEVELOPMENT OF NOVEL INTEGRATED BEAD AND FIBER ANTIBODY FILTERS FOR SPECIFIC REMOVAL OF ANTI-A ANTIBODIES FROM BLOOD

Azadeh Hajy Alikhani, Ph.D.

University of Pittsburgh, 2010

Removal of anti-A/B antibodies from blood in the peri-transplantation period eliminates the risk of hyperacute rejection in ABO-incompatible transplantation. We are developing anti-A/B immunoadsorption devices, compatible with whole blood perfusion. In this study we developed a new antibody filtering device based on integrated microfiltration fibers with antibody capturing beads distributed within the interstitial fiber space (BSAF device). As blood flows through the fibers in BSAF devices, Starling flow carries plasma from the inner fiber lumen to the beads in the shell compartment where antibodies diffuse and bind to covalently attached antigens within the shell-side porous beads. We first investigated the possibility of using synthetic blood group A/B-trisaccharide epitopes, conjugated with poly-N hydroxyethylacrylamide spacers, as the immunoadsorbent material in our antibody filtering devices. The glycopolymers were equipped with biotin tags and deposited on streptavidin-coated sensor chips. Antibody removal capacity per unit surface area and kinetics of antibody binding to immobilized glycoconjugates were quantified using surface plasmon resonance. We then developed a simple mathematical model to guide the choice of key design and operational parameters for a clinical BSAF device. The model demonstrated that for a given flow rate and reservoir volume, antibody removal rate in a BSAF was dependent on the magnitude of a lumped dimensionless parameter, $k_L m_B / Q_s$, which characterized the ratio of antibody uptake rate by the beads to the Starling flow rate in the device. The highest antibody removal rate was predicted for a perfusion limited regime, when

$k_L m_B / Q_s \to 10$. Once this maximum limit was obtained, any further increase in the antibody removal rate was only possible by increasing the flow rate in the device. Key model predictions were validated in a series of in vitro monoclonal anti-A antibody capture studies in BSAF devices packed with anti-A specific beads. Once validated, we used the model to design a BSAF device that would generate a clinically relevant rate of anti-A removal. We fabricated and tested scaled down prototypes of the "clinical" BSAF device and showed significant reduction in IgM and IgG anti-A antibody titers within two hours of whole blood perfusion through our fabricated BSAF devices.

TABLE OF CONTENTS

LIST OF TABLES

LIST OF FIGURES

ACKNOWLEDGEMENTS

Graduate school has been a wonderful and fulfilling experience for me and I am thankful for all the people who have contributed and befriended me in this journey. First and most of all, I would like to deeply express my gratitude for my advisor Dr. William Federspiel, who has kindly mentored me for the past 6 years. My research would have not been possible without his support, encouragement, and patient guidance. I am very proud of the work I have done with him. I am grateful for the many opportunities provided by Dr. Federspiel for my research, one of which, being able to attend national conferences that provided me with the opportunity to present my research to the scientific community. Thanks for providing a wonderful lab atmosphere that has been my second home for the past 6 years. I am deeply grateful for all the lessons I have learned from him.

I would also like to deeply thank my committee members, Dr. David Cooper, Dr. Steven Little and Dr. Alan Russell for their generosity in serving in my committee for the past 3 years, and for kindly donating their time, expertise, and advice, which has contributed greatly in completing my research.

I am very grateful for the financial support from National Institutes of Health (NIH), National Heart, Lung, and Blood Institute (Grant Number HL69956-01), National Institute of Health Training Grant in Biotechnology (Grant Number 5T32GM065100-03) and the University of Pittsburgh Provost's Development Fund. I would also like to thank ICX-Agentase

Technologies for giving me the opportunity to gain an extremely valuable industrial experience at their company.

I would like to thank all the personnel of Medical Devices Lab for their help and friendship for the past 6 years. Over the years, I have made so many wonderful friends here and I will always cherish the memories from working with each and every one of them.

I would like to thank my very dearest family for their love and support, without which this work would not have been possible. To my beloved husband Arash, for being my best friend and companion throughout the years, for his love, kindness, patience, and support. To my parents, who have always been my best advocates in life. To my brothers Orang and Ehsan who have always been my best friends and to Sanaz, for her friendship and her kind assistance in producing the beautiful diagrams in my thesis! Last, but not least, a big thank you to my dearest daughter, Aveen, for bringing joy, happiness, hope and energy in my life. I will always love you.

1.0 INTRODUCTION

The number of patients awaiting organ transplantation far exceeds the number of available cadaveric donor organs [1]. The average waiting time to obtain an ABO-compatible deceased donor kidney is approximately 3 years (UNOS/OPTN). Living donor organ transplantation provides a solution to the shortage of cadaveric donor organs, but an estimated 30-40% of living organ donor-recipient pairs are turned down due to ABO-incompatibility [2]. The main barrier to ABO-incompatible transplantation is the risk of hyperacute and acute allograft rejection [3]. Both types of rejection are triggered by binding of the host pre-existing anti-A/B antibodies to A/B antigens on the graft endothelium [3-5]. Antibody-antigen binding interactions activate the complement pathway and result in endothelial cell disruption, platelet adhesion and intravascular thrombosis. Hyperacute organ rejection follows as a result of insufficient blood circulation in the graft [6]. However, immediate peri-transplantation removal of host anti-A/B antibodies eliminates the risk of hyper acute rejection and reduces the possibility of acute antibody mediated rejection to less than 30% [7]. Following initial successful ABO-mismatch renal transplantations reported by Alexandre et al. in 1985 [8], and Bannett et al. in 1987 [9] and the subsequent successful long term outcomes [10],[11],[12]. several protocols have been developed and used in ABO-mismatch kidney, liver and heart transplantation in a few transplantation centers around the world [10], [13],[14],[15], [16],[17], [18], [19].

Both selective and nonselective antibody removal techniques have been used to reduce host anti-A/B antibody titers prior to ABO-incompatible transplantation [20]. The nonselective methods include plasma exchange with fresh frozen donor plasma or replacement albumin solution and double filtration plasmapheresis [10, 21-23]. Selective antibody removal occurs through plasma or whole blood immunoadsorption in packed sorbent columns, containing immobilized synthetic A/B-trisaccharide epitopes [13-14, 17, 19, 24-25]. As it appears, the outcome of an ABO-incompatible transplantation primarily depends on the peri-transplantation anti-A/B antibody titer, and does not correlate with the use of any specific method of antibody removal [20]. Nevertheless, nonselective antibody removal techniques have been generally associated with higher risks of procedure related complications and morbidities [26-27]. Most of the complications have been attributed to the use of donor plasma or replacement albumin solution [28]. Total plasma exchange with fresh frozen donor plasma is limited by donor supply and is also associated with the risks of infection transmission and immunological reactions to non-autologous plasma. Whereas, replacement with albumin solution depletes the recipient of requisite proteins, protective immunoglobulins and clotting factors [28]. Plasma immunoadsorption requires minimal replacement fluid, but nonetheless, involves the same risks associated with plasmapheresis [28]. Direct hemoperfusion through sorbent columns eliminates the need for a complicated plasmapheresis procedure, but meanwhile direct contact between blood cells and the sorbent material increases the chances of hemolysis and loss of platelets or red blood cells [29],[30].

Our group previously reported development of a fiber based anti A/B immunosorption device (SAF) in which Neutr-AB®, animal based A/B glycoprotein antigens, were covalently attached to the luminal surface of hollow fiber membranes [31]. Hollow fibers were perfused

with whole blood and the SAF devices selectively removed anti-A/B antibodies in a one step process through high affinity interaction between immobilized A or B antigens and the corresponding antibodies. Subsequently, SAF devices were developed in which synthetic blood group A antigens were used as the immobilized ligands [32]. **Figure 1-1** shows a schematic of antibody removal in the luminal surface of a single fiber in a SAF device. The SAF devices present the advantage of eliminating a complicated plasmapheresis procedure [31], [33], [32]. Additionally, blood flow through hollow fiber membranes is associated with significantly less resistance than blood flow in a sorbent column [34]. Yet, limited surface area for antigen immobilization restricts antibody removal capacity of SAF devices and further effort is required to enhance the immobilized antigen density [32].

In this study we had two main objectives: our first objective (as described in detail in Chapter 3.0 was to investigate the possibility of enhancing antibody removal capacity of our SAF devices by using synthetic blood group A/B trisaccharide antigens conjugated with high molecular weight polyacrylamide spacers as the immobilized ligands. We approached this goal by performing the following series of studies:

1. We conjugated synthetic blood group A/B-trisaccharide epitopes with poly-N hydroxyethylacrylamide spacers of 30 and 1000 kDa. The glycopolymers were equipped with biotin tags and deposited on streptavidin-coated sensor chips.
2. Samples of different clones of IgM monoclonal anti-A antibodies and polyclonal anti-A antibodies in plasma were injected over the surface of sensor chips on which glycopolymers were immobilized. Using surface plasmon resonance (SPR), the effect of the polyacrylamide spacer size (30 kDa or 1000 kDa) on antibody removal capacity of glycopolymers was assessed.

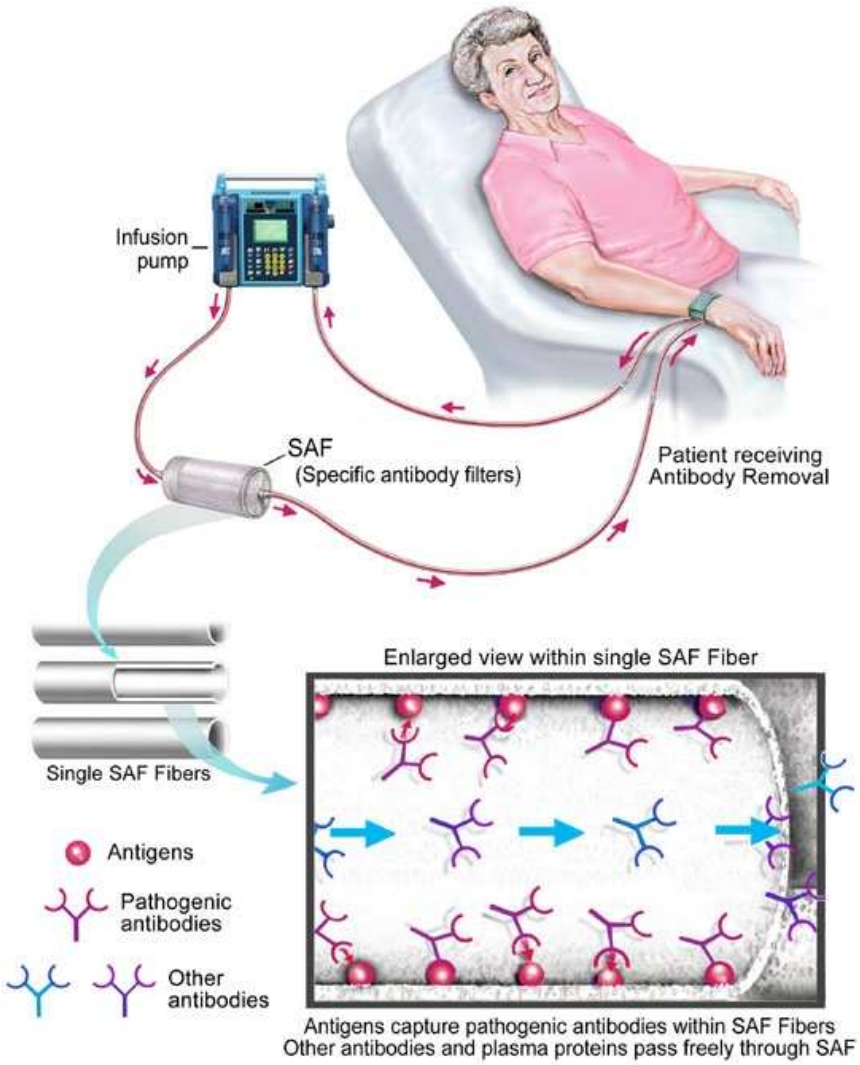

Figure 1-1: Schematic of the blood perfusion loop and antibody removal in the luminal surface of a single fiber in a SAF device. Figure is from the McGowan Institute for Regenerative Medicine website.

3. We also assessed the effect of the carbohydrate content (20 mol% or 50 mol%) on antibody removal capacity of glycopolymers in their interactions with monoclonal and polyclonal anti-A antibodies.
4. We quantified binding kinetics of Anti-A antibodies to immobilized glycopolymers.

The results of this study suggested that by immobilization of the high molecular weight (1000 kD) polyacrylamide glycoconjugates on the luminal surface of hollow fibers in the SAF devices, we could potentially achieve a target anti-A antibody titer reduction of three to four titer steps in each device.

Our second objective (as described in detail in Chapters 4.0, 5.0 and 6.0) was to develop a new antibody filtering device: Integrated Bead and Fiber Antibody Filter (BSAF). The BSAF device contains microfiltration hollow fibers combined with antibody capturing beads uniformly distributed within the fiber interstitial space. As blood flows through the fibers, Starling flow carries plasma from the inner fiber lumen to the beads in the shell compartment where antibodies diffuse and bind to covalently attached polyacrylamide glycoconjugates within the shell-side porous beads **(Figure 1-2)**. We envisioned the following advantages for BSAF devices:

1. Selectivity in antibody removal: unlike nonselective techniques of antibody removal such as plasma exchange, double filtration plasmapheresis or antibody adsorption in protein A columns, BSAF devices provide selective antibody removal and do not deplete blood of essential proteins, clotting factors or other immunoglobulins.
2. Compatibility with direct whole blood perfusion: BSAF devices are compatible with whole blood perfusion. This simplifies the blood circuit and eliminates the need for a separate plasmapheresis unit.

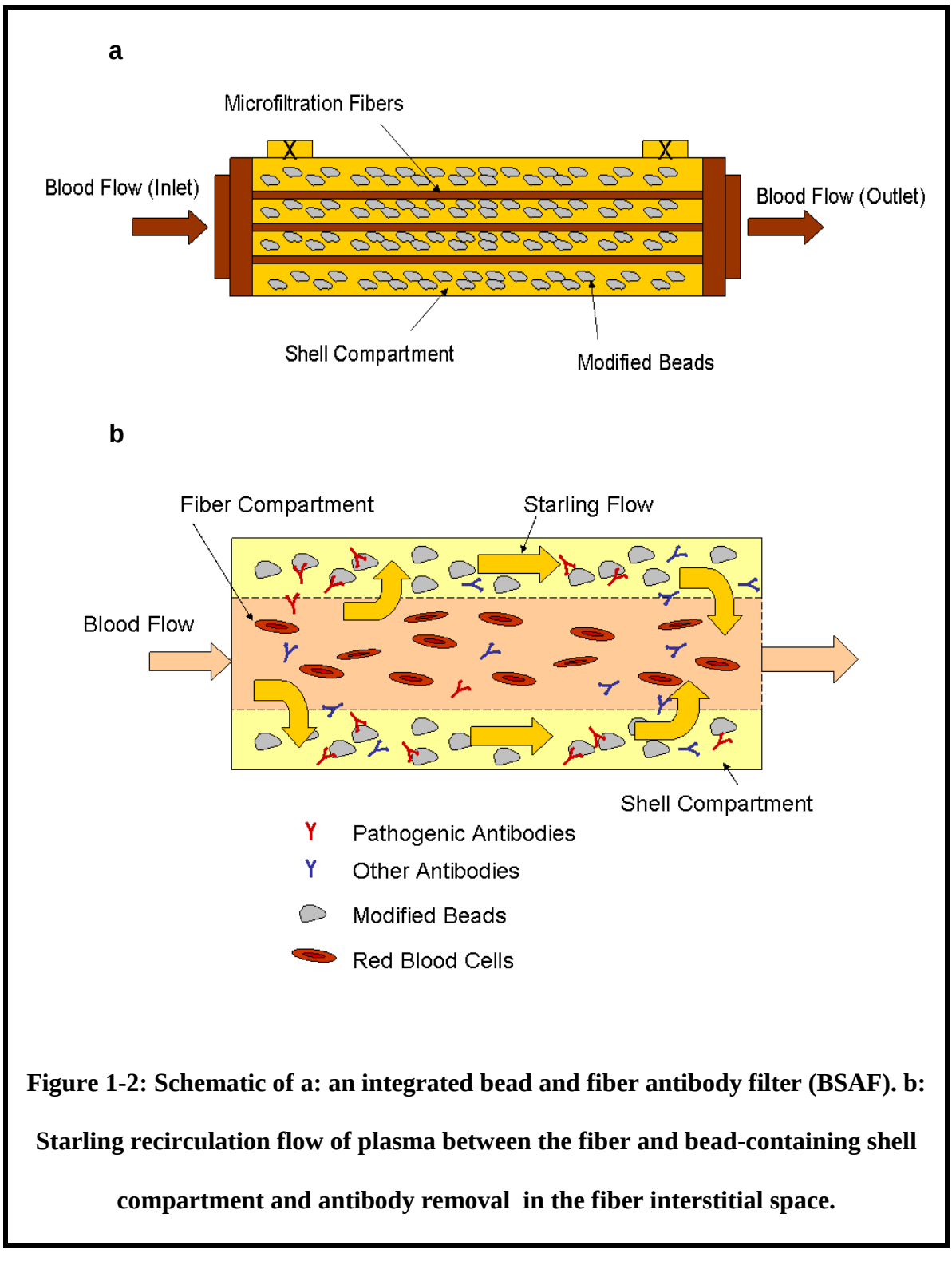

Figure 1-2: Schematic of a: an integrated bead and fiber antibody filter (BSAF). b: Starling recirculation flow of plasma between the fiber and bead-containing shell compartment and antibody removal in the fiber interstitial space.

3. Blood compatibility: there is no direct contact between blood cells and the sorbent material in BSAF devices. Therefore, the risks of hemolysis, loss of platelets or red blood cells and other biocompatibility concerns associated with a direct contact between blood cells and the sorbent material are eliminated.
4. Fast antibody removal: the sorbent particles in BSAF devices are maintained in suspension. Therefore, there is significantly less flow resistance in the fiber interstitial space compared to plasma flow in a packed sorbent column. This enables higher flow rates and increases the overall antibody removal rate in BSAF devices.
5. Unlimited antibody removal capacity: antibody removal capacity of BSAF devices is practically infinite in relation to the maximum amount of antibodies in blood. Therefore, clinically relevant antibody removal rate and capacity can be achieved in one single device. This potentially provides a solution to the limited adsorption capacity of our first prototype SAF devices.
6. Consistency in antibody removal: the sorbent particles are maintained in a uniformly distributed and well mixed suspension within the fiber interstitial space. Therefore, uniform and consistent antibody removal characteristics are expected between devices. Conversely, in a sorbent column the particles pack further with fluid flow and time of use [29]. Therefore, antibody removal characteristics of the beads change over time and may not be consistent between devices.
7. Simplicity in operation: the same blood circuit in hemodialysis is adaptable for use with BSAF devices. Therefore antibody removal in BSAF devices could be performed in clinical facilities which are already equipped with hemodialysis machinery.

We developed our BSAF devices by performing the following series of studies:

1. We developed a mathematical design model that incorporated the mechanisms underlying antibody capture in the BSAF and predicted antibody removal rate based on key design and operational parameters (Chapter 4.0).
2. We measured the parameters of our mathematical model and compared key predictions of the model with experimental antibody capture data in a series of in-vitro monoclonal anti-A antibody capture in BSAF devices packed with anti-A specific beads (Chapter 4.0).
3. Based on the mathematical model predictions of antibody removal rate in BSAF devices and experimental data, we designed a BSAF device that would generate a clinically relevant rate of anti-A removal (Chapter 4.0).
4. We evaluated the effect of bead mixing on antibody removal rate in BSAF devices. A conceptual design for an integrated bead mixing system was proposed. We fabricated appropriately scaled down prototypes of our conceptual clinical BSAF device and obtained "proof of concept" experimental data in capture of monoclonal anti-A antibodies from buffer solution (Chapter 5.0).
5. We tested anti-A antibody removal from whole blood in appropriately scaled down prototypes of the "clinical" BSAF device and showed that the designed BSAF devices effectively and specifically removed anti-A antibodies directly from whole blood (Chapter 6.0).

2.0 BACKGROUND

2.1 AN OVERVIEW OF IMMUNE RESPONSE TYPES AND MEDIATORS

Immune responses protect multicellular organisms from potentially harmful invading pathogens [36]. Innate immunity is the simplest form of an immune response and utilizes an array of primitive and nonspecific defensive tools including physical barriers, toxic molecules and phagocytic cells to non-discriminately eliminate pathogens from body [36]. In vertebrates innate immunity works in parallel with adaptive immunity, a very sophisticated immune response, which utilizes a diverse group of specialized agents to specifically recognize and destroy pathogens [36]. Two types of adaptive immune responses are recognized: cellular immunity, mediated by T lymphocytes, and humoral immunity, mediated by an enormous collection of immunoglobulins, produced by B lymphocytes [37]. Both B and T cell precursors develop from the same pluripotent hemopoietic stem cells [36]. In mammals, B cells develop in bone marrow and T cells develop in the thymus. Hence both thymus and bone marrow are referred to as central or primary lymphoid organs. Mature B and T lymphocytes are transferred to secondary or peripheral lymphoid organs including spleen, appendix and lymph nodes [36]. The mature lymphocytes continuously recirculate between blood and peripheral lymphoid organs in search of antigens [36]. An antigen is any foreign substance (usually a carbohydrate or protein structure) that induces the adaptive immune responses. Circulating lymphocytes contain

membrane bound receptors with different specificities through which they specifically recognize and bind the antigens they encounter. Through this receptor-antigen binding interaction, those lymphocytes with specificity for the encountered antigens both proliferate and differentiate. This adaptive stimulation of B and T cells is referred to as clonal selection [36].

The membrane-bound receptors of T cells are composed of two disulfide bonded transmembrane polypeptide chains (known as α and β). Each chain is approximately 280 amino acids long, containing an amino-terminal variable region and a carboxyl-terminal constant region. Two variable amino-terminals cooperate to form a single antigen binding site on the T cell receptor [36]. Two general classes of T cells exist: cytotoxic or killer T cells, and helper T cells. Cytotoxic T cell receptors specifically recognize antigenic peptides bound to class 1 major histocompatibility complex (MHC) molecules (HLA class 1 in human) [36]. Cytotoxic T cell receptor-antigen binding interaction leads to release of perforin and granzymes into the antigen presenting cells to signal cell apoptosis [36],[6]. Helper T cells specifically recognize peptides bound to class 2 MHC molecules (HLA class 2 in human). Although, helper T cells have no cytotoxic or phagocytic activity, they play a major role in magnifying immune responses through secreting a variety of cytokines which act as local mediators and help activate macrophages, B cells and cytotoxic T cells [36],[6].

The membrane-bound receptors of B cells are specialized glycoproteins called immunoglobulins or antibodies. Once an antibody on the cell surface of a naïve B cell binds a specific antigen, the antibody-antigen complex is engulfed and digested by the antibody-bearing B cell. The B cell then displays antigenic fragments on the cell surface to elicit T cell stimulation and B cell proliferation and differentiation. The B cell progeny, called effecter B cells, secrete large amounts of the antigen specific antibodies into blood. Antibodies specifically bind

antigens, employ complement proteins and initiate a cascade of reactions to destroy the antigen containing pathogens [36],[6]. A small population of the progeny B cells turns into memory B cells which can elicit a secondary and more potent response in a second encounter of the same antigen [6]. Each antigen may have several antigenic determinants, called epitopes. Each epitope elicits production of a unique antibody with specificity for that epitope. Thus a single antigen may activate various clones of B cells, resulting in production of polyclonal antibodies. All antibody clones in a polyclonal population bind the same antigen, but antibody-antigen binding interactions occur through different antigenic epitopes and affinity of the interactions varies [36],[6, 37].

The simplest antibodies are composed of two identical 23 kDa light (~ 220 amino acids) and two identical 53-75 kDa heavy (~440 amino acids) polypeptide chains [37]. Both heavy and light chains constitute a variable and a constant region. The constant and variable regions each constitute about 110 amino acids [37]. All four chains are associated by disulfide bonds and by noncovalent interactions to form a roughly Y shaped symmetric molecule **(Figure 2-1)**. The amino-terminus tips of both heavy and light chains in each arm form an antigen binding site. Therefore, each Y-shaped antibody has two identical antigen binding sites. The entire light chain and the amino-terminal of the heavy chain in each arm is known as a Fab fragment. The carboxyl- terminal portion of two heavy chains is known as the Fc fragment [36],[6].

In mammals antibodies are found in five major classes: IgA, IgD, IgE, IgG and IgM, distinguished by the differences in their heavy chain compositions known as α, δ, ε, γ and μ respectively [6],[36]. The amino acid sequence of the constant region of the heavy chain is the same between all antibodies in a specific class and subclass. Hence all antibodies of IgM class have the μ heavy chain and so forth [37].

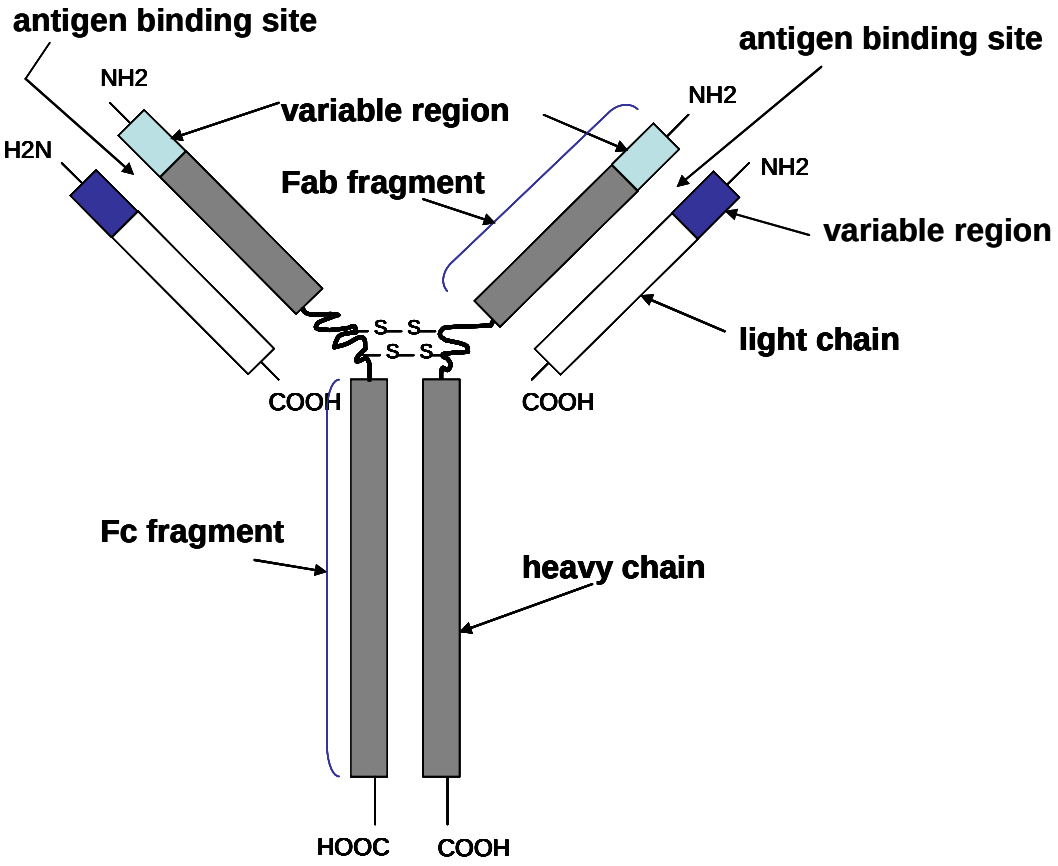

Figure 2-1: Schematic of an immunoglobulin in the monomeric form.

On first exposure to an antigen, the major class of antibodies that is secreted into blood is IgM isotype [36]. IgM antibodies are presented in monomeric form as cell-bound receptors and in pentameric form containing 5 –four chain units with 10 antigen binding sites when secreted into blood **(Figure 2-2)**. The five subunits in an IgM antigen are held together by disulfide bonds. A single J chain which is disulfide bonded between two heavy μ chains, conforms IgM antibodies into its pentameric structure [37]. IgM antibodies make about 10% of the total

immunoglobulins in human blood [36]. They are also the most potent antibody class to activate complement system [36],[6], [3]. IgG isotype is the major class of antibodies found in human blood and makes up to 75% of total human immunoglobulin concentration [36]. Each IgG antibody is composed of one four chained monomer with the heavy chain known as γ chain. This isotype is also capable of activating the complement system but is a weaker activator compared to IgM isotype [36]. IgG antibodies are produced mainly during the secondary responses. There are four IgG subclasses: IgG1, IgG2, IgG3 and IgG4 with γ1, γ2, γ3 and γ4 heavy chains, respectively [36]. IgG antibodies bind Fc receptors on macrophages and neutrophils and facilitate digestion and destruction of antigen coated microorganisms [6]. IgG antibodies are the only isotype that cross placenta and are secreted into mother's milk [36]. IgA is found in body secretions including saliva, tears, milk, respiratory and intestinal secretions [36]. IgA is found in the form of a four chain monomer in blood and is present as an eight chain dimer in secretions **(Figure 2-3)**. IgA antibodies constitute 15% of total human antibody concentration [36]. The last two isotypes: IgE and IgD each constitute less than 1% of total antibody concentration. They are both found as 4 unit monomers. IgE antibodies bind to receptors on mast cells and basophils and induce release of a variety of cytokines and biologically active amines such as histamine. IgD antibodies are expressed mainly on mature B cell surfaces and function as antigen receptors. The very specific functionality of this class of antibodies is not yet completely understood [36].

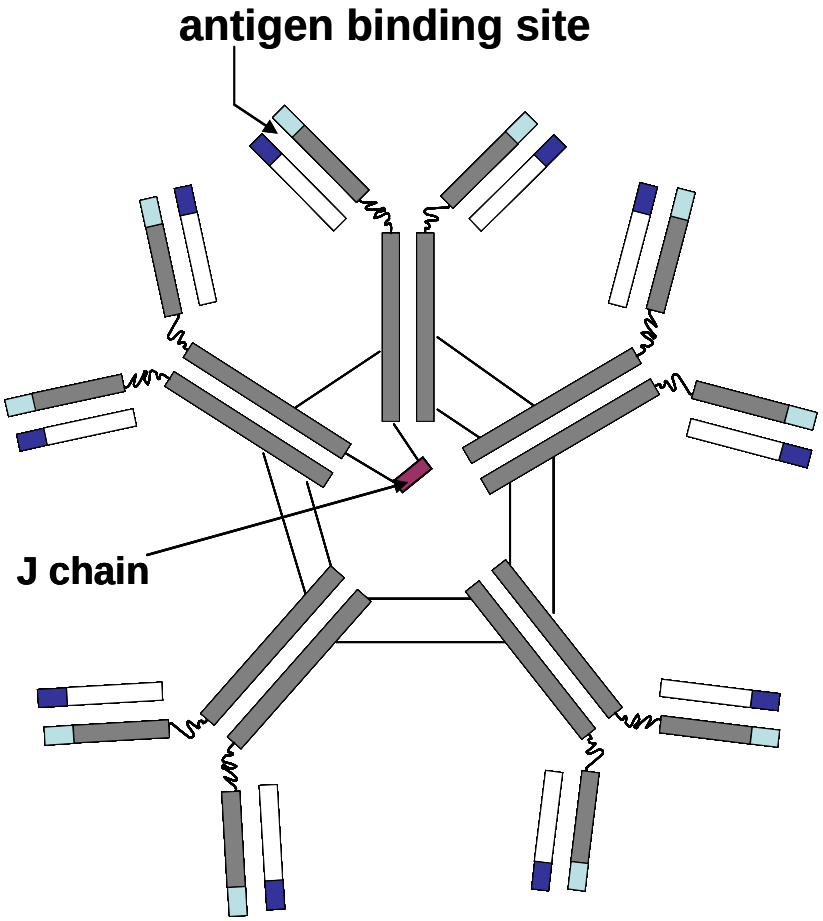

Figure 2-2: Schematic of an IgM immunoglobulin in the pentameric form, containing 5-four chain units with 10 antigen binding sites.

2.2 IMMUNE RESPONSES IN SOLID ORGAN TRANSPLANTATION

Allograft and xenograft transplantation elicit immune responses in organ recipients due to host recognition of “non-self” antigens on the graft cells [3],[38]. Three structurally related antigens play the major role in inducing humoral mediated immune responses in solid organ transplantation: A, B and α-Gal antigens [39]. In addition to antibody mediated immune responses, cellular rejection, accommodation and tolerance are possible immunological reactions in solid organ transplantation [39]. In the following section, an overview of the major immune responses in solid organ transplantation will be presented.

2.2.1 Humoral Mediated Rejection in ABO-Incompatible Solid Organ Transplantation

ABO antigens, also known as histo-blood group antigens, are carbohydrate structures, expressed as glycoproteins or glycolipids on almost all cells in the human body [4],[5]. There are three antigens in ABO blood group system: A, B and O (H). A and B antigens are characterized by two structurally related, but distinct trisaccharides: GalNAcα1−3 [Fucα1−2]Galβ− and Galα1−3 [Fucα1−2]Galβ−, respectivly [5].

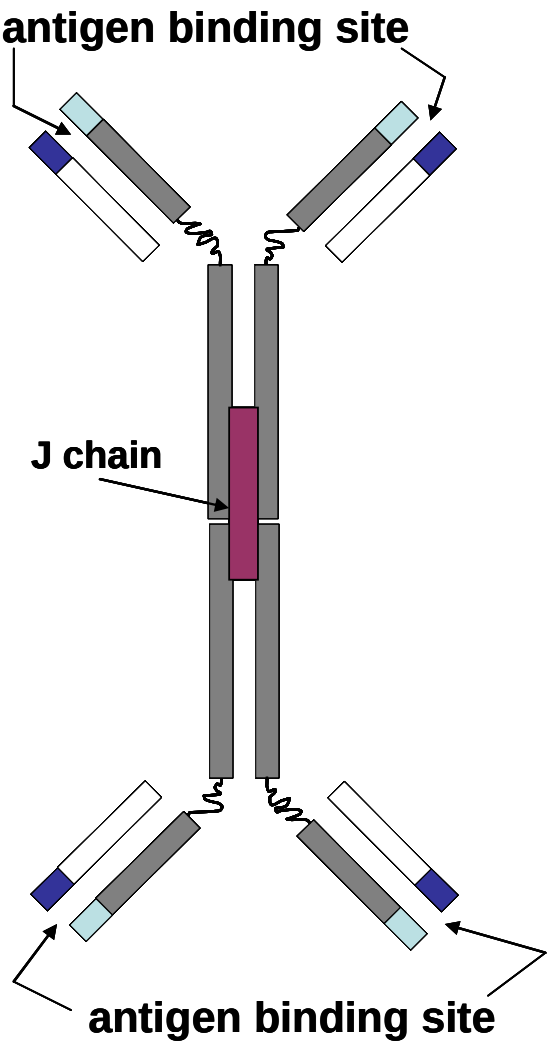

Figure 2-3: Schematic of an IgA immunoglobulin in dimeric form.

The immunodominant sugar structure in O antigen is a disaccharide: [Fucα1−2]Galβ1-[5]. The immunodominant sugars of A, B and O antigens are expressed on four different types of core saccharide chains [4]:

Type 1 chain: Galβ1-3GlcNAcβ1-R

Type 2 chain: Galβ1-4GlcNAcβ1-R

Type 3 chain: Galβ1-3GalNAcα1-R

Type 4 chain: Galβ1-3GalNAcβ1-R

Expression of core saccharide chains and the number of ABO epitopes varies in different organs [4]. ABO gene in humans is located on chromosome 9 and encodes synthesis of two enzymes: glycosyltransferase A (GTA) and glycosyltransferase B (GTB), which catalyze the biosynthetic pathways in synthesis of A and B antigenic determinants, respectively [40]. The terminal fucose residue in O antigen provides the basis for synthesis of both A, and B trisaccharides [5]. In synthesis of A antigens, GTA transfers the monosaccharide N-acetylgalactosamine (GalNAc) from the donor substrate (uridine diphosphate- N-acetylgalactosamine) to fucosylated galactosyl residue of the O antigen. Similarly, in synthesis of B antigens, GTB catalyzes transfer of the nucleotide donor uridine diphosphate-galactose to the fucosylated galactosyl residue on O antigen [40],[5]. There are four phenotypes in ABO blood group system: A, B, AB and O. Blood group A phenotype expresses only A antigens, whereas blood group B expresses only B antigens. Individuals of type AB express both A and B antigens and type O individuals lack functional glycosyltransferases, hence express neither A nor B antigens. Blood group A is divided into two subgroups: A1 and A2 [4]. A1 individuals express a larger number of A antigens compared to A2 subjects. Additionally, all four chain types are identified in A1 phenotype. Whereas, A2 antigens have only been associated with type 1 and 2

chains [4]. Individuals who express ABO antigens on soluble glycoproteins in their body secretions are known as secretors [4]. Group A or B non-secretors lack the enzyme α–1,2-fucosyltransferase type 2 (FUT2) which is responsible for synthesis of H antigen in secretions [4]. ABO antigens are expressed on virtually all cells in human body including the vascular endothelium, the convoluted distal tubules and the collecting tubules of kidneys, the hepatic arteries, portal veins, capillaries, sinusoidal lining cells and bile duct epithelium of liver tissues and on the surface of the epicardium and on the vascular endothelium of human heart tissues [4],[41].

According to Landsteiner's law, humans produce antibodies against those ABO antigens that are missing on their tissues [4],[5]. Antigen expression and antibody secretion patterns as well as the population distribution of each blood type within ABO blood group system in the United States are summarized in **Table 2-1**. Anti-A and anti-B antibodies are believed to be produced in the human body in response to carbohydrate antigens expressed by intestinal bacteria [4],[3],[35]. These antibodies bind to A/B antigens due to cross reactivity [4],[3],[5]. Anti-A/B antibodies circulate in blood and are predominantly in IgM isotype but are also present in the IgG form [42].

In ABO-incompatible solid organ transplantation, pre-existing anti-A/B antibodies in the organ recipient recognize A/B antigens on the graft endothelium as non-self antigens [6],[3]. Antibody-antigen complex formation activates the classical pathway of complement system through fixation of C1q (a subunit of C1 protein). Fixation of C1q by at least two antibody Fc regions is a crucial complement activation step [3],[43]. Therefore, IgM antibodies which provide five Fc regions in close proximity are more potent complement activators than IgG isotype [3]. Fixation of C1q by antibodies induces conformational changes in C1q and leads to

Table 2-1: Antigen expression, antibody secretion and US population distribution of different blood types within ABO blood group system.

Blood Type (genotype)	Antigen Expression (Phenotype)	Antibody Secretion (Phenotype)	US Donor Percentage
A (AA,AO)	A	Anti-B	42%
B (BB,BO)	B	Anti-A	10%
AB (AB)	A and B	None	4%
O (OO)	O (H)	Anti-A and Anti-B	44%

activation of the subsequent proteins in the cascade, ultimately resulting in formation of membrane attack complexes (MAC) [43]. MAC complexes insert themselves into cell membranes and induce cell lysis and endothelial cell disruption [43]. This is followed by platelet aggregation, interstitial hemorrhage, edema, and formation of fibrin thrombi [3]. Ultimately, rapid swelling of the graft, vascular thrombosis and loss of graft function will occur. This rapid and humoral mediated hyperacute graft rejection occurs within 24 hours upon resuming blood flow in the transplanted organ [3].

Hyperacute organ rejection is the major, but not the only risk factor in ABO-incompatible transplantation. Host anti-donor antibodies could also induce acute vascular or accelerated cellular rejection. Acute vascular rejection occurs days to months after transplantation [3]. Unlike cell-mediated rejection which responds very well to immunosuppressant treatments, humoral mediated rejection including: hyper acute, acute vascular and accelerated cell mediated rejection are resistant to immunosuppressive therapy [3]. The exact mechanisms underlying acute vascular and accelerated cell mediated rejection are yet not completely understood. However, both humoral and cell mediated responses are believed to affect these types of rejection [3].

2.2.2 Humoral Mediated Rejection in Xenotransplantation

Discordant xenotransplantation without any manipulation of immune system results in hyper acute rejection of the graft within minutes to few hours [44],[38]. Hyperacute rejection in xenotransplantation is triggered by binding of abundantly produced anti-Gal antibodies to α-Gal epitopes (Galα1-3Gal) expressed on pig and other nonprimate mammalian cells [45-46], [39], [44]. Anti α–Gạl antibodieș are present in human plasma and, similar to anti- A/B antibodies, are

produced in response to expression of α-Gal epitopes by intestinal bacteria [44]. Current research in xenotransplantation is focused on genetically disrupting α1,3 galactosyltransferase (α1,3GT) gene in pigs, hence producing pigs which lack α-Gal epitopes [47], [48]. Additionally, removal of anti-α-Gal antibodies from circulating blood or depletion of complement proteins reduces the risk of hyper acute rejection in xenotransplantation [45], [45, 49],[30, 50-52]. However, as anti-α-Gal antibody titers rebound, acute vascular graft rejection occurs in days to weeks post transplantation [44],[3].

2.2.3 Cellular Rejection

Major histocompatibility complex antigens in humans are known as human leukocyte antigens (HLA). Class 1 HLA antigens are found on the surface of most nucleated cells. Class 1 HLA antigens present endogenous antigen fragments to cytotoxic T cells upon binding CD8 receptors on killer T cells [36]. Class 2 HLA antigens are expressed on most immune cells including macrophages, dendritic cells and B cells. These antigens bind CD4 receptors on helper T cells and present exogenous antigens to these cells [36]. Cellular organ rejection occurs when donor HLA antigens are recognized as foreign substances by host T cells. Graft cells undergo apoptosis via perforin/ granzyme released by cytotoxic T cells or are subject to lysis via lytic enzymes released by macrophages [36]. HLA-incompatible transplantation also triggers hyperacute rejection in some recipients who are pre-sensitized to donor HLA antigens through

blood transfusion, prior transplants or pregnancy [3]. Hyperacute rejection in these cases is mediated by pre-exisitng host anti-HLA antibodies which bind HLA antigens and activate classical pathway of complement system [3]. Cell-mediated rejection can be prevented or reversed by immunosuppressive therapy [3].

2.2.4 Accommodation and Tolerance

Accommodation occurs when a transplanted organ is accepted by recipient as self organ despite the existence of anti-donor antibodies in host circulating blood and continued expression of foreign antigens on the graft [39],[53-54]. The exact biological pathways leading to accommodation are not yet fully understood. Some experimental models in xenotransplantation have demonstrated that graft cells undergo genetic changes and produce anti-apoptotic and cytoprotective proteins which protect endothelial cells against immunological assaults [53-55]. Other studies have demonstrated a decrease in expression of incompatible carbohydrate antigens by graft cells and/or production of protective antibodies in the host [55]. Tolerance refers to a state of accommodation when host antibodies against donor antigens are suppressed in long term. Evidence of tolerance has been observed in ABO-incompatible heart transplantations in infants who never produce anti-donor antibodies in long term [56].

2.3 PERI-TRANSPLANTATION REMOVAL OF ANTI-DONOR ANTIBODIES IN SOLID ORGAN TRANSPLANTATION

As discussed in the previous section, antigens expressed on donor graft elicit immune responses in the transplant recipient. In human allograft transplantation, ABO-incompatibility imposes the greatest barrier to solid organ transplantation [4]. However, the number of patients awaiting organ transplantation is significantly greater than the number of ABO-compatible donor organs that become available [1]. The capability to perform ABO-incompatible transplantation could increase the donor pool availability by 30 to 40% [2]. Numerous studies have shown that purification of blood from pre-existing anti-donor antibodies in the peri-transplantation period significantly reduces the risk of hyperacute graft rejection in ABO-incompatible transplantation [10, 13-15, 17-19, 57-58], [7], in xenotransplantation [45], [49],[30, 50-52] and in pre-sensitized recipients of HLA-incompatible allografts [59],[60]. Additionally studies have shown that despite the rebound of anti-A/B titers following the immediate peri-transplantation period, accommodation occurs and the risk of humoral mediated organ rejection in ABO-incompatible transplantation is reduced to less than 30% [7],[39],[15]. In the next section, a short review of prior clinical experiences with allograft ABO-incompatible and HLA-incompatible transplantation will be presented. Additionally, a short review of the effect of antibody removal in prevention of hyperacute rejection in xenotransplantation will be presented.

2.3.1 Clinical Experiences in ABO-Incompatible Kidney Transplantation

Early experiences in ABO-incompatible kidney transplantation in 1950s and 1960s resulted in very poor graft survival rates and crossing ABO blood group barrier was considered unsafe for

decades [4]. Initially Porter [61] speculated that graft rejection in ABO-incompatible transplantation was mediated by binding of anti-A/B antibodies to A/B antigens on the graft endothelium [61]. Additionally, by late 1960s, it was already understood that renal grafts from A2 blood group individuals expressed A antigens at a much weaker level than A1 individuals [62],[4]. Based on these two facts, the first clinical trials in crossing ABO barrier were performed by transplanting A2 renal grafts to type O recipients [63]. All 20 patients who participated in this study, received a standard immunosuppressive therapy, but did not undergo any other procedure for antibody removal. Eight of the kidneys were lost within 1 month, while 12 grafts showed long term survival [63]. After this initial successful attempt, several groups adapted the same procedure in transplantation of A2 kidneys to O recipients [64],[65]. Nelson et al. reported a 10-year large scale study, involving transplantation of A2 and A2B kidneys to B and O patients [64]. The acceptable anti-A titer in recipients at the time of transplantation was reported 1:4 titer units or below. The reported 2 year graft survival rate was 94% [64]. The first successful large scale ABO-incompatible kidney transplantation which included donors other than A2 or A2B blood groups was performed by Alexandre et al [8]. This group reported a series of successful ABO-incompatible kidney transplantations, following depletion of host blood from anti-A/B antibodies using plasma exchange and donor specific platelet transfusion [8]. Six out of nine patients showed graft survival for at least 2 to 16 months after transplantation. Following this initial successful trial, several other groups adapted an antibody removal procedure and demonstrated successful ABO-incompatible organ transplantations with 1-year graft survival rates of nearly 90% [7, 10-15, 17-19, 21, 39]. Tanabe et al. showed in a study of 52 end-stage renal patients that peri-transplant reduction of anti A/B titers to 1:16 or below resulted in graft and patient survival rates of 78 and 91% at 5 years [21]. No significant difference in patient or

graft survival rates was observed in ABO-compatible (n=723) versus ABO-incompatible (n=52) transplantations [21]. A follow up study of 67 patients over 8 years indicated no significant difference in ABO-compatible and ABO-incompatible graft survival rates after year 3. But patient survival rate was the same during all 8 years of the study [10]. Other long term survival rates have also been very encouraging [10-12]. Ishida et al. [23] reported a 10 year large scale study including 101 living related kidney transplantations. In all cases, plasmapheresis and immunoadsorption were used to reduce pre-transplantation anti-A/B antibody titers of graft recipients to 1:4 or below. Patient survival rate was reported 94% after 1 year and 92% after 5 years. Graft survival rate was 76% after 1 year and 73% after 5 years. The same study indicated that 75% of patients showed no increase in anti-A/B titers following transplantation [23]. Graft loss was only observed in 12% of patients, 9% of which lost grafts within 2 months and 4% lost grafts within a year. Graft loss was observed in all patients who had postoperative anti-donor titers of 1:64 or higher [23]. Toma et al. reviewed long term patient and graft survival rates in 213 patients who underwent ABO-incompatible renal transplantation at 41 centers in Japan between January 1989 and 1998. Antibody titers were reduced to 1:16 or lower through several sessions of plasma exchange, double filtration plasmapheresis or plasma immunoadsorption. Patient and graft survival rates were reported to be 91% and 82% at 1 year and 75% and 57% at 9 years, respectively [12]. No significant difference in patient or graft survival rates were observed between ABO-compatible and ABO-cross matched transplantations [12].

2.3.2 Clinical Attempts in ABO-Incompatible Liver Transplantation

ABO-incompatible liver transplantation has been performed only in emergency cases of hepatic failure, when the only organ available has been ABO-incompatible [4]. ABO-incompatible liver

transplantation rarely results in hyper acute rejection. However, graft survival rates are poor and liver transplants fail due to vascular thrombosis and bile duct complications [4]. Gordon et al. [66] reported a series of 672 liver transplants in 1986, with a 3 year graft survival rate of 56% in 520 ABO-identical grafts, 39% in 91 ABO-compatible and 36% in 31 ABO-incompatible liver transplants [66],[4]. Fifteen cases of ABO-incompatible liver transplantation were reported from the Mayo clinic with a 1 year patient and graft survival rates of 57 and 46%, respectively [67]. Mor et al. reported a study in which preoperative plasmapheresis was used to reduce anti- A/B titers to 1:16 or below in 10 patients undergoing ABO-incompatible liver transplantation. Patient and graft survival rates were 80% and 60%, respectively at a follow up time of 5-17 months [16]. Hanto et al. used double volume plasma exchange in 14 cases of ABO-incompatible liver transplantation, and reported 1 year graft survival rate of 71.4% [15]. No immunological graft losses were observed in any of the cases [15]. Skogsberg et al reported results of ABO-incompatible cadaveric liver transplantation in 12 blood group O adult patients [18]. No pre-operative plasmapheresis was performed but three patients underwent plasmapheresis post transplantation [18]. Patient and graft survival rates were 83% and 67%, respectively, with a 6.5 month follow up median [18]. Slightly better graft survival rates have been observed in pediatric liver transplantation. Tanaka et al reported patient and graft survival rates of 77% in a series of 13 pediatric ABO-incompatible related living kidney transplantations [68]. In a report published by Varela-Fascinetto et al, the 10 year patient and graft survival rate in 28 ABO-incompatible liver transplantations was 71% and 67%, respectively. No significant difference in ABO-incompatible, ABO-compatible or ABO-identical liver transplantations was observed [69].

2.3.3 Clinical Attempts in ABO-Incompatible Heart and Lung Transplantation

Very few cases of ABO-incompatible heart and/or lung transplantation have been reported and the success rates have been generally very low. A series of ABO-incompatible heart transplantation in small children were reported by West et al. which used plasma exchange during cardiopulmonary bypass [56]. Seven out of 10 transplanted grafts survived in a follow up time of 11 months to 4.6 years. Pierson et al. reported the first successful ABO-mismatch lung transplantation, following inadvertent transplantation of type A lung to a type B patient [70]. Following rebound of anti-A titers, patient underwent plasmapheresis and plasma immunoadsorption. Patient was reported "clinically well" three years after transplantation. Recently, Struber et al reported one intentional case of transplantation of a lung from a deceased type AB donor to type O recipient. Anti-A/B antibodies were removed from circulating blood by plasmapheresis and immunoadsorption. The patient was reported well and at home at nine months follow up [71].

2.3.4 Clinical Attempts in HLA-Incompatible Allograft Transplantation

Anti-human leukocyte antigen (HLA) antibodies are produced in pre-sensitized patients mainly due to prior pregnancy, repeated blood transfusions or chronic dialysis [3]. Renal and cardiac HLA-incompatible transplantation results in a high rate of hyperacute rejection and graft loss following binding of recipient anti-HLA antibodies to donor HLA antigens. Pre-transplantation removal of recipient anti-HLA antibodies is performed by plasma exchange or by plasma immunoadsorption through protein A columns with relatively high success rates. In a study of eighteen HLA-incompatible kidney transplantations, Sonnenday et al. removed anti-donor HLA

antibodies in an average of three plasma exchange sessions and reported 94% graft survival rate at 1 to 44 months post transplant [60]. Ross et al. removed anti-HLA antibodies through plasma immunoadsorption in protein A columns and reported 80% graft survival rate for 3 to 34 months post transplant [59].

2.3.5 Clinical Attempts in Xenotransplantation

The major barrier to successful xenotransplantation is binding of natural anti-α-Gal antibodies to Galα1-3Gal (α-Gal) antigenic determinants expressed abundantly on nonprimate mammalian grafts [72],[73],[45-46, 74]. These naturally occurring antibodies mediate hyperacute and acute rejection of nonprimate mammalian grafts transplanted into primates. Pre-transplantation removal of anti-α-Gal antibodies through plasma exchange or immunoadsorption through beaded columns containing α-Gal oligosaccharides significantly reduces the risk of hyperacute rejection [45],[49],[30, 50-52]. However, rapid rebound of anti-α-Gal antibody titers results in delayed humoral rejection. In an in-vivo study, Taniguchi et al. showed that serum anti-α-Gal antibodies were reduced significantly in baboons following plasma immunoadsorption in columns containing macroporous glass beads, on which polyacrylamide-synthetic Gal conjugates were immobilized [51]. Although both IgM and IgG anti-α-Gal antibody titers were significantly reduced, antibody titers rebound within a week following the last immunoadsorption session [51]. Kozlowski et al. showed in a series of in-vivo baboon plasma perfusion through immunoaffinity columns that both IgM and IgG anti-α-Gal antibody titers were reduced by 81-97% immediately after immunoadsorption. However, the antibody titers rapidly rebound to the pre-immunoadsorption levels within 1-6 days [52]. Following perfusion of separated plasma or

whole blood through immunoadsorbent columns containing α-Gal epitopes, Xu et al demonstrated that removal of anti-α-Gal antibodies from blood was sufficient to prevent hyperacute rejection of a transplanted pig kidney [30]. The same study also indicated that perfusion of whole blood through beaded columns was associated with a 30% decrease in hematocrit and 40-50% decrease in platelet count [30]. A combination of hemodilution and nonspecific removal of red blood cells was reported responsible for the decrease in hematocrit. Hemoperfusion also resulted in transient reduction in total immunoglobulin, platelet, complement, total protein, albumin and fibrinogen concentrations due to hemodilution [30]. Despite the success in complete removal of anti-α-Gal antibodies in immunoadsorption columns prior to xenotransplantation, delayed antibody mediated rejection following rebound of anti-α-Gal antibodies remains an obstacle in xenotransplantation. Current efforts in this area are directed towards production of transgenic pigs which do not express α-Gal antigens [47-48],[75], hence eliminating the need for removal of anti-α-Gal antibodies.

2.4 ANTIBODY REMOVAL TECHNIQUES

As discussed in the previous section, antibody removal is performed to prevent hyperacute rejection in ABO-incompatible organ transplantation [8, 10, 22],[21, 71], in xenotransplantation [30, 51, 76-78] and in HLA-incompatible allograft transplantation in pre-sensitized organ recipients [60], [59]. Additionally antibody removal is used in treatment of many autoimmune

diseases [79],[80],[81],[82]. Both selective and nonselective techniques of antibody removal have been used previously. In the following section, a short overview of each of these techniques will be presented.

2.4.1 Plasmapheresis or Therapeutic Plasma Exchange

In plasmapheresis or therapeutic plasma exchange, plasma is separated from blood cells and is replaced with either fresh frozen donor plasma or 5% albumin solution [28],[83]. Plasma exchange is used for fast removal of the factors that associate with certain diseases [83],[79],[81]. Examples include removal of pathogenic autoantibodies which mediate autoimmune diseases, immune complexes, thrombotic factors and cholesterol containing lipoproteins [83],[79]. Plasmapheresis is also used to remove high and middle molecular weight blood proteins that participate in the inflammatory processes such as activated complement products, fibrinogen and possibly cytokines [83]. Other examples include removal of anti-A/B [8, 10, 22],[21, 71], [56], [18], [84], anti-HLA [60] and anti-α-Gal antibodies [85],[77] to facilitate ABO-incompatible, HLA- incompatible or xenotransplantation.

Therapeutic plasmapheresis is performed either by centrifugation or by membrane filtration [83]. A centrifugal plasmapheresis device typically consists of a bell shaped bowl which rotates at about 16000 rpm [28]. Venous blood is withdrawn from patient and is pumped into the device at a typical flow rate of 100 ml/min [28]. Blood cells and plasma are separated due to centrifugal forces and plasma is removed through a central outlet port on top of the bowl. Each cycle has to be disrupted once the bowl is full of red blood cells. The packed blood cells will be collected and returned to patient after addition of substitution fluid [28],[83]. Each cycle usually removes approximately 400 to 700 ml of plasma [28]. Continuous flow and intermittent

centrifugation are similar in principles. However, in the continuous process, there are outlet ports for simultaneous removal of both plasma and blood cells [83]. The extracorporeal volume is smaller (220 to 350 ml) in the continuous flow centrifugation. Therefore, this type of plasmapheresis is more appropriate for treatment of patients with severe anemia or cardiovascular impairment [83], [28]. In a continuous flow centrifuge, approximately 3L of plasma can be removed within 90 minutes [86].

Membrane based filters contain microfiltration hollow fibers with pore sizes ranging between 0.2 and 0.77 μm [83],[28]. In these devices blood cells are separated from plasma due to transmembrane pressure. The maximum limit for transmembrane pressure is typically 70-100 mm-Hg, due to the risk of fiber rupture [28]. The optimal blood flow rate for plasma filtration is usually 100 ± 20 ml/min and the filtration flow rate is typically 15-50 ml/min [28]. The optimum filtration flow rate is determined based on the filtration characteristics of the fibers. Usually as filtration flow rate exceeds a certain range, the plasmapheresis yield declines due to the increased rate of fiber fouling [28].

Total plasma exchange with fresh frozen donor plasma is limited by donor supply and is also associated with the risks of infection transmission and immunological reactions to non-autologous plasma [28]. The risk factor associated with the use of 5% albumin solution as the replacement fluid is depletion of blood from the requisite proteins, such as clotting factors, platelets, and immunoglobulins [28].

2.4.2 Double Filtration Plasmapheresis

Double filtration plasmapheresis provides semi-selectivity in removal of target molecules from blood. In double filtration plasmapheresis, two membrane based plasmapheresis devices with

different pore sizes are used successively. Blood cells are separated from plasma in the first filter with a pore size of approximately 0.2 μm. Plasma is then passed through a second filter whose pore size is 0.03 μm [83],[87]. Cleared plasma is recombined with blood cells and returns to patient. Total amount of discarded plasma is 500-600 ml. Therefore minimal replacement fluid is required [87]. Inlet blood flow rate is typically 50-100 ml/min and approximately 3-4 L of plasma is obtained over 2-3 hours [87]. Double filtration plasmapheresis is used in a limited number of transplantation centers to remove anti-A/B antibodies in ABO-incompatible transplantation [12],[23].

2.4.3 Protein-A Columns

Protein A columns provide the advantage of semi-selective removal of plasma immunoglobulins [80],[82]. Antibody removal in protein-A columns is preferred over nonselective antibody removal techniques, such as plasmapheresis, as no replacement solution is required. However protective immunoglobulins, other than the targeted pathogenic antibodies, are also removed in this process. Two protein-A containing columns: Prosorba® and Immunosorba® are currently FDA-approved and are used in treatment of rheumatoid arthritis, idiopathic thrombocytopenic purpura and hemophilia with inhibitors [80], [82], [88]. In Prosorba® columns, protein A is immobilized on silica beads. Immunosorba® columns contain protein-A, covalently attached within the pores of Sepharose particles. Both columns are commercially available through Fresenius Hemocare (Redmond, WA).

2.4.4 Selective Bead-Based Immunoadsorption

Immunoadsorption columns have been developed to selectively remove antibodies from whole blood or plasma. These columns typically contain porous beads within the pores of which antigens with affinity for the target antibodies are immobilized [89],[24],[25],[30]. Biosynsorb® from Chembiomed (Alberta, Canada) [90], BioSorbent A and B developed by Rieben et al. [24] and Glycosorb® from Glycorex transplantation AB (Lund, Sweden) [25] are affinity columns specifically made for removing anti-A/B antibodies from human plasma or whole blood. Biosynsorb® columns were previously available but are no longer in the market [90],[89]. These columns contained synthetic A or B antigens immobilized on silica beads [90]. The bead also contained a thin coating of polystyrene which made them compatible with whole blood perfusion [90]. Nonetheless, significant loss of hematocrit and platelet count was observed in some studies during perfusion of whole blood through these columns [30]. In BioSorbent A and B columns, synthetic A or B –trisacchsride antigens were conjugated with poly-N hydroxyethylacrylamide spacers and were covalently attached to macroporous glass beads with a pore diameter of 200 nm [24]. Currently, only Glycosorb columns are commercially available through Glycorex transplantation AB (Lund, Sweden). In Glycosorb columns, synthetic A or B antigens are conjugated via short aliphatic hydrocarbon chains (up to 6 carbon atoms in length) within the pores of Sepharose particles [25]. Glycosorb columns are approved for human clinical use is Europe and have been used to reduce anti-A/B antibody titers to 1:8 or below in ABO-incompatible kidney, liver and lung transplantation [13],[19-20],[91],[14, 17, 70, 92-97].

Similarly affinity columns for removal of anti-α-Gal antibodies have been developed and used in in-vitro and in-vivo [30, 51, 76-78] studies to remove anti-α-Gal antibodies in baboons.

Taniguchi et al. developed immunoadsorption columns for specific removal of anti-α-Gal antibodies by immobilizing spacered α-galactose disaccharide conjugated with poly-N hydroxyethylacrylamide to macroporous glass beads [51]. Xu et al. developed affinity columns by immobilizing two types of α-Gal trisaccharides on silica beads and demonstrated that type 6 α-Gal trisaccharides were more efficient in removing anti-α-Gal antibodies. Efficiency of antibody removal and safety of these columns were later confirmed in a large scale study [76].

Immunoadsorption columns offer the advantage of specifically removing the target antibodies. Nonetheless, in most cases a complicated plasmapheresis procedure is coupled with immunoadsorption to eliminate any risks associated with direct contact of blood cells with the immunoadsorbent material [13],[19-20],[91],[14, 17, 70, 92-97]. The risks associated with plasmapheresis include haemodynamic and cardiovascular complications [28]. Conversely, the adverse effects of direct hemoperfusion through columns usually include loss of platelets, decrease in hematocrit, increase in coagulation time and electrolyte imbalances [29-30]. In some cases the beads have been coated with a biocompatible polymer to make them compatible with direct hemoperfusion [90]. However, the coating significantly reduces the removal capacity of the beads and may not completely eliminate all the risk factors associated with direct hemoperfusion through columns [30]. Additionally, there are a number of practical and safety difficulties associated with the use of sorbent columns [29]. Most sorbent columns are compressible and cause a large pressure drop across the columns. The smaller the beads are, the greater the cost of pressure drop will be. Therefore, blood flow rate has to be maintained at a typically low range (10-20 ml/min) to maintain pressure drop in a manageable range [29]. In practical terms, the size of the beads in columns can not be smaller than 20-50 μm as pressure drop across the column length for smaller beads becomes unmanageable [29].

2.4.5 Selective Fiber-Based Immunoadsorption

Similar to affinity columns, the fiber based immunoadsorption devices use immobilized ligands with specific affinity for the target antibodies. However, in fiber based immunoadsorption, antigens are directly immobilized on the inner, outer or internal surfaces of dialysis or microfiltration fibers. Several groups have developed fiber based immunoadsorption devices for removal of target antibodies from blood or plasma [31],[33],[32, 98-99]. Our own group previously developed specific antibody filtering devices (SAF) designed for removal of antibodies directly from whole blood without the need for prior plasmapheresis [31-33]. In these devices, ligands specific to the targeted antibodies were immobilized on the luminal surfaces of dialyzer fibers potted into modules. Whole blood perfusion through the fibers resulted in antibody capture at the fiber walls **(Figure 1-1)**. The first predecessor SAF was fabricated and tested by Hout et al. [31]. This device incorporated Neutr-AB®, an animal based A and B glycoprotein antigen, immobilized on the lumenal surfaces of modified Hemophan® dialysis fibers. Bench-top experiments demonstrated that anti-A and anti-B titers of average to high titer type O blood could be reduced to 1:2 or below from 300-400 ml of whole blood recirculating through this device [31]. Purification of Neutr-AB prior to immobilization to remove a lower molecular weight non-antigenic fraction further increased the apparent binding capacity of the predecessor SAF by six fold [31]. Based on these preliminary results, it was estimated that two to three dialyzers modified with purified Neutr-AB were required to significantly reduce anti-A/B antibody titers in 3-5 L of blood [31]. Gautam et al. developed a SAF device for removal of anti-A antibodies which used synthetic blood group A-trisaccharide antigens conjugated to polyacrylamide spacers as the immobilized ligands [32]. Using a mathematical model of antibody removal and in vitro anti-A capture data obtained in appropriately scaled down

modules, these studies indicated that a minimum antibody binding capacity of 0.0045 nmol/cm^2 would be required for a clinically effective device. This removal capacity was 5 to 6 fold higher than the antibody binding capacity achieved based on current immobilization methods [32] . As we will discuss in more detail, efforts have been ongoing to increase antibody removal capacity of the SAF modules by using high molecular weight spacers and by increasing the surface area for antigen immobilization through use of fibers with larger pore sizes [100].

2.5 INTEGRATED FIBER AND BEAD ANTIBODY FILTERS (BSAF)

2.5.1 Integrated Sorbent Suspension/Fiber Devices

Integrated sorbent suspension/fiber is referred to a class of blood detoxification devices in which sorbent particles are suspended in the interstitial space of microfiltration fibers and rely on Starling recirculation flow of plasma between the fiber and the bead-containing shell compartment to transfer target molecules from blood to the sorbent material (similar to our BSAF devices). Previously Falkenhagen and his group developed microspheres-based detoxification system (MDS), for blood detoxification in liver failure and sepsis [101-107]. In MDS the dialysate side of a standard plasma filter is combined with a secondary extracorporeal flow loop in which adsorbent particles are suspended. The volume of this secondary loop is approximately 300 ml per 1 L of processed blood [104] . Blood flow rate is typically 200 ml/min and the bead suspension flow rate is 4-6 L/min [102, 104]. Weber et al. immobilized anti-TNF antibodies on cellulose beads (1-10 μm) and used these beads in MDS to remove TNF from human plasma [104, 107]. The same group has also applied a combination of a hydrophobic

neutral resin and an anion exchange resin as sorbent material in MDS to remove albumin-bound substances such as unconjugated birilubin or cholic acid and non protein-bound substances such as phenol from blood [101]. Overall, the efficacy of MDS in removal of small and middle molecular weight blood proteins such as endotoxins, digitoxin, unconjugated birilubin and tryptophan has been shown in several publications [101-108].

The suspended sorbent particles in integrated sorbent suspension/ fiber devices cause significantly less flow resistance in the fiber interstitial space compared to plasma flow in a packed sorbent column. As a result, flow rate in the fiber interstitial space can be up to 10-fold higher than blood/plasma flow rate in a packed sorbent column. Additionally as pressure drop is much smaller along the length of the modules, smaller beads can be used in sorbent suspension/fiber devices [29]. All this increases the overall removal rate and capacity of these devices. The upper limit for blood flow rate is mainly dictated by hemodynamic stability of patient as well as the capability of fibers to withstand transmembrane pressure at the given flow rate [29]. Typically blood flow rate in the range of 100-500 ml/min may be applied. The lower limit of the bead size is dictated by the size of the fiber pores.

2.5.2 BSAF Devices for Specific Removal of Anti-A/B Antibodies from Blood

A new class of antibody removal devices, the integrated bead and fiber specific antibody filters (BSAF), are under development in out laboratory,. BSAF devices are composed of microfiltration hollow fibers, potted into modules with immunoadsorbent beads uniformly distributed in suspension within the fiber interstitial space **(Figure 1-2)**. The blood perfusion loop in BSAF devices is similar to the perfusion loop used in our first prototype SAF devices **(Figure 1-1)**. Antibody removal in BSAF occurs as a result of Starling recirculation flow

between the fibers and the shell compartment, along with antibody diffusing and binding to novel synthetic antigens, immobilized within the shell side porous beads. As we will discuss in detail in the following chapters, we have developed a mathematical model to quantify antibody adsorption rate in BSAF devices as a function of key design and operational parameters. We have validated the mathematical model in appropriately scaled down capture system of monoclonal anti-A antibodies in physiological buffer solution . We used this model to design full scale BSAF devices and showed in our studies that appropriately scaled down prototypes of our designed BSAF modules are capable of depleting up to 100% of reservoir anti-A antibody concentration within two hours from buffer and whole blood. A list of potential advantages of antibody removal in BSAF devices was presented in Chapter 1.0. One major challenge in development of full scale BSAF devices is to integrate a bead mixing mechanism within the device to maintain the bead slurry in a continuously mixed condition. In the following chapters we will discuss the theoretical and experimental studies performed to develop BSAF devices for antibody removal from whole blood and we will further discuss our envisioned design of an integrated bead mixing mechanism for our BSAF devices.

Our first prototype BSAF modules were developed for removal of anti-A antibodies due to the widespread clinical application of anti-A removal in ABO-incompatible transplantation (see **Table 2-1**). However, as mentioned in the previous section, antibody removal is required in various other clinical applications. Therefore, the same approach could be easily applied to develop BSAF devices for specific removal of other pathogenic antibodies. Additionally, the work presented here will provide a basis to design other blood purification devices which aim at removal of toxins from blood. Examples of such applications are in treatment of hypercholesterolemia, liver failure and sepsis [88, 109-110].

3.0 ANALYSIS OF BINDING INTERACTIONS BETWEEN A- TRISACCHARIDE-POLYACRYLAMIDE GLYCOCONJUGATES AND ANTI-A ANTIBODIES USING SURFACE PLASMON RESONANCE TECHNOLOGY

As discussed in chapter 2.0, specific immunoadsorption of anti-A/B antibodies from plasma or whole blood provides a superior alternative to nonselective or semi-selective antibody removal techniques, since only anti-A/B antibodies are removed from plasma and minimal replacement fluid is required. Our group has been developing fiber based anti-A/B immunoadsorption devices, designed for specific removal of blood group antibodies directly from whole blood, without the need for prior plasmapheresis [31-33, 100]. In chapter 2.0, we described development of our first specific antibody filters (SAF), which were composed of dialyzer hollow fiber membranes potted into cartridges, with blood group A or B antigens covalently attached on the luminal surfaces of the fibers [31-32]. Initially, an animal based A and B glycoprotein antigen (Neutr-AB®) was used as the immunoadsorbent material in our SAF devices [31]. Antibody capture in Neutr-AB® -based SAF devices resulted in reduction of anti-A and anti-B titers of 300-400 ml of type O blood by 75-98% [31]. Purification of Neutr-AB prior to immobilization to remove a lower molecular weight non-antigenic fraction further increased the binding capacity by six fold [31]. However, the SAF antibody removal capacity was still significantly lower than the required level for a clinically effective device [31]. In an effort to further improve both antibody removal capacity and biocompatibility of SAF devices, Gautam et

al. used synthetic blood group A-trisaccharide antigens conjugated to 30 kDa poly N-hydroxyethylacrylamide spacers (Atri-PAA^{30}) as the immobilized ligands in the SAF device [32]. Using a mathematical model of antibody removal and in-vitro anti-A antibody capture data obtained in appropriately scaled down modules, these studies indicated that a minimum antibody binding capacity of 0.0045 nmol/cm^2 would be required for a clinically effective device [32]. This level of immobilized antigen is 5 to 6 fold higher than the antibody binding capacity achieved based on our current immobilization methods.

In this study, we conjugated blood group A-trisaccharide antigens to high molecular weight (1000-2000 kDa) poly N-hydroxyethylacrylamide spacers (Atri-PAA^{1000}). This new, high molecular weight glycoconjugate was investigated as an alternative synthetic A antigen for antibody removal devices. The glycopolymers equipped with biotin tags (Atri-PAA^{30}-biotin and Atri-PAA^{1000}-biotin) were deposited on streptavidin coated sensor chips and the affinity and kinetics of anti-A antibodies binding to these glycoconjugates were studied using surface plasmon resonance (SPR). Antibody removal capacity of the high molecular weight glycoconjugate (Atri-PAA^{1000}-biotin)-immobilized surface was 2-3 times higher than with the low molecular weight glycoconjugate (Atri-PAA^{30}-biotin) immobilized surface. The carbohydrate content in Atri-PAA^{1000}-biotin (20 mol% or 50 mol %) did not affect antibody binding capacity of the glycoconjugate. To assess the strength of the binding interactions, the kinetics and affinities in interactions between several clones of anti-A antibodies and (Atri-PAA^{1000}-biotin) were measured and compared to reference values for monoclonal antibody-

antigen interactions. The results suggest that anti-A/B immunoadsorption devices, especially hollow fiber-based antibody filters which are limited in surface area for antigen immobilization, may greatly benefit from the new synthetic high molecular weight polyacrylamide glycoconjugates.

3.1 MATERIALS AND METHODS

3.1.1 Instrumentation

All experiments were performed using a Biacore® 3000 optical biosensor (Biacore AB, Uppsala, Sweden), equipped with research grade streptavidin-coated sensor chips (SA) (Biacore AB, Uppsala, Sweden). The temperature of the instrument was set at 25^{o}C and data were collected at a collection rate of 5 Hz. The Biacore instrument uses surface plasmon resonance technology (SPR) to quantitatively measure the rate of binding of a soluble ligand to an immobilized binding partner in real time [111]. The SPR signal is expressed in resonance units (RU) and is a measure of mass concentration at the sensor chip surface [111]. . A satisfactory linear relationship has been found between resonance units and surface concentration of proteins, sugars and DNA [111]. This technology has been used for measurement of the kinetic rate constants, as well as the equilibrium constants in biomolecular interactions [112] [113] [114].

3.1.2 Reagents

All reagents and chemicals were obtained from Biacore AB (Uppsala, Sweden) unless otherwise specified. Filtered and degassed HBS-EP buffer at pH 7.4 contained 0.01 *M* *N*-2-hydroxyethyl-piperazine-*N*'-2-ethanesulfonic acid (HEPES), 0.15 *M* sodium chloride (NaCl), 3 m*M* ethylenediaminetetraacetic acid (EDTA) and 0.005% polysorbate-20 (v/v). HBS-N buffer contained 0.01 *M* HEPES and 0.15 *M* NaCl, at pH 7.4.

3.1.3 Monoclonal Anti-A Antibodies

Murine monoclonal anti-A antibodies were all of immunoglobulin M (IgM) class; Clone F98 7C6-4 (401 μg/ml) was obtained from Dominion Biologicals, Ltd. (Dartmouth, NS, Canada), Clone A-16 (37 μg/ml) was from Hematological Center (Moscow, Russia), and the Anti-A series1 (47 μg/ml) was from Immucor Inc. (Norcross, GA, USA). The stock concentration of each of the monoclonal antibodies was measured by enzyme linked immunosorbent assay (ELISA) as described previously [116].

3.1.4 Plasma

Samples of fresh frozen plasma type B from three different healthy donors were obtained from the Central Blood Bank of Pittsburgh. Blood typing and measurement of anti-A/B antibody titers were performed according to the standard blood bank procedure for hemagglutination assay [117]. Briefly, plasma samples were serially diluted in 0.9% Saline solution. One drop of either A1 or B reference red blood cells (Immucore Inc., Norcross, GA, USA) was added to each tube

and tubes were centrifuged for 1 minute at 3300 rpm. Tubes were then examined for agglutination of A1 and B red blood cells. Anti-A and anti-B titers were recorded as the reciprocal of the largest dilutions that agglutinated A1 and B reference blood cells, respectively. As expected for type B plasma, all three samples agglutinated type A but not type B blood cells. Anti-A antibody titer in plasma samples (#2) and (#3) were 16 and in sample (#1) the measured titer was 32.

3.1.5 Synthesis of Polyacrylamide Glycoconjugates

All polyacrylamide glycoconjugates were synthesized at Shemyakin and Ovchinnikov Institute of Bioorganic Chemistry (Russian Academy of Sciences, Moscow, Russia). Specific determinant fragments of blood group A-trisaccharide antigen (Atri), GalNAcα1−3[Fucα1−2]Galβ−, and B-trisaccharide antigen (Btri), Galα1−3[Fucα1−2]Galβ−, were synthesized as ω-aminopropyl glycosides as previously described [119]. 30 kDa poly(4-nitrophenyl acrylate) ($pNPA^{30}$) and 1000 kDa poly(N-oxysuccinimidyl acrylate) ($pNSA^{1000}$) were synthesized as previously described [120-121]. The glycoconjugates containing 20 or 50 mol % of the A or B -trisaccharides and 5 mol% of biotin were also prepared according to the previously described method [120]. Briefly, aminopropyl glycosides (2 or 5 mmol) and biotin-$NH(CH_2)_6NH_2$ (0.5 mmol) were added to a solution of 10 mmol activated polymer ($pNPA^{30}$ or $pNSA^{1000}$) in dimethyl sulfoxide (DMSO). The reaction mixture was kept at 40^{o}C for 24 hours. The exhaustive immobilization of the aminoligands to the polymers was confirmed by thin layer chromatography (TLC). The remaining active ester groups in the polymer were quenched by treatment with ethanolamine. The synthesized glycoconjugates were purified by gel-permeation chromatography.

3.1.6 Immobilization of Synthetic Antigens on SA Sensor Chips

Flow cells of SA sensor chips were primed with running buffer (HBS-EP), followed by three consecutive injections of 90µl of 1 *M* NaCl in 40 m*M* sodium hydroxide (NaOH) at a flow rate of 90 µl/min. The immobilization protocol varied slightly for kinetic and binding capacity studies. In binding capacity experiments, antigens were immobilized at maximum surface loading capacity, which ensured that antibody removal was not limited by the amount of immobilized antigens on the surface. Glycoconjugate solution (5 µg/ml in HBS-N buffer) was injected over the surface at a flow rate of 2µl/min until a plateau in the binding curve was observed, signifying that equilibrium had been reached. This typically happened within five minutes of sample injection. Repeated injections of the glycoconjugate solution after reaching equilibrium did not increase the surface loading density. For kinetic studies, a low level of antigen loading was desired to minimize the effect of diffusion limitation on the kinetic analysis [122]. Immobilization was performed by injecting 5 µl of the glycoconjugate solution (1 µg/ml in HBS-N buffer) over the specified flow cells at a flow rate of 2µl/min. The amount of glycoconjugates immobilized on each surface was quantified by subtracting the baseline response level of the glycoconjugate solution before the injection from the baseline level after injection. Thus variations of synthetic A antigens (Atri-PAA^{1000}-biotin or Atri-PAA^{30}-biotin) were immobilized on test sensor chips. Control surfaces for measurement of non-specific binding levels included immobilized synthetic B antigens (Btri-PAA^{1000}-biotin or Btri-PAA^{30}-biotin) or immobilized spacers (PAA^{1000}-biotin).

3.1.7 Measurement of Anti-A Antibody Removal Capacity of Immobilized Antigens

Samples of different clones of IgM monoclonal anti-A antibodies (A16, Anti-A series1 and F98 7C6-4) were diluted to one-half their original stock concentrations in HBS-EP buffer. Each sample was then injected at a flow rate of 20 µl/min over the surface of a sensor chip specifically prepared for binding capacity studies. Each injection was continued until a plateau in the response sensogram indicated that equilibrium was reached. After injections, the surfaces were regenerated by a single 30 second injection of 50m*M* NaOH solution and consequently, monoclonal antibody samples, diluted to 75% of their original concentrations were injected over regenerated surfaces. Similar binding levels of monoclonal antibodies diluted to 50% and 75% their original concentrations ensured that the reported binding levels represented the maximum surface removal capacity for a given antibody. Similarly, polyclonal anti-A antibodies in plasma type B were injected over sensor chips. Unlike monoclonal antibodies, we did not dilute plasma samples because initial measurement of anti-A antibody titer in plasma samples indicated several folds lower antibody concentrations in plasma samples compared to the stock solution of monoclonal antibodies. Anti-A antibody removal capacity of immobilized antigens in each case was considered to be the equilibrium binding level in resonance units (RU). All surfaces were regenerated, by a single 30 second injection of 50m*M* NaOH solution at a flow rate of 90 µl/min to remove bound monoclonal or plasma antibodies. This regeneration protocol resulted in complete removal of bound antibodies from surface. Repeated injections of monoclonal antibodies or plasma samples over each regenerated surface resulted in reproducible antibody binding levels on the surface which indicated that immobilized glycoconjugates were stable.

3.1.8 Statistical Analysis

The significance of the difference between the binding levels on different surfaces were evaluated using a two-tailed student's t-test with $p<0.05$ indicating a significant difference. The difference between binding levels of different plasma samples on different surfaces were compared using one-way analysis of variance (ANOVA).

3.1.9 Measurement of the Kinetics of Antibody-Antigen Interactions

Monoclonal antibodies were all diluted in the dilution buffer (HBS-EP) to the following final concentrations: 0.01, 0.02, 0.04, 0.08, 0.15, 0.30, 0.61 and 1.22 n*M* for A-16 antibodies; 0.7, 1.4, 2.9, 5.8, 11.7 and 23.5 n*M* for Anti-A series1; and 0.1, 1.7, 3.5, 6.9, 13.9, 55.6 and 111.1 n*M* for clone F98 7C6-4 antibodies. The range of antibody concentrations was chosen to cover a complete range of binding levels to immobilized Atri-PAA^{1000}-biotin. Antibodies at each concentration were injected twice over the control and test surfaces. Injections were performed at a flow rate of 75 µl/min for three minutes in a random concentration order. Each injection was followed by a 10 minute dissociation time and a single injection of 10 m*M* glycine-hydrochloric acid (Glycine-HCl) (pH 1.5) at a flow rate of 90 µl/min for 30 seconds to remove the bound antibodies from the surface. A two minute stabilization time after the regeneration step followed each cycle. In all of the above experiments, a blank injection of the running buffer was included.

3.1.10 Kinetic Analysis

We used the approach given by Fagerstam et al. [111] to obtain kinetic constants for interactions between immobilized Atri antigens (*Ag*) and monoclonal anti-A antibodies (*Ab*). Assuming a simple 1:1 interaction model, the net rate of antibody-antigen complex formation (*Ab-Ag*) is given by :

$$d[Ab-Ag]/dt = k_a[Ab][Ag] - k_d[Ab-Ag] \qquad \textbf{(3-1)}$$

where k_a and k_d represent the association and dissociation rate constants, respectively and t represents time. Equation **(3-1)** can be expressed in terms of the resonance signal, R :

$$dR/dt = k_a C(R_{\max} - R) - k_d R \qquad \textbf{(3-2)}$$

where R is the binding level at time t and is assumed proportional to the amount of *Ab-Ag* complexes formed, C represents concentration of the antibodies in the solution and $R_{\max}$ represents antibody removal capacity of the immobilized antigens in resonance units. Equation **(3-2)** can be rearranged to give:

$$dR/dt = -k_s R + k_a C R_{\max} \qquad \textbf{(3-3)}$$

where,

$$k_s = k_a C + k_d \qquad \textbf{(3-4)}$$

Following equation **(3-3)**, dR/dt was linearly regressed against R at various antibody concentrations and the slopes of the regression yielded k_s. A linear regression of k_s against C then yielded k_a according to equation **(3-4)**. During the dissociation phase, antibody concentration is zero and equation **(3-2)** simplifies to:

$$dR/dt = -k_d R \qquad \textbf{(3-5)}$$

The solution to equation **(3-5)** is:

$$\ln(R_o / R) = k_d t \qquad \textbf{(3-6)}$$

where R_o represents the response at the beginning of the dissociation phase. Dissociation rate constants (k_d) were calculated by a linear regression of $\ln(R_o / R)$ versus t according to equation **(3-6)**. Equilibrium dissociation constants (K_D) were calculated as the ratio of k_d over k_a. For each anti-A antibody clone, k_a was reported as the average of two independent measurements and k_d was measured as the average of a series of measurements for the range of antibody concentrations studied in the experiment.

3.2 RESULTS

3.2.1 Effect of the size of PAA on Antibody removal Capacity of Glycopolymers

Our goal was to evaluate the effect of molecular weight of polyacrylamide scaffold on the antibody removal capacity of Atri-PAA-biotin conjugates. Atri-PAA^{30}-biotin and Atri-PAA^{1000}-biotin (containing 20 mol% carbohydrate and 5 mol% biotin) were synthesized. Analogous glycoconjugates containing B antigens (Btri-PAA^{30}-biotin and Btri-PAA^{1000}-biotin) and the polymer without carbohydrate residues (PAA^{1000}-biotin) were used as controls for the SPR experiments. All glycoconjugates were immobilized on flow cells of SA sensor chips. Immobilization was performed until maximum loading on each surface was reached. The maximum loading capacity of surface was estimated 1 ng/mm^2 for both 30 and 1000 kDa glycoconjugates **(Figure 3-1)**. Since in both 30 and 1000 kDa glycoconjugates 20 mol% of the active acrylate groups were replaced with trisaccharide antigens, equal immobilization level (1 ng/mm^2) of 30 and 1000 kDa glycoconjugates resulted in equal loading of the chips with blood group A or B trisaccharide antigens. Three clones of monoclonal anti-A antibodies and three different samples of plasma type B (polyclonal anti-A antibodies) were injected over immobilized antigens on control and test surfaces to measure maximum antibody removal capacity of each surface. The nonspecific binding level of monoclonal antibodies on the control surfaces (Btri-PAA^{30}-biotin and Btri-PAA^{1000}-biotin) was less than 10% of their binding level on all test surfaces. To obtain the net binding levels, the nonspecific binding levels on control surfaces were subtracted from the binding levels on test surfaces. **Figure 3-2** shows the net amounts of three clones of monoclonal anti-A antibodies binding to immobilized conjugates (Atri-PAA^{30}-biotin or Atri-PAA^{1000}-biotin). Atri-PAA^{1000}-biotin showed greater capacity for

monoclonal antibody removal compared to Atri-PAA^{30}-biotin. The percentage of increase in capacity was significant ($P<0.05$), but different between the three clones of antibodies (60% for A16, 30% for Anti-A series1 and 15% for F98 7C6-4).

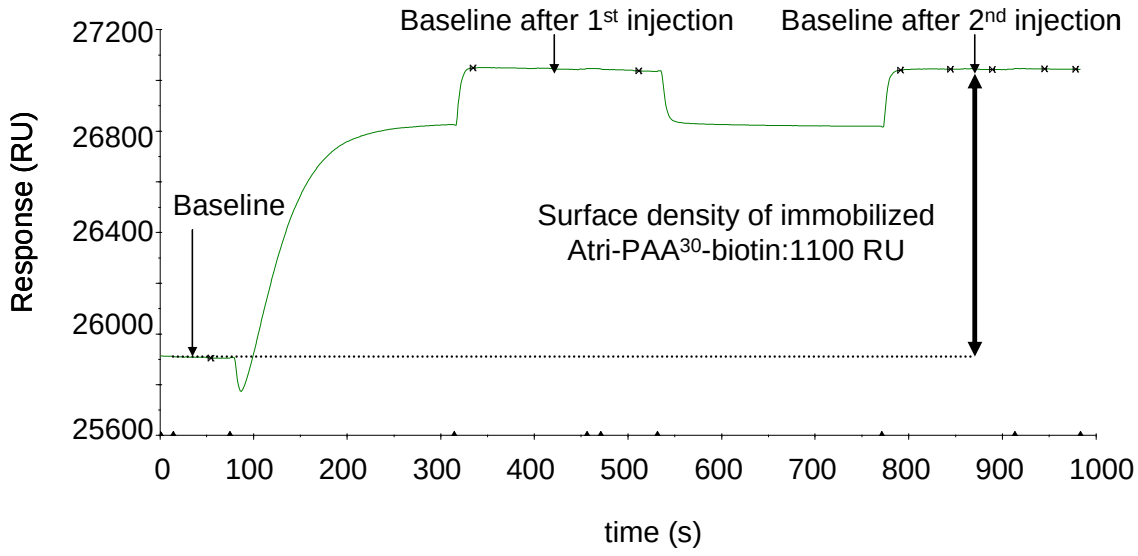

Figure 3-1: **Immobilization of Atri-PAA^{30}-biotin on streptavidin-coated sensor chips.**

Figure 3-3 shows the removal capacity of different surfaces in interactions with anti-A antibodies present in three plasma samples of type B donors. Anti-A antibody binding levels to Atri-PAA^{1000}-biotin increased by 150% for two of the plasma samples (#1 and #3) and by 88% for sample (#2) compared to their binding level on Atri-PAA^{30}-biotin. Average nonspecific binding levels of plasma antibodies to control surfaces were 50% and 24% of their specific

binding to test surfaces containing immobilized Atri-PAA^{30}-biotin and Atri-PAA^{1000}-biotin, respectively. Antibodies in all three plasma samples showed equal binding levels to both Btri-PAA^{1000}-biotin and Btri-PAA^{30}-biotin. Thus, increase in the size of the PAA linker did not increase the nonspecific binding on surface. Additionally, there was no difference in the nonspecific binding levels to Btri-PAA^{1000}-biotin, Btri-PAA^{30}-biotin or PAA^{1000}-biotin.

3.2.2 Effect of the Carbohydrate Content on Antibody Removal Capacity of Glycopolymers

We hypothesized that in polyacrylamide glycoconjugates such as Atri-PAA-biotin, the space between the carbohydrate residues is not fixed. A randomly coiled flexible polyacrylamide backbone could provide multivalent binding with antibodies by adjusting the spacing between copies of A- trisaccharides. Based on this hypothesis, an increase in carbohydrate content of Atri-PAA^{1000}-biotin from 20 mol % to 50 mol % could affect the antibody removal capacity of glycopolymers by changing their flexibility. To check this hypothesis, Atri-PAA^{1000}-biot with 20 mol % and 50 mol % of blood group A- trisaccharide content were synthesized. We did not observe a significant difference in antibody removal capacity of Atri-PAA^{1000}-biot with 20 or 50 mol % A-trisaccharide content **(Figure 3-4)**. Any further increase in the A-trisaccharide content is unlikely to improve the binding capacity of surface, possibly due to an increase in the steric hindrance between the binding antibodies when PAA becomes too closely populated with conjugated A-trisaccharides.

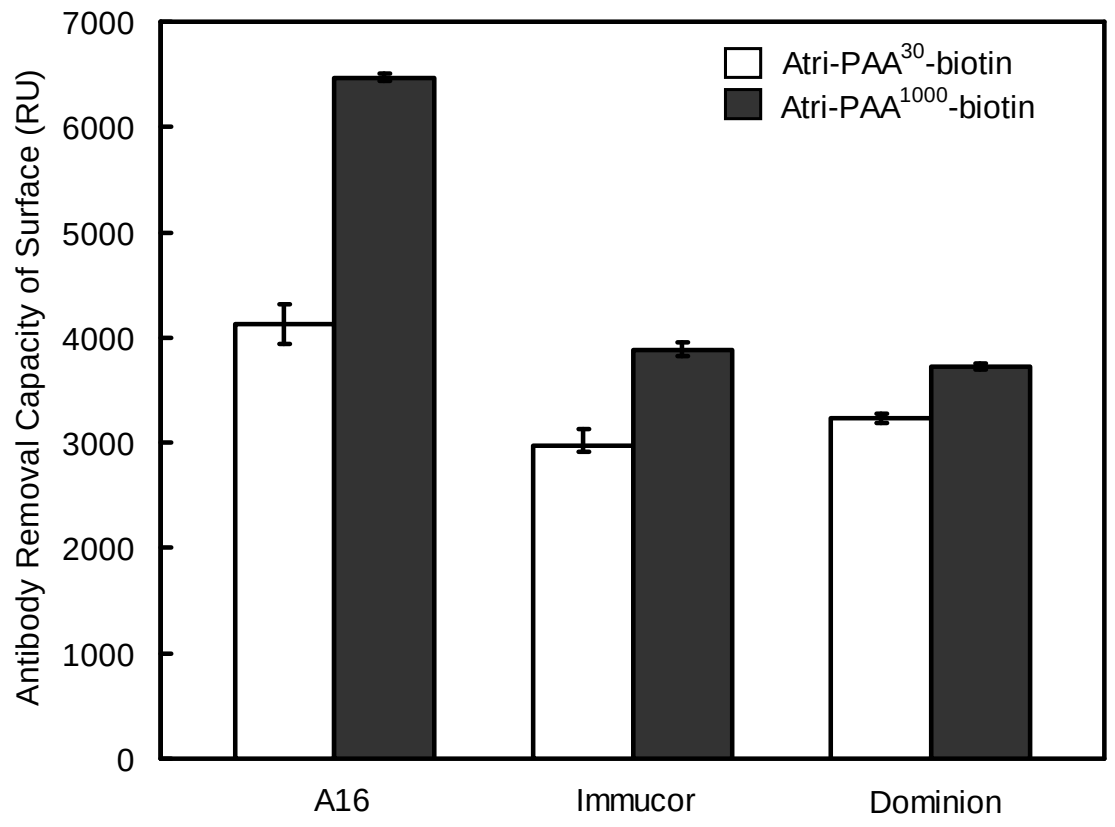

Figure 3-2: Antibody removal capacity of glycopolymer immobilized surfaces. Low (Atri-PAA^{30}-biot) and high (Atri-PAA^{1000}-biot) molecular weight glycopolymers were deposited on streptavidin-coated sensor chips at the loading density of 1 ng/mm^2. Three clones of IgM anti-A antibodies (A16, Immucor and Dominion) were injected over glycopolymer immobilized surfaces until equilibrium was reached. The nonspecific binding levels on control surfaces were subtracted from the binding levels on test surfaces. The amount of bound antibodies per unit surface area was measured in resonance units (1000 RU~ 1 ng/mm^2).

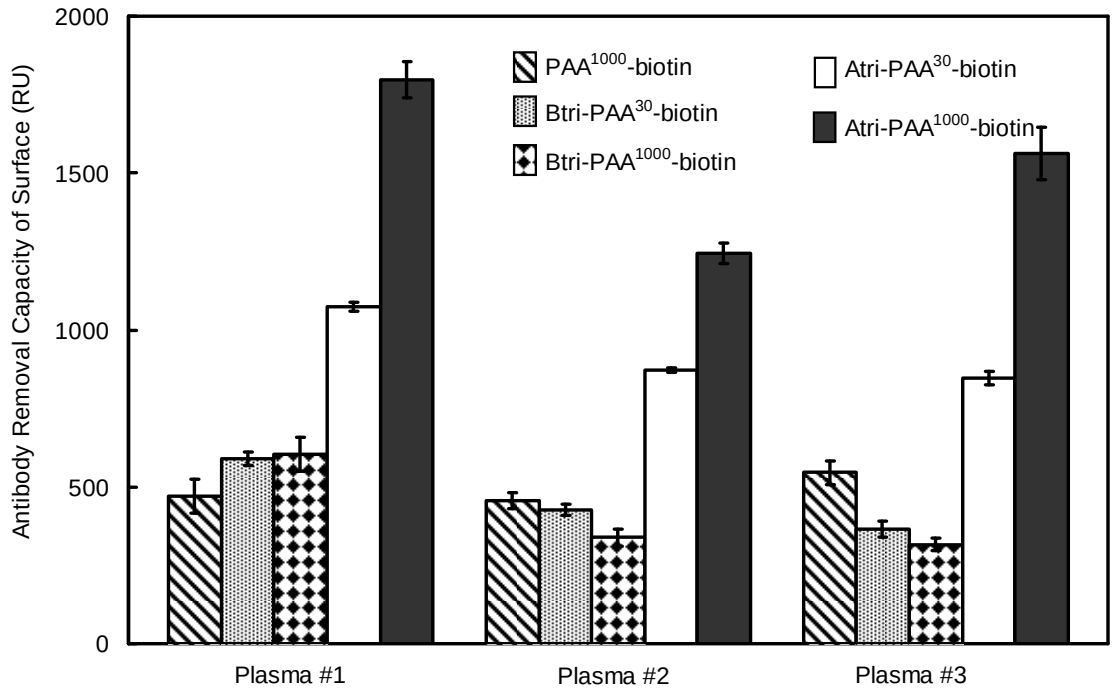

Figure 3-3: Antibody removal capacity of glycopolymer immobilized surfaces (Atri-PAA^{30}-biot and Atri-PAA^{1000}-biot) in their interactions with polyclonal anti-A antibodies. Analogous glycoconjugates containing B antigens (Btri-PAA^{30}-biotin and Btri-PAA^{1000}-biotin) and the polymer without carbohydrate residues (PAA^{1000}-biotin) were used as controls. Anti-A antibody titer in plasma samples #1, #2 and #3 were 32, 16 and 16, respectively.

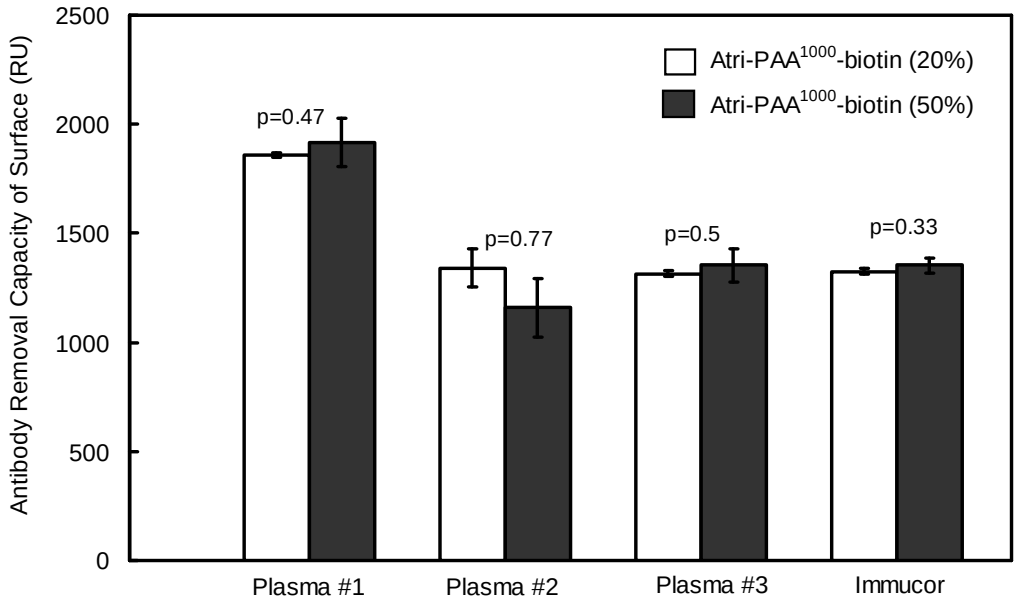

Figure 3-4: Effect of the carbohydrate content on antibody removal capacity of glycopolymer immobilized surfaces. Atri-PAA^{1000}-biot molecules with 20% or 50% A-trisaccharide content were deposited on streptavidin-coated sensor chips. Three plasma samples and a sample of monoclonal IgM anti-A antibodies (Immucor) were injected over glycopolymer immobilized surfaces until equilibrium was reached. Anti-A antibody titer in plasma samples #2 and #3 and Immucor antibodies were 16 and in plasma sample #1 the antibody titer was 32.

3.2.3 Binding Kinetics of Anti-A Antibodies to High Molecular Weight Glycopolymers

We chose Atri-PAA^{1000}-biot as the candidate synthetic A antigen because it enhanced antibody binding capacity of surface by two to three fold compared to the surfaces equally immobilized with Atri-PAA^{30}-biot. We then measured the kinetics of binding between Atri-PAA^{1000}-biot and monoclonal anti-A antibodies. Atri-PAA^{1000}-biot and Btri-PAA^{1000}-biot were immobilized on test and control flow cells of SA sensor chips at loading levels of 0.046 and 0.056 ng/mm^2, respectively. **Figure 3-5** shows net binding curves during double injections of A-16 antibodies (with concentrations ranging between 0.01 and 1.22 n*M*) over Atri-PAA^{1000}-biot at 25 ^{o}C. Net binding curves were obtained by subtracting response levels on control flow cells form response levels on test flow cells. Our regeneration protocol resulted in complete surface regeneration after each cycle. Repeated injection of antibodies at each concentration following surface regeneration resulted in reproducible antibody binding levels, indicating that immobilized Atri-PAA^{1000}-biot were stable on test surfaces throughout the experiment. The net binding curves were analyzed in terms of the kinetic model described in section (3.1.10). Initially first order rate constants (k_s) were obtained as the slope of the plots after regression of dR/dt against R, according to equation **(3-3)**, during the association phase **(Figure 3-6)**. Subsequently, association rate constants (k_a) for each set of monoclonal antibody-Atri conjugate interaction were obtained from equation **(3-4)** as the slope of the plots by linear regression of k_s against C **(Figure 3-7).** There was good agreement between our experimental data during the association phase and the fitting curves generated based on the 1:1 interaction model (R^2>0.96 for all fits). To obtain dissociation rate constants, response levels from the dissociation phase were transformed into a plot of $\ln(R_o/R)$ versus time, see equation **(3-6)**. **Figure 3-8** shows a transformed dissociation

phase during 10 minutes dissociation time for A-16 antibodies. The dissociation phase demonstrated two stages, with faster antibody release occurring during the initial stage. This data deviated from the 1:1 interaction model, most likely due to bivalent or multivalent binding of a fraction of the binding IgM antibody population. Due to the comparable sizes of IgM and high molecular weight glycoconjugates, multivalent binding interaction between IgM antibodies and

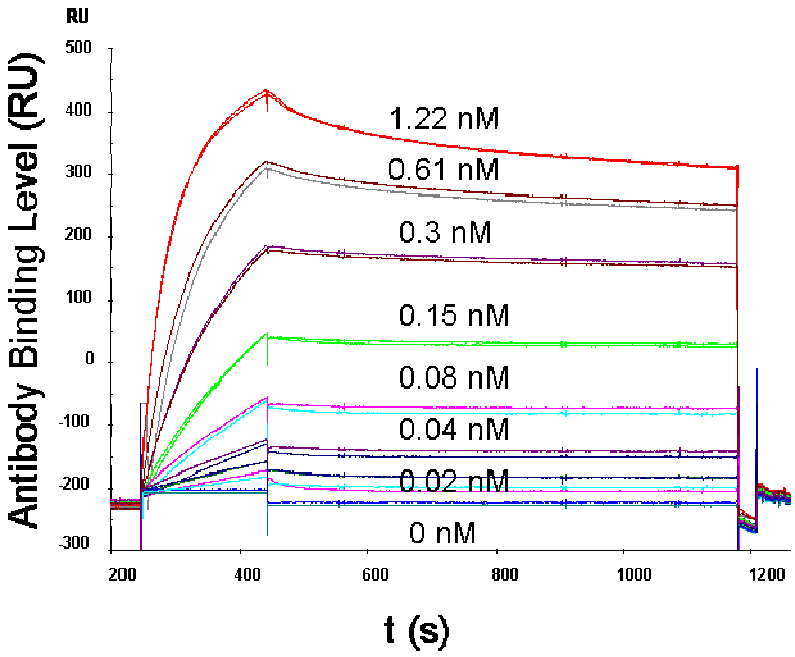

Figure 3-5: Real time plot of monoclonal anti-A antibody (A16) binding level on Atri-PAA^{1000}-biot immobilized surface.

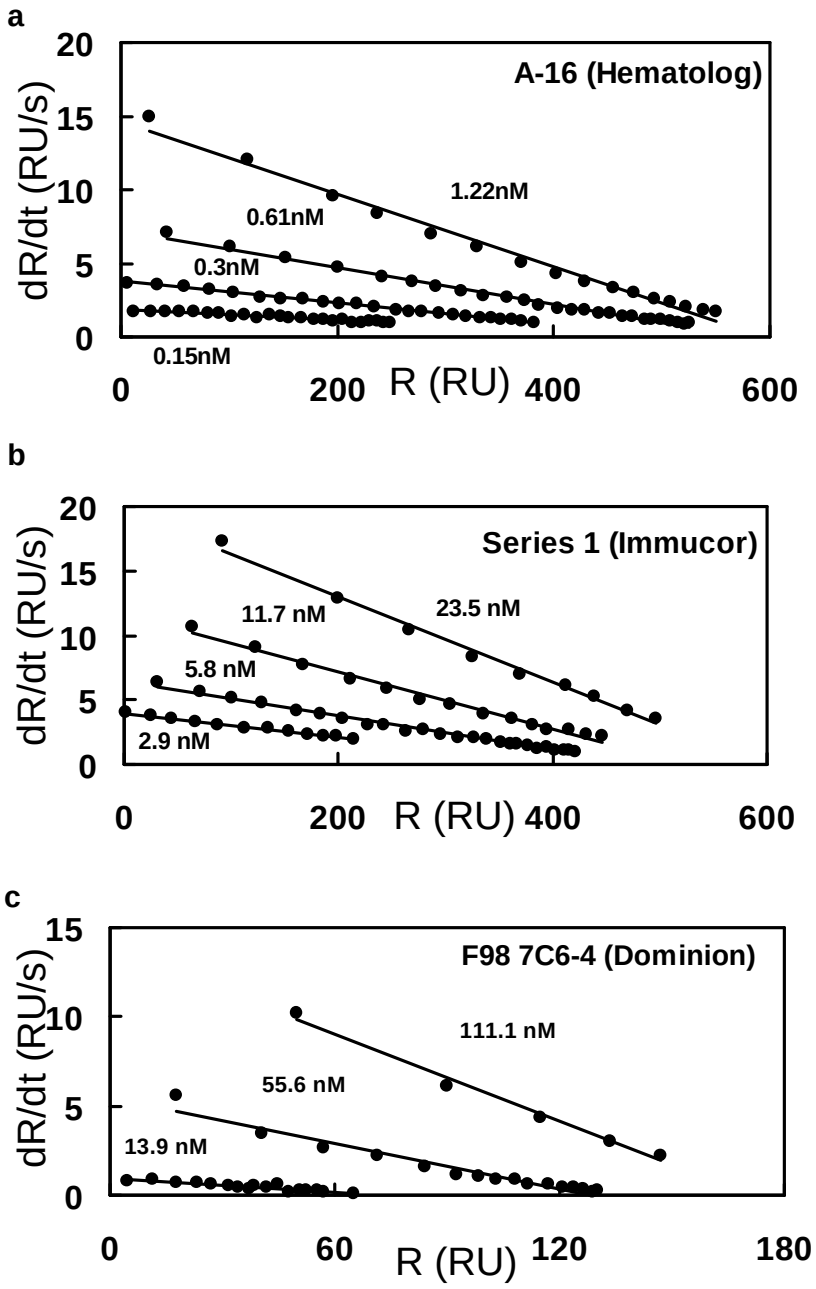

Figure 3-6: Plots of dR/dt versus R for three sets of monoclonal anti-A antibodies binding to immobilized Atri-PAA^{1000}-biot. a: A-16 (Hematological Center) , b: Series1 (Immucor) c: F98 7C6-4 (Dominion).

Atri-PAA^{1000}-biot is expected. To minimize these effects in our analysis, we adopted the method explained by Morton et al. [123] and utilized only the initial stage of dissociation data in our analysis **(Figures 3-8 and 3-9)**. This method excludes the population of antibodies that show smaller dissociation rate constants due to multivalent binding to immobilized A-trisaccharides. The initial dissociation time range in each case was arbitrarily chosen from t=0 to the time point at which ln (Ro/R) reached 40% of its equilibrium value (**Figure 3-8**). The coefficient of determination (R^2) for linear regression of ln (Ro/R) versus time during the initial dissociation phase was greater than 0.96 in all cases. **Table 3-1** summarizes the association and dissociation rate constants obtained for the three clones of anti-A antibodies.

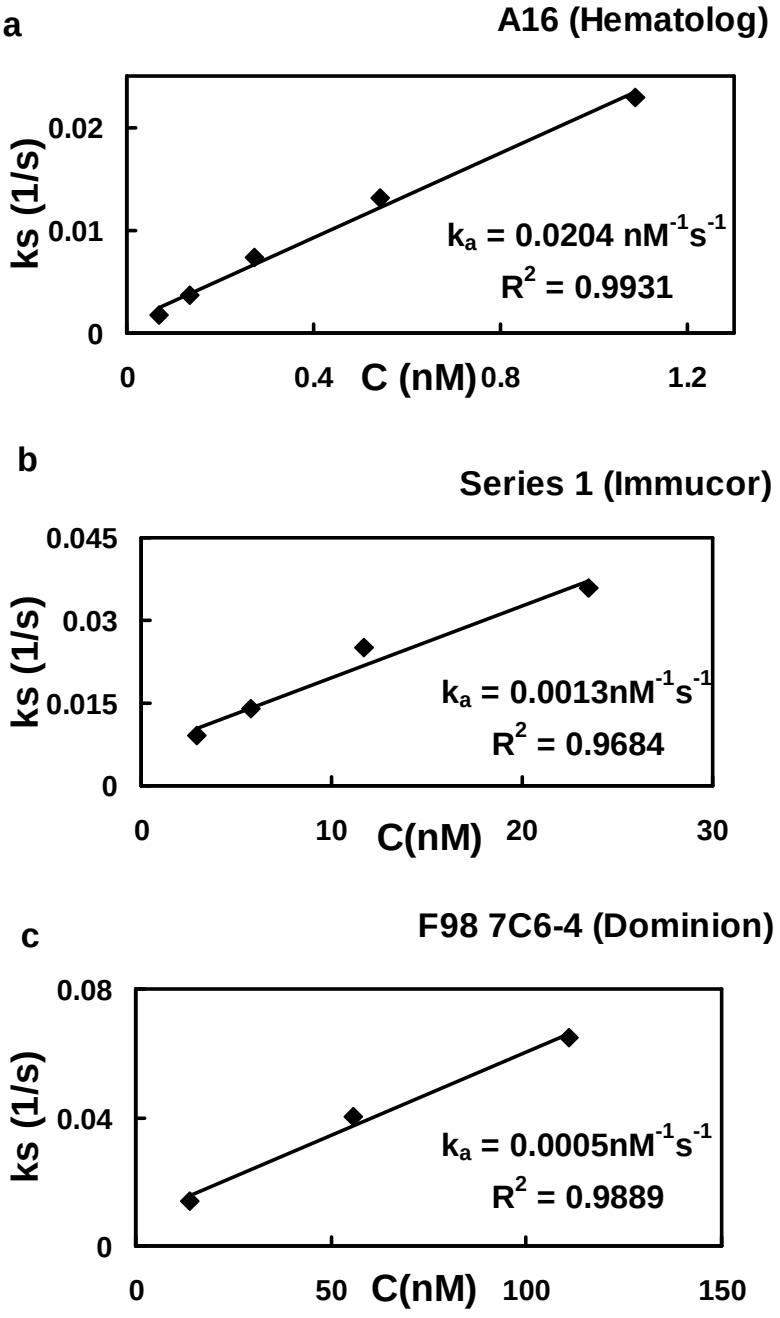

Figure 3-7: Plot of the pseudo first order rate constant (k_s) versus monoclonal antibody concentration (C) for a: **A-16 (Hematolog),** b: **Series1 (Immucor),** c: **F98 7C6-4 (Dominion).**

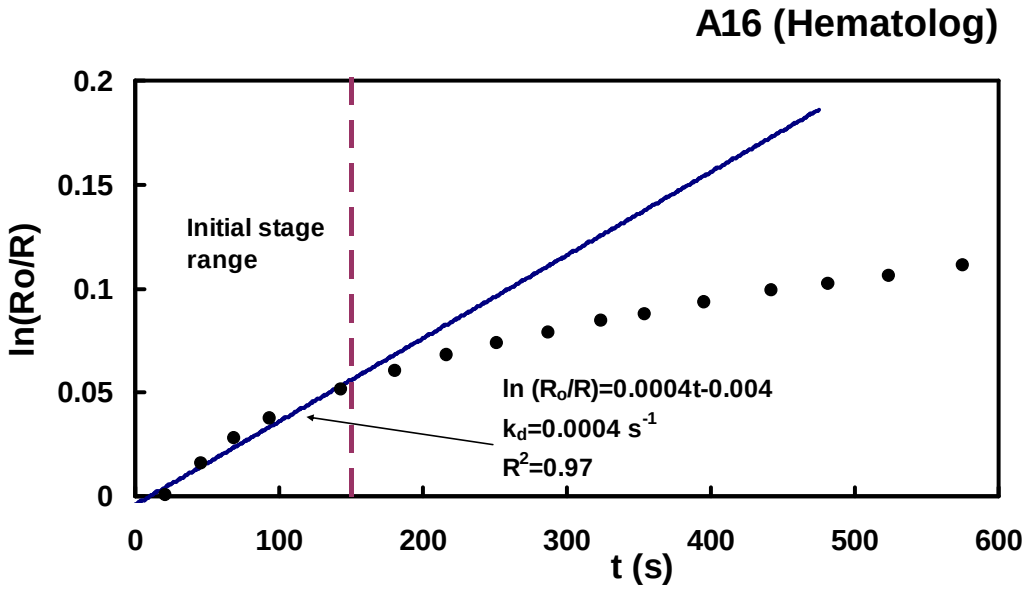

Figure 3-8: Plot of ln (R_o/R) versus time demonstrates two stages of dissociation phase with faster antibody release occurring during the initial stage. R and R_o represent the antibody binding level on surface at any time point (t) and at the beginning of the dissociation phase, respectively. The plot shows the dissociation phase following injection of A16 monoclonal antibodies, at a concentration of 0.0055 nM.

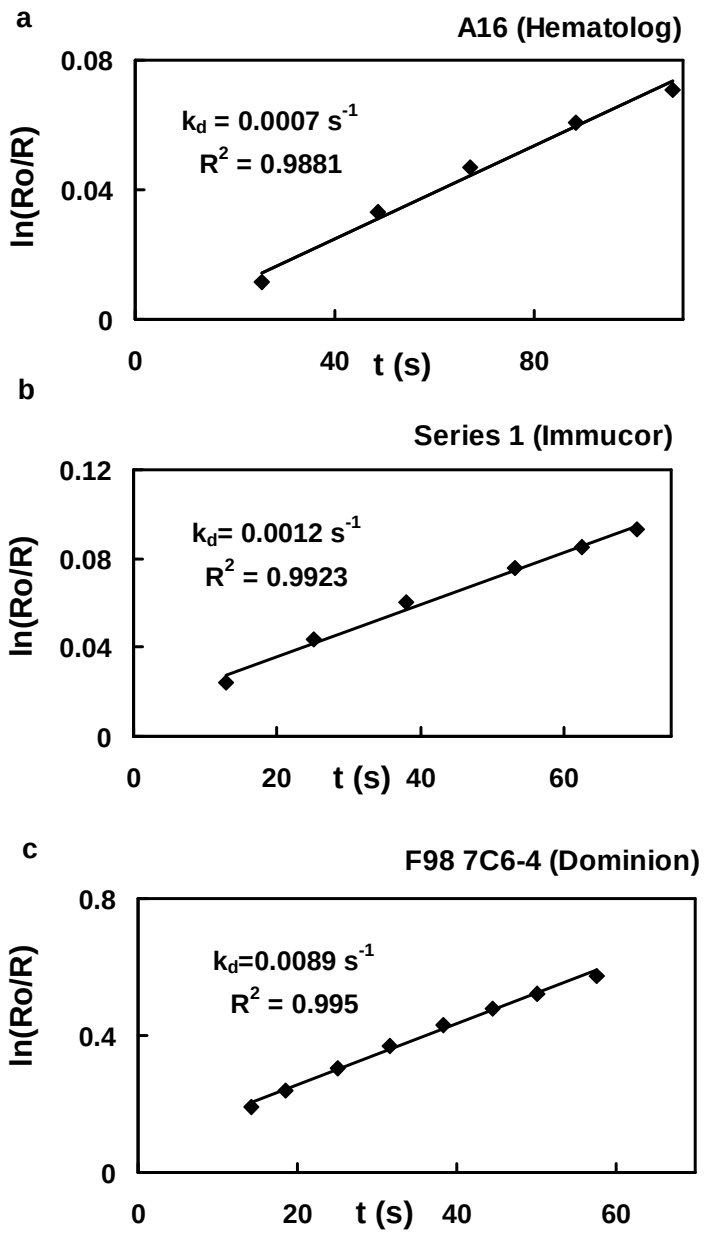

Figure 3-9: Measurement of dissociation constant for binding interactions between a: **A-16 (Hematolog),** b: **Series1 (Immucor),** c: **F98 7C6-4 (Dominion). antibodies and Atri-PAA^{1000}-biot immobilized surface. The slope of the plot corresponds to the dissociation constant, k_d.**

Table 3-1: Kinetic and equilibrium affinity constants for binding interactions between three clones of IgM anti-A and Atri-PAA^{1000}-biot.

Antibody Clone/ Source	k_a ($M^{-1}s^{-1}$)	k_d (s^{-1})	K_D (M)	$Da = (\frac{k_a C_s^i a}{D})$
A-16 (Hematological Center)	$(1.8\pm0.1)\times10^{7}$	$(3.8\pm2.2)\times10^{-4}$	2.1×10^{-11}	785
Series1 (Immucor)	$(1.2\pm0.2)\times10^{6}$	$(1.4\pm0.7)\times10^{-3}$	1.2×10^{-9}	52
F98 7C6-4 (Dominion)	$(5.2\pm1.2)\times10^{5}$	$(6.4\pm3.7)\times10^{-3}$	1.2×10^{-8}	23

3.3 DISCUSSION

Polymer beads or hollow fiber membranes on which synthetic antigenic determinants of A and B blood groups are immobilized have been previously used for specific removal of anti-A or anti-B antibodies [24-25, 32]. Membranes are associated with less pressure drop, faster flow rates, and less diffusion limitations than packed beds of porous beads [34] making them the more attractive option as support matrices in hemoperfusion systems. However, lower removal capacity due to limited surface area for ligand immobilization is a major obstacle in membrane adsorption

techniques. Affinity and accessibility of small haptens (such as blood group A and B trisaccharides) for target binding molecules (such as anti-A and anti-B antibodies) could be greatly enhanced by using a flexible spacer in linking the small molecule to the support matrix. Flexible spacers increase lateral mobility of immobilized haptens and facilitate the binding interaction. The use of spacers is even more crucial when hollow fibers are used as support matrices because of their limited surface area for ligand immobilization. Polymeric spacers such as polyethylene glycol (PEG), poly-L-Lysine (PLL) and polyacrylamide (PAA) have been previously proposed as linkers to enhance binding affinity and removal capacity of immobilized ligands. Synthetic A and B antigens have been used both with relatively short aliphatic chains (6-17 carbon atoms in length) as in Synsorb® and Glycosorb® columns or with longer multivalent PAA spacers (30-50 kDa). Nevertheless, limited antibody binding capacity is still the major challenge especially with hollow fiber based antibody removal devices (92). In this work, we conjugated 1000 kDa PAA spacers to synthetic blood group A-trisaccharide antigens and compared their anti-A removal capacity with the previously used 30 kDa glycoconjugates [32]. The increase in the size of PAA conjugates resulted in two to three fold increase in removal capacity per unit surface area. With this estimated increase in capacity, a hollow fiber based antibody removal device (such as the SAF device) with a surface area of about 1.5 to 2 m^2 would provide sufficient capacity for 100% antibody capture from blood in a single device.

Few studies have been performed to evaluate the effect of the size of PAA on affinity and removal capacity. Shilova et al. [121] observed no difference in the anti-B antibody binding levels on to low (30-50 kDa) or high (1000-2000 kDa) molecular weight Btri-PAA glycoconjugates physically adsorbed on ELISA plates. However, high molecular weight Btri-PAA conjugates inhibited type B erythrocyte agglutination at a 100 times lower concentration

than low molecular weight Btri-PAA in the solution phase reaction [121]. We hypothesized that PAA glycoconjugates immobilized on streptavidin covered surfaces are presented in two ways. In one scenario, Atri-PAA-biotin molecules are coupled to surface by all of their biotin residues thereby adopting the "stretched" conformation **(Figure 3-10-a)**. This conformation reduces mobility of the polymer backbone and interferes with interaction of the glycoconjugates with antibodies. In the stretched conformation antibodies will interact equally with Atri-PAA-biotin glycopolymers regardless of their molecular weight. In the second situation, Atri-PAA-biotin polymers bind to the surface by one or a few biotin molecules, and the glycopolymers keep their conformation close to a random coil **(Figure 3-10-b)**. The diameter of Atri-PAA^{1000}-biotin and Atri-PAA^{30}-biotin molecules in the random coil conformation is estimated to be 500-600 Å and 90 Å, respectively [120]. IgM antibodies (about 300-400 Å) are comparable in size to Atri-PAA^{1000}-biotin and are therefore capable of binding to most of the immobilized glycopolymer molecules, whereas the size of IgM antibodies does not allow binding of them to each of immobilized Atri-PAA^{30}-biotin molecules **(Figure 3-10-b)**. Our results agreed well with the second mechanism, i.e. high molecular weight glycoconjugates provided better accessibility of blood group A-trisaccharides for antibody binding. The second mechanism could also explain the earlier observed difference between antibody binding levels to glycoconjugates of different molecular weights in the solution phase [121].

We measured the kinetics of interaction between our candidate glycoconjugates (Atri-PAA^{1000}-biotin) and anti-A antibodies to show that conjugation of synthetic A-trisaccharides to polyacrylamide spacers and immobilization of the conjugates on surfaces did not adversely interfere with A-trisaccharide-anti-A antibody binding interactions. Association rate constants ranging between 10^3 and 10^7 $M^{-1}s^{-1}$ and dissociation rate constants ranging between 10^{-6} and 10^{-2}

s^{-1} have been previously reported for interactions between various pairs of monoclonal antibodies and their specific antigens [124], [125], [126], [127], [112, 128]. The kinetic and affinity constants calculated in this study fall within the range of antibody-antigen interaction kinetic constants, with a trend towards higher affinity interactions.

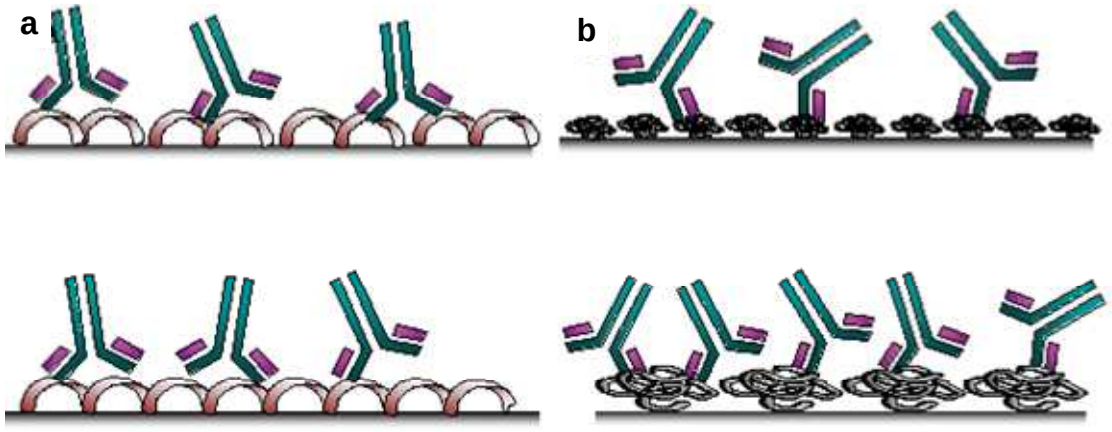

Figure 3-10: Two hypothetical presentations of immobilized glycopolymers on surface. a: Atri-PAA-biotin polymers are coupled to surface by all of their biotin residues thereby adopting the "stretched" conformation. b: Atri-PAA-biotin polymers bind to the surface by one or a few biotin molecules, and the glycopolymers keep their conformation close to random coil.

Two different levels of antigen loading on SA sensor chips were used in our studies. For our kinetic analysis, we attempted to immobilize the minimum amount of Atri-PAA^{1000}-biot (0.046 ng/mm^2) on SA sensor chips to minimize the effect of mass transfer on the kinetic analysis [122],[129],[130],[131]. The low loading level of antigens also minimizes crowding of antigens on the surface and as a result, multivalent interactions between binding IgM antibodies and immobilized antigens are minimized. This behavior was ideal for quantification of the kinetics of interaction between single antibody binding sites (Fab) and immobilized Atri-PAA^{1000}-biot. However, to mimic the real application in SAF when measuring the binding capacity of surface, antigens needed to be immobilized on the surface at their maximum loading capacity (1 ng/mm^2). This ensured that the steric effects in interactions between immobilized glycoconjugates and antibodies were similar in our experimental set up and in the real application.

We previously developed a mathematical model capable of predicting the dependence of antibody removal rate on key design parameters in our proposed SAF devices [33],[32]. This mathematical model established that maximum antibody removal rate could only be achieved in SAF devices under a diffusion limited antibody transport regime. In other words, optimum capture rate occurs only when antibody removal becomes independent of antibody-antigen reaction rates. The dimensionless Damkohler number (*Da*) defined as ($Da = \frac{k_a C_s^i a}{D}$) was used to determine the conditions needed for antibody transport to occur in a diffusion-limited regime. Based on this model a *Da* number of 10 or greater was required to achieve maximum antibody removal rate in the proposed SAF design. Both the surface binding capacity (C_s^i) and the intrinsic association rate constant (k_a) for antibody-antigen interaction are required for

calculation of *Da* and an assessment of our design of antibody filters. The intrinsic association constants (k_a) were directly measured for three sets of monoclonal anti-A antibodies and were found to be 18, 1.2 and 0.52 cm^3/nmol.s for clones A16, series 1 and F98 7C6-4. The magnitude of *Da* was then calculated for each set of monoclonal antibodies binding to Atri-PAA^{1000}-biot assuming a surface capacity (C_s^i) of 0.0017 nmol/cm2 (twice the surface capacity measured previously for Atri-PAA^{30}-biot by Gautam et al. [32]). The antibody diffusivity coefficient (D) was assumed to be 3.9×10^{-7} cm^2/s and the fiber inner radius (a) was 0.01 cm. The value of *Da* for each monoclonal antibody is listed in **Table 3-1**. Values of *Da* for all three antibody clones were greater than 10, supporting the hypothesis that antibody removal rate becomes diffusion limited and independent of the specific affinity for antibody-antigen interaction in an Atri-PAA^{1000}-biotin-immobilized hollow fiber based antibody removal device.

Further experimental work is required to establish the bioactivity and biocompatibility of Atri-PAA^{1000}-biotin in antibody capture from whole blood in the SAF device. Rieben et al. previously characterized the biocompatibility of Atri-PAA^{30} immobilized on porous particles in their interaction with plasma antibodies [24]. Hout et al. described the feasibility of antibody capture from whole blood in an earlier-generation SAF device with Neutr-AB®, an animal based A and B glycoprotein antigen, immobilized on inner lumens of the hollow fibers [31]. We propose that the custom-made high molecular weight glycopolymer we have presented is a promising synthetic A antigen for construction of anti-A immunoadsorption devices. A SAF device which incorporates these high molecular weight glycoconjugates as synthetic A antigens may aid in meeting the target anti-A antibody titer reduction of three to four titer steps.

4.0 DEVELOPMENT OF A SIMPLE MATHEMATICAL MODEL OF ANTI-A/B ANTIBODY CAPTURE IN INTEGRATED BEAD AND FIBER ANTIBODY FILTERS

In Chapter 2.0, we discussed development of our previous prototype antibody filtering devices (SAF), in which synthetic A-trisaccharide (Atri) antigens conjugated to low molecular weight (30-50 kDa) poly-N hydroxyethylacrylamide (PAA) spacers were immobilized on the luminal surfaces of dialyzer fibers potted into modules [32]. As we also discussed in Chapter 2.0, initial evaluation of anti-A antibody removal capacity and capture rate in appropriately scaled down SAF devices indicated that a 5 to 6-fold increase in removal capacity per unit surface area of the modules was required to achieve 100% antibody removal in a clinically relevant time scale [32]. In Chapter 3.0, we showed that by using high molecular weight (1000-2000 kDa) polyacrylamide glycoconjugates as the immunoadsorbent material in SAF devices, antibody removal capacity per unit surface area could be increased by 2-3 fold. We concluded that by immobilizing high molecular weight glycoconjugates on the luminal surface of SAF fibers, we would achieve a target anti-A antibody titer reduction of three to four titer steps in each device. However, so far we have faced a number of difficulties in obtaining consistent immobilized antigen densities in SAF devices during immobilization of high molecular weight polyacrylamide glycoconjugates. While parallel efforts were ongoing in our team to improve antigen immobilization chemistry and further increase antibody removal capacity of SAF devices, we started developing a new antibody removal device, based on integrated

microfiltration fibers with antibody capturing beads uniformly distributed within the interstitial fiber space (BSAF device). Antibody removal in BSAF devices occurs by Starling recirculation flow of plasma between the fiber and bead-containing shell compartment in combination with antibody diffusing and binding within the shell-side porous beads. Similar to our SAF devices, the BSAF modules are compatible with whole blood perfusion and remove blood group antibodies in a one step process that does not require a separate plasmapheresis unit. Additionally, due to the vast surface area of the beads for antigen immobilization, antibody removal capacity of the BSAF modules is practically infinite, in relation to the range of anti-A/B antibody concentrations naturally found in blood.

In this chapter, we will describe development of a simple mathematical model to guide the choice of key design and operational parameters for a clinical BSAF device. The model demonstrates that for a given flow rate and reservoir volume, antibody removal rate in a BSAF depends on the magnitude of a lumped dimensionless parameter, $k_L m_B / Q_s$. This term characterizes the ratio of antibody uptake rate by the beads to the Starling flow rate in the device. Three distinct antibody removal regimes were observed with the following approximate boundaries: diffusion limited ($k_L m_B / Q_s \leq 1$), intermediate ($1 < k_L m_B / Q_s < 10$) and perfusion limited ($k_L m_B / Q_s \geq 10$). For a given BSAF geometry, fiber hydraulic permeability, reservoir volume and flow rate, the highest antibody removal rate is predicted for the perfusion limited regime, when $k_L m_B / Q_s \to 10$. The model also shows that once perfusion limited antibody removal rate in a BSAF device is obtained, further increase in antibody removal rate is possible,

solely by increasing the flow rate in the device. We validated the key predictions of the model in a series of in vitro monoclonal anti-A antibody capture studies in BSAF devices, packed with anti-A specific beads. Once validated, the model was used to conceptually design a BSAF device that would generate a clinically relevant rate of anti-A removal.

4.1 MODEL ANALYSIS

4.1.1 Model geometry

The BSAF system is modeled as a bundle of N identical cylindrical microfiltration hollow fibers of inner diameter, d_i , and length L. The fibers are equally spaced and fixed in a cylindrical housing of length L. A slurry of beads in buffer solution is recirculated through the interstitial space between the fibers. The bead recirculation loop serves solely to maintain a well-mixed and uniformly distributed bead slurry within the fiber interstitial space.

4.1.2 Quantification of Starling Flow

Starling flow is the flow of fluid out of the fiber into the shell side that returns back into the fibers [132-133]. Starling flow occurs due to a transmural pressure gradient between the two compartments. Assuming a constant pressure, P_s, in the shell side, a mass balance on a differential element Δz of any single fiber yields the governing mass transfer equation:

$$\frac{-dq}{dz} = K\pi d_i[P(z) - P_s] \qquad \textbf{(4-1)}$$

where $q(z)$ is the steady state flow rate inside a single fiber as a function of the axial position z, K is the hydraulic permeability of each fiber and $P(z)$ is the pressure in the fiber. The axial pressure gradient inside each hollow fiber is obtained assuming a fully developed laminar viscous flow [134]:

$$\frac{dP}{dz} = \frac{-128\mu}{\pi d_i^4} q(z) \qquad \textbf{(4-2)}$$

where, μ is the viscosity of the fluid.

Combining equations **(4-1)** and **(4-2)**, a governing differential equation for the flow through a fiber is obtained:

$$\frac{d^2q}{dz^2} - \beta^2 q(z) = 0 \qquad \textbf{(4-3)}$$

where, $\beta^2 = \frac{128\mu K}{d_i^3}$. There is no net ultrafiltration flow in the BSAF. Therefore, the boundary conditions for equation **(4-3)** are: $q(z=0) = q(z=L) = Q/N$, where Q is the flow rate in the device. The analytical solution to equation **(4-3)** with associated boundary conditions is:

$$q(z) = \frac{Q}{N}[\cosh(\beta z) + \frac{1-\cosh(\beta L)}{\sinh(\beta L)}\sinh(\beta z)] \quad \textbf{(4-4)}$$

The Starling flow, Q_s, is the integrated total flow out of the fibers to the shell side and is given by:

$$Q_s = Q - Nq(z = L/2) = Q[1-\cosh(\frac{\beta L}{2}) - \frac{1-\cosh(\beta L)}{\sinh(\beta L)}\sinh(\frac{\beta L}{2})] \quad \textbf{(4-5)}$$

4.1.3 Quantification of Antibody Capture Rate in BSAF

The shell compartment of the BSAF is modeled as a well-mixed slurry of beads. The inlet stream to the shell compartment is the Starling flow through the first half of the fibers, which has an antibody concentration, $C(t)$, equal to the concentration of antibodies in the inlet stream of the BSAF. The outlet stream from the shell compartment is the Starling flow back into the second half of the fibers with an antibody concentration, $C_s(t)$, which is obtained from an antibody mass balance in the shell compartment.

Assuming that BSAF devices have an infinite antibody adsorption capacity in relation to the maximum amount of antibodies in the reservoir (see section 4.3.1 for justification), the rate of antibody adsorption per unit mass of the beads is obtained from the following first order relation:

$$\frac{dR}{dt} = k_L C_s(t) \quad \textbf{(4-6)}$$

where, $R(t)$ is the amount of antibody adsorbed per unit mass of the beads as a function of time and k_L is a first order rate constant that accounts for antibody diffusion and adsorption into the beads.

Assuming a quasi steady state adsorption in the shell compartment, the governing equation for capture of antibodies in the shell is obtained from:

$$Q_s[C(t) - C_s(t)] = m_B \frac{dR}{dt} = m_B k_L C_s(t) \qquad \textbf{(4-7)}$$

where m_B is the mass of beads. This yields the following equation for $C_s(t)$:

$$C_s(t) = C(t)[\frac{Q_s}{Q_s + k_L m_B}] \qquad \textbf{(4-8)}$$

Our interest is to obtain an equation for the antibody concentration in the reservoir, $C(t)$. A mass balance for antibody in the fiber side yields: $V_R \frac{dC}{dt} = Q_s[C_s(t) - C(t)]$, where V_R is the volume of the reservoir. Using equation **(4-8)**, the antibody mass balance is :

$$\frac{dC}{dt} = \frac{-Q_s}{V_R}[1 - \frac{Q_s}{Q_s + k_L m_B}]C(t) \qquad \textbf{(4-9)}$$

Assuming an initial reservoir antibody concentration, C_i, this leads to the following analytical solution for $C(t)$:

$$C(t) = C_i \exp[\frac{-Q_s}{V_R}(1 - \frac{Q_s}{Q_s + k_L m_B})t] \quad \textbf{(4-10)}$$

4.2 MATERIALS AND METHODS

4.2.1 Preparation of Affinity Beads

All chemicals were obtained from Fisher Scientific (Pittsburgh, PA) unless specified. Specific determinant fragments of blood group A-trisaccharide antigen (Atri), GalNAcα1−3[Fucα1−2]Galβ−, and B-trisaccharide antigen (Btri), Galα1−3[Fucα1−2]Galβ−, conjugated to activated poly(4-nitrophenyl acrylate) of molecular weight 30 kDa ($pNPA^{30}$) were synthesized at Shemyakin and Ovchinnikov Institute of Bioorganic Chemistry (Russian Academy of Sciences, Moscow, Russia) as described previously [119], [120]. The synthesized polyacrylamide glycoconjugates contained 20 mol% of the A or B trisaccharides (Atri-$pNPA^{30}$ or Btri-$pNPA^{30}$).

Cyanogen bromide (CNBr) activated, cross linked Sepharose® CL-4B beads (Sigma-Aldrich, St. Louis, MO) were initially left to swell in cold (4°C) 1m*M* hydrochloric acid (HCl) for 30 minutes. The gel was then rinsed and transferred to an equal volume of 0.1 *M* sodium carbonate buffer (pH 9.6) containing 1*M* ethylenediamine. The reaction mixture was left at 22°C for 24 hours. The gel was then rinsed and suspended in an equal volume of 10% dimethyl

sulfoxide (DMSO) in 0.1 *M* sodium carbonate buffer (pH 9.6) containing 0.15 mg/ml of Atri-pNPA[30] or Btri-pNPA[30] . The reaction mixture was left at 22^{o}C for another 24 hours. Finally, to block the unreacted active acrylate sites, the gel was left in an equal volume of 10% DMSO in 0.1 *M* sodium carbonate buffer (pH 9.6) containing 10% 2-aminoethanol at 22^{o}C for 24 hours. The gel was then rinsed and suspended in an equal volume of cold (4 ^{o}C) 1.1 *M* sodium bicarbonate solution containing 5% acetic anhydride for 30 minutes to deactivate any remaining free amine groups. The resin was thoroughly rinsed with water and stored in phosphate buffered saline (PBS) (pH 7.4) at 2-8 ^{o}C.

Cross linked Sepharose® CL-6B beads (Sigma-Aldrich, Louis, MO) were not available in already activated form and were activated using a standard CNBr activation chemistry [135]. Briefly, the gel was suspended in an equal volume of distilled water. CNBr (Sigma-Aldrich, St. Louis, MO) was added to the gel suspension (0.2 g/ml) and the pH of the reaction mixture was kept at 11.0 by dropwise addition of 10*N* sodium hydroxide (NaOH) while maintaining the temperature of the reaction at 23-25 ^{o}C. This reaction proceeded for approximately 15 minutes until the pH stabilized. The gel was quickly washed with ice cold water and ice cold 0.1*M* sodium bicarbonate buffer (pH 9.6). The gel was then aminated and modified using the same protocol as described above for the CL-4B beads.

4.2.2 Determining Adsorption Capacity and Antibody Uptake Kinetics within Modified Beads

One ml polypropylene Rezorian cartridges (Supelco**,** St Louis**,** Mo) equipped with luer plugs, caps and polyethylene frits were packed with 0.2 g of CL-4B or CL-6B beads on which synthetic A or B antigens were immobilized, as previously described. The packed columns were initially

primed with 5 ml of PBS buffer containing 0.05% Tween (PBS/0.05% Tween). Antibody solution was prepared by diluting murine monoclonal anti-A IgM antibodies (Anti-A series1, Immucor Inc., Norcross, GA, USA) in PBS/0.05% Tween to the final concentration of 15 μg/ml. Various volumes (3 to 20 ml) of the antibody solution were then recirculated through the columns at two different flow rates, 0.5 and 1.5 ml/min, for 90 minutes to ensure that antibody uptake kinetics were not dependent on flow rate. Small samples (10 μl) were taken from the reservoir at time points: 0, 5, 10, 15, 30, 60 and 90 minutes. The concentration of antibodies in the reservoir were determined by enzyme-linked immunosorbent assay (ELISA) as described previously [116] Antibody removal capacity of the beads was calculated from the difference between the antibody concentrations of reservoir in the beginning and in the end of capture experiment for those columns in which the beads reached their saturation limit.

The first order rate constant, k_L, was determined by analyzing antibody removal by packed bead columns, through which 3 ml of antibody solution was recirculated at two flow rates of 0.5 and 1.5 ml/min. Assuming that the local rate of antibody removal in the packed bead column is governed by equation **(4-6)**, the governing differential equation for the axial variation of antibody concentration in the packed bead column is:

$$\frac{-dC_c}{dz} = \frac{m_B k_L}{L_c Q_c} C_c(z) \qquad \textbf{(4-11)}$$

where $C_c(z)$ is the pseudo steady state concentration of antibodies in the liquid phase as a function of the axial position z within the column, L_c is the length of the column and Q_c is the

flow rate within the column. Integrating equation **(4-11)** over the length L_c of the column, the antibody concentration in the outlet stream is:

$$C_{cL}(t) = C(t)\exp(\frac{-m_B k_L}{Q_c}) \qquad \textbf{(4-12)}$$

where $C(t)$ is the concentration of antibodies in the reservoir as a function of time. Combining equation **(4-12)** with an antibody mass balance in the reservoir: $V_R \frac{dC}{dt} = Q_c[C_{cL}(t) - C\ (t)]$, and integrating with respect to time yields:

$$C(t) = C_i \exp\{\frac{-Q_c}{V_R}[1 - \exp(\frac{-m_B k_L}{Q_c})]t\} \qquad \textbf{(4-13)}$$

The reservoir antibody concentration, $C(t)$, measured at time points: 0, 5, 10 and 15 minutes was fit to equation **(4-13)** using the "nlinfit" function in Matlab (Matlab 7.0, The MathWorks, Inc., Natick, MA) to determine the first order rate adsorption constant, k_L.

4.2.3 Fabrication of the BSAF Modules

A polycarbonate tube (K-mac Plastics, Wyoming, MI) of 25 cm length, 0.635 cm inner diameter and 1.27 cm outer diameter was used as the shell case of our BSAF module. Two circular holes (0.5 mm) were placed in the outer surface of the case at 1 cm from each end of the module and

two polycarbonate female luer fittings (Value Plastics, Fort Collins, CO) were glued to each hole using UV light curing (DYMAX, Torrington, CT). Twenty polyethersulfone microfiltration hollow fiber membranes (MicroPES®, Membrana GmbH, Wuppertal, Germany) of 0.03 cm inner diameter and 0.01 cm wall thickness were aligned and placed in the center of the polycarbonate housing in a manner to leave approximately 3 cm protruding from each end of the housing. The ends were filled with hot glue, and the excess glue was tomed with a razor blade once hardened. Polycarbonate caps with luer fittings were fabricated and attached to both ends of the devices using UV light curing adhesive.

4.2.4 Measurement of Hydraulic Permeability of Fibers

Figure 4-1-a shows a schematic of the experimental set up for measurement of hydraulic permeability of fibers. Distilled water was pumped into the modules with the outlet of the device sealed to force ultrafiltration flow into the shell side. Inlet pressure in the fiber compartment, P_o, and the pressure in the shell compartment, P_s, were measured at various flow rates, Q. Using the appropriate boundary conditions for the described experimental set up: $q(z=0)=Q/N, q(z=L)=0$, the Q versus $P_o - P_s$ is derived from equation **(4-1)**:

$$Q = \frac{NK\pi d_i \sinh(\beta L)}{\beta \cosh(\beta L)}(P_o - P_s) \qquad \textbf{(4-14)}$$

where $\beta^2 = \frac{128\mu K}{d_i^3}$. Assuming $\mu = 1.25\times10^{-7}$ mm - Hg.min, hydraulic permeability, K, was calculated from the inverse slope of the plot of $P_o - P_s$ versus Q using an Excel solver tool (Microsoft® Office Excel 2003, Redmond, WA).

4.2.5 Model Validation Experiments

The model was validated by performing three different types of experiments. First, we compared antibody capture rates in BSAF devices loaded with equal mass (1.5 g) of either CL-4B or CL-6B beads to test whether the model could predict changes in antibody removal rate due to changes in the first order rate constant of the beads, k_L. The second set of experiments explored the effect of change in mass of beads of a given k_L on antibody adsorption rate by comparing antibody removal rates in BSAF devices loaded with either 1.5 g or 3 g of the same

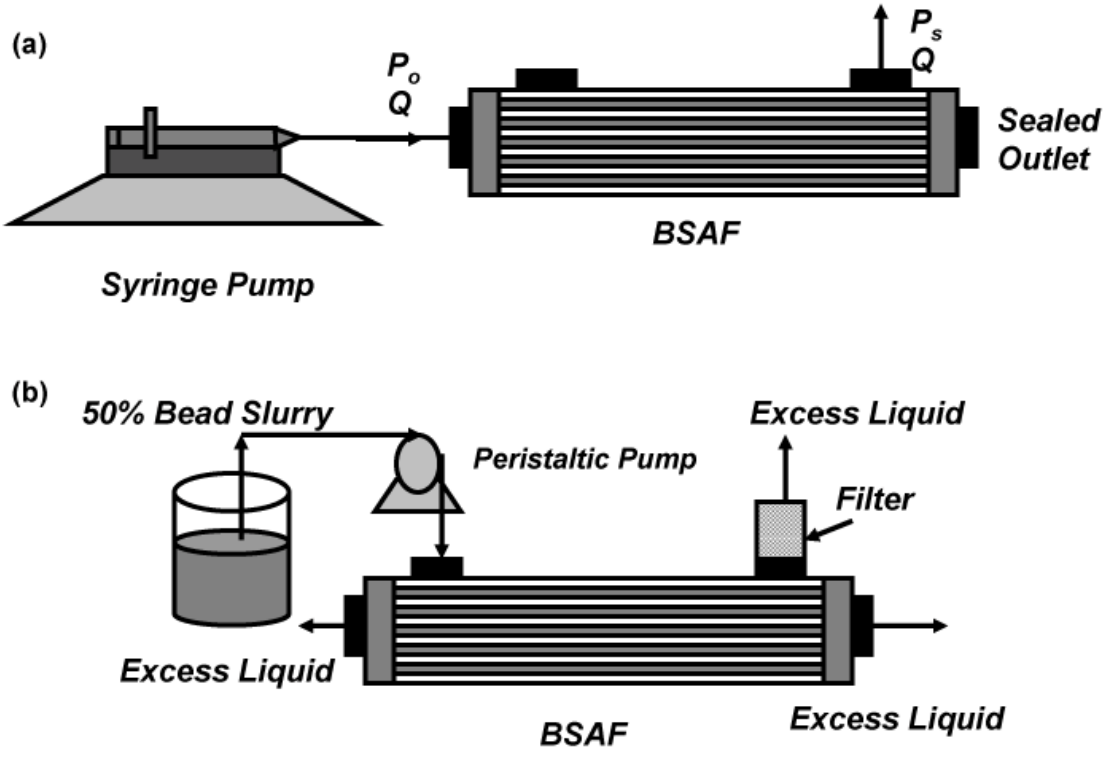

Figure 4-1: Experimental set up for: a: measurement of hydraulic permeability of fibers. b: loading a BSAF device with modified beads.

type of beads. For all experiments, the adsorption capacity of the BSAF devices was at least three times greater than the maximum amount of antibodies in the reservoir. In the last set of experiments, the reservoir volume was increased from 12 ml to 35 ml while the flow rate was maintained at 2.2 ml/min. This was to test whether the model was able to predict the decrease in antibody removal rate associated with an increase in the reservoir volume. All experimental parameters were set at the baseline values summarized in **Table 4-1**, unless otherwise specified.

Table 4-1: Description of the parameters of the mathematical model and the respective values in the model validation experiments.

Parameter name	Description	Baseline value
D_i	Inner shell diameter (cm)	0.635
d_i	Fiber inner diameter (cm)	0.03
L	Module length (cm)	25
m_B	Mass of beads (g)	3
N	Number of fibers	20
K	Fiber hydraulic permeability (cm/mm-Hg.min)	0.056
k_L	First order rate constant (ml/g.min)	3.27 (CL-6B) 1.03 (CL-4B)
μ	Viscosity (mm-Hg.min)	1.25×10^{-7}
C_i	Initial concentration of antibodies in reservoir (μg/ml)	10
Q	Volumetric flow rate (ml/min)	2.2
V_R	Reservoir volume (ml)	12 or 35

The shell side of a BSAF device was packed with modified beads as follows **(Figure 4-1-b)**: a 50% bead slurry in PBS (pH 7.4) was placed in a beaker, which was connected to one of the luer fittings of the shell using a piece of Tygon® tubing (Cole-Parmer, Vernon Hills, IL) via a Masterflex peristaltic pump (Cole-Parmer, Vernon hills, IL). A 1 ml polypropylene Rezorian cartridge equipped with polyethylene frit which acted as a filter was connected to the other luer fitting in the shell compartment. The bead slurry was then pumped into the shell side at a flow rate of 6 ml/min while filtering out the extra liquid through the adjacent shell port and the fiber outlet ports. In the end we connected the two shell ports with a piece of Tygon® tubing, primed with PBS buffer. Subsequently, the tubing was connected to a Masterflex peristaltic pump and the flow rate was set at 6 ml/min.

Figure 4-2 shows a schematic of a typical recirculation loop used for antibody removal in a BSAF device and **Figure 4-3** shows an actual experimental set up of in-vitro antibody capture in a BSAF device. The reservoir solution was prepared by diluting monoclonal IgM anti-A antibodies (Anti-A series1, Immucor Inc., Norcross, GA, USA) to 10 μg/ml in PBS with 0.05% Tween and 5% bovine serum albumin (BSA) (Sigma-Aldrich, St. Louis, MO). The inlet and outlet of the fiber side of the BSAF module were connected to the reservoir using Tygon® tubing. The antibody solution was recirculated through the module at a flow rate of 2.2 ml/min by a Masterflex pump attached to the inlet tubing. Samples were taken from the reservoir at time points: 0, 5, 10, 15, 30, 60, 90 and 120 minutes and assayed for the concentration of the antibodies using ELISA.

4.2.6 Data Analysis

The model predictions of antibody capture in the BSAF given by equation **(4-10)** were generated based on the baseline parameter values summarized in **Table 4-1** and a theoretical $\theta = Q_s(1 - \frac{Q_s}{Q_s + k_L m_B})$ parameter was calculated for each experiment. To validate the mathematical model we fit the experimental capture data to equation **(4-10),** using the "nlinfit" function in Matlab (Matlab 7.0, The Mathworks, Inc, Natick, MA), to determine an experimental θ parameter for each experiment. The model predictions were compared to the experimental results by computing the percentage of the relative difference between the experimental and theoretical θ values in each experiment as the following: % relative difference$= \frac{\theta_{experimental} - \theta_{theoretical}}{\theta_{theoretical}} \times 100$. Similarly, we calculated the % relative difference

between the experimental and theoretical $t_{1/2}$ values, where $t_{1/2}$ is the time point at which 50% of the initial reservoir antibody concentration is removed by the BSAF and is calculated from: $t_{1/2} = \frac{-V_R \ln(0.5)}{\theta}$.

4.3 RESULTS

4.3.1 Measurement of Model Parameters and Adsorption Capacity of Modified Beads

Experiments were performed to determine two parameters of our mathematical model: the hydraulic permeability of fibers and the first order rate constant of the modified beads. Another series of experiments were performed to determine the adsorption capacity per unit mass of the modified beads. This data enabled us to calculate the minimum mass of beads required in the BSAF devices to maintain an excess of anti-A antibody binding sites in relation to the maximum amount of antibodies in the reservoir (hence we justified our assumption of a first order antibody removal rate by the beads in BSAF devices, see section 4.1.3). Hydraulic permeability of fibers was calculated in each of the fabricated BSAF modules from the inverse slope of the plot of inlet transmembrane pressure ($P_o - P_s$) versus flow rate (Q), see equation **(4-14)**. **Figure 4-4** shows a typical plot of transmembrane pressure versus flow rate. Across the eighteen devices that we fabricated and tested for our studies, the average hydraulic permeability was 0.056±0.004 cm/mm-Hg.min.

First order rate constant, k_L, of the modified beads was calculated from analyzing antibody removal by packed bead columns at recirculation flow rates of 0.5 and 1.5 ml/min. In

each case, k_L was calculated from fitting the reservoir antibody concentrations at various times to equation **(4-13)**. The results of the fits of equation **(4-13)** to experimental antibody removal rate data and the best-fit values of k_L, along with R^2 values, for each set of modified beads (CL-4B and CL-6B) are shown in **Figure 4-5**. As the recirculation flow rate was increased from 0.5 to 1.5 ml/min, k_L increased by 4 % (from 0.92 to 1.03 ml/g.min) for CL-4B beads and by 24 % (from 2.48 to 3.27 ml/g.min) for CL-6B beads. The values of k_L, calculated at the flow rate of 1.5 ml/min, were used in our antibody capture rate model.

The modified bead adsorption capacities were also calculated from analyzing antibody removal by packed bead columns in the recirculation mode. Various volumes (3 to 20 ml) of antibody solution were recirculated through columns for 90 minutes. Adsorption capacity of modified beads, in the columns that became saturated with bound antibodies, was calculated from the difference between initial and final reservoir antibody concentrations **(Figure 4-6)**. The antibody adsorption capacity of CL-4B and CL-6B beads was each estimated 153 and 788 μg/g. Nonspecific adsorption of anti-A antibodies by control beads, modified with B antigens, was not significant.

4.3.2 Model Predictions

For a given reservoir volume and Starling flow rate, antibody removal rate in a BSAF nonlinearly increases by increasing a dimensionless lumped parameter: $k_L m_B / Q_s$. A maximum limit of antibody capture rate is achieved when $k_L m_B / Q_s$ approaches infinity **(Figure 4-7)**. Three distinct antibody removal regimes with the following approximate boundaries are shown

in **Figure 4-7**: diffusion limited ($k_L m_B / Q_s \leq 1$), intermediate ($1 < k_L m_B / Q_s < 10$) and perfusion limited ($k_L m_B / Q_s \geq 10$). In a diffusion limited regime ($k_L m_B / Q_s \leq 1$) antibody removal rate

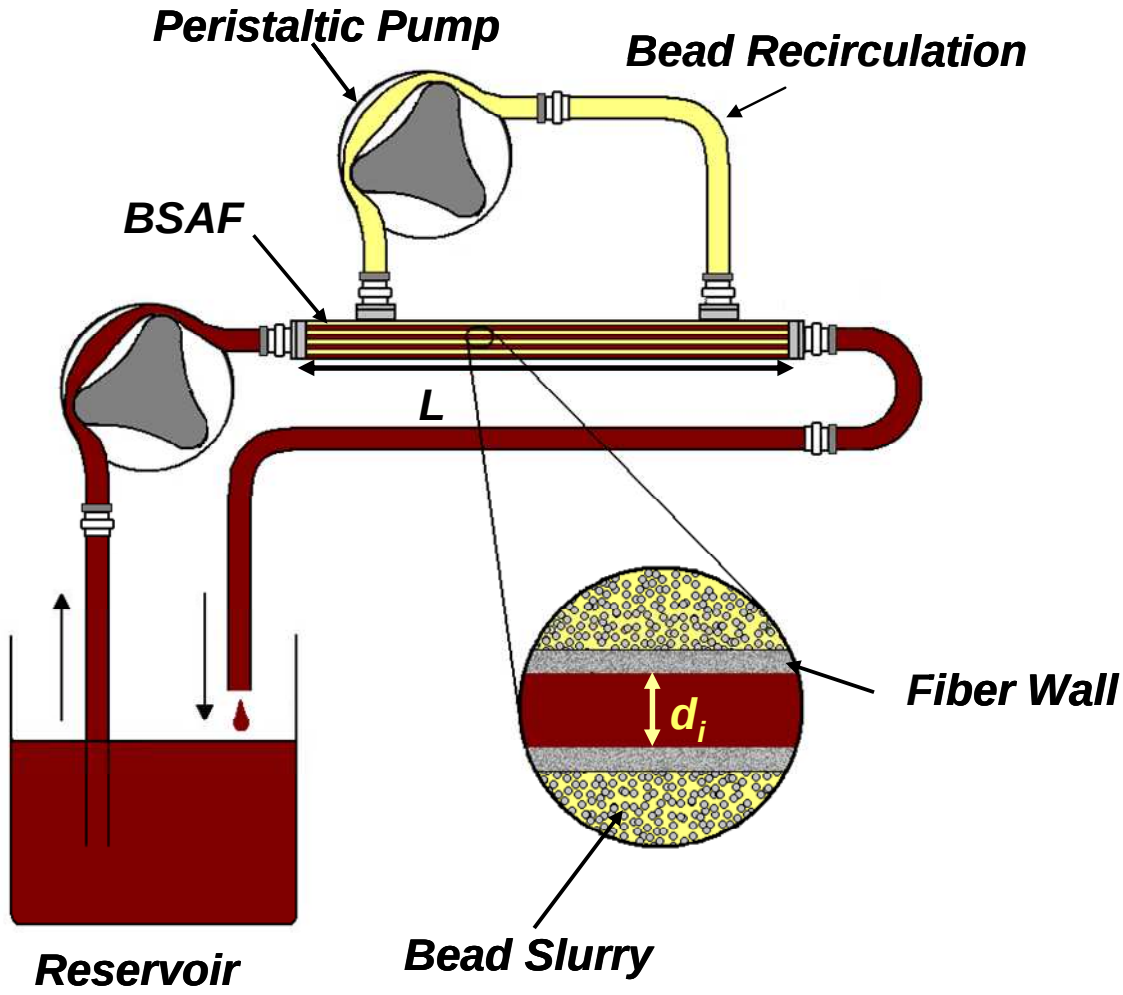

Figure 4-2: Schematic of the BSAF device and a typical set up of the recirculation loop for antibody capture.

primarily depends on antibody diffusion to the binding sites within the porous beads. Hence, antibody removal rate in the diffusion limited regime increases substantially as $k_L m_B / Q_s$ increases, but changes insignificantly in relation to an increase in Starling flow rate relative to the reservoir volume (Q_s / V_R). Antibody removal is perfusion limited when $k_L m_B / Q_s \geq 10$.

In a perfusion limited regime antibody removal rate is solely dependent on the magnitude of Starling flow rate relative to the reservoir volume (Q_s / V_R). No significant increase in the antibody removal rate is expected by further increasing the magnitude of $k_L m_B / Q_s$ in a perfusion limited regime. An intermediate regime ($1 < k_L m_B / Q_s < 10$) is distinguished in which antibody

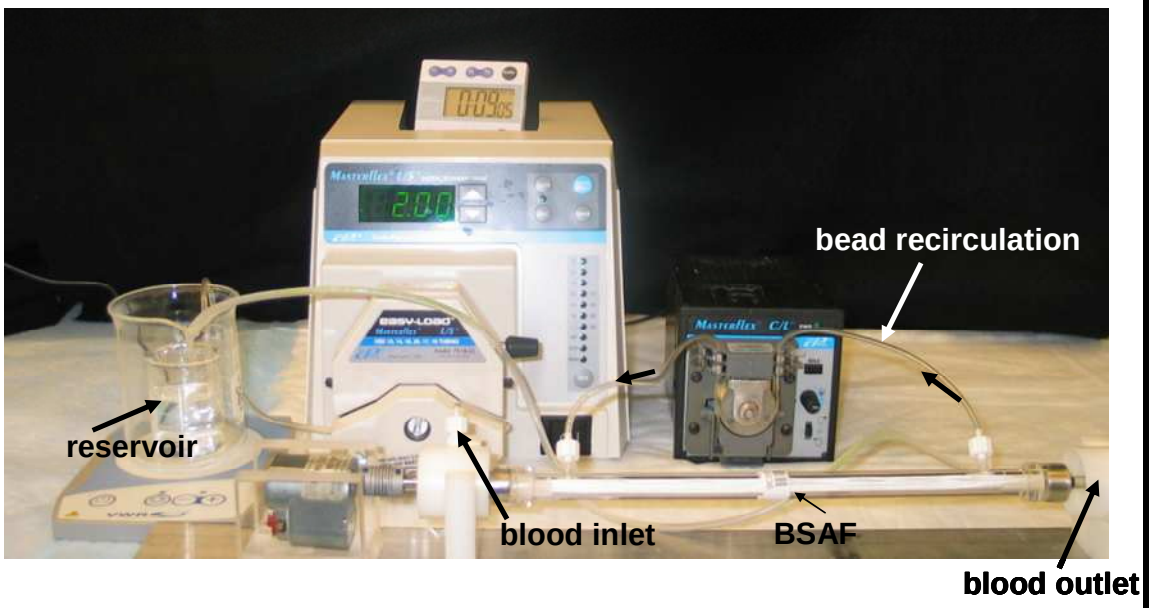

Figure 4-3: An actual experimental set up of in-vitro antibody capture in BSAF devices in model validation experiments.

removal rate is affected by a combination of antibody diffusion and Starling flow rate in the device. For any given value of $k_L m_B / Q_s$ and reservoir volume, a greater rate of antibody removal rate is obtained for a higher value of Starling flow rate **(Figure 4-8)**.

Figure 4-9 shows that for a given flow rate, reservoir volume, mass of beads and first order rate constant, antibody removal rate in a BSAF device increases by increasing the module length.

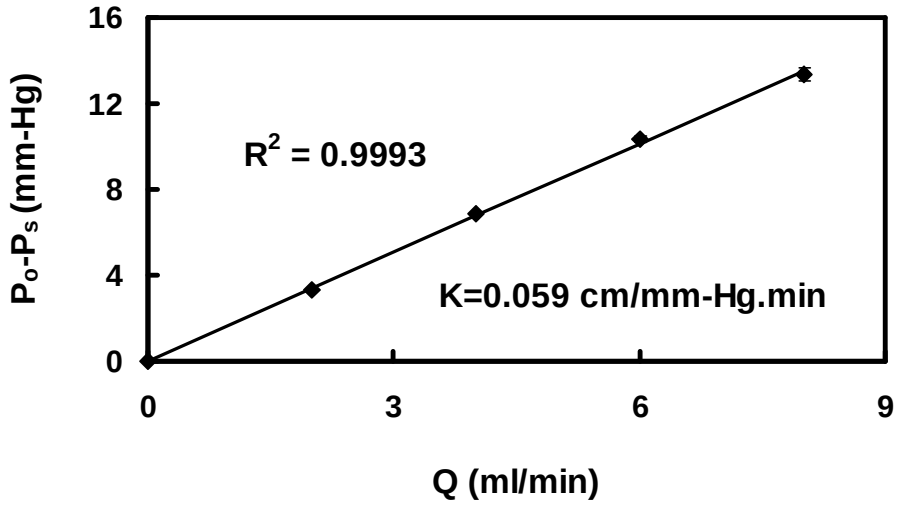

Figure 4-4: A typical plot of transmembrane pressure (P_o-P_s) versus flow rate (Q) from which fiber hydraulic permeability is calculated.

4.3.3 Validation of the BSAF Antibody Capture Rate Model

To validate the model, we first tested its ability to predict changes in antibody removal rates associated with changes in $k_L m_B / Q_s$ for a given BSAF geometry, flow rate and reservoir

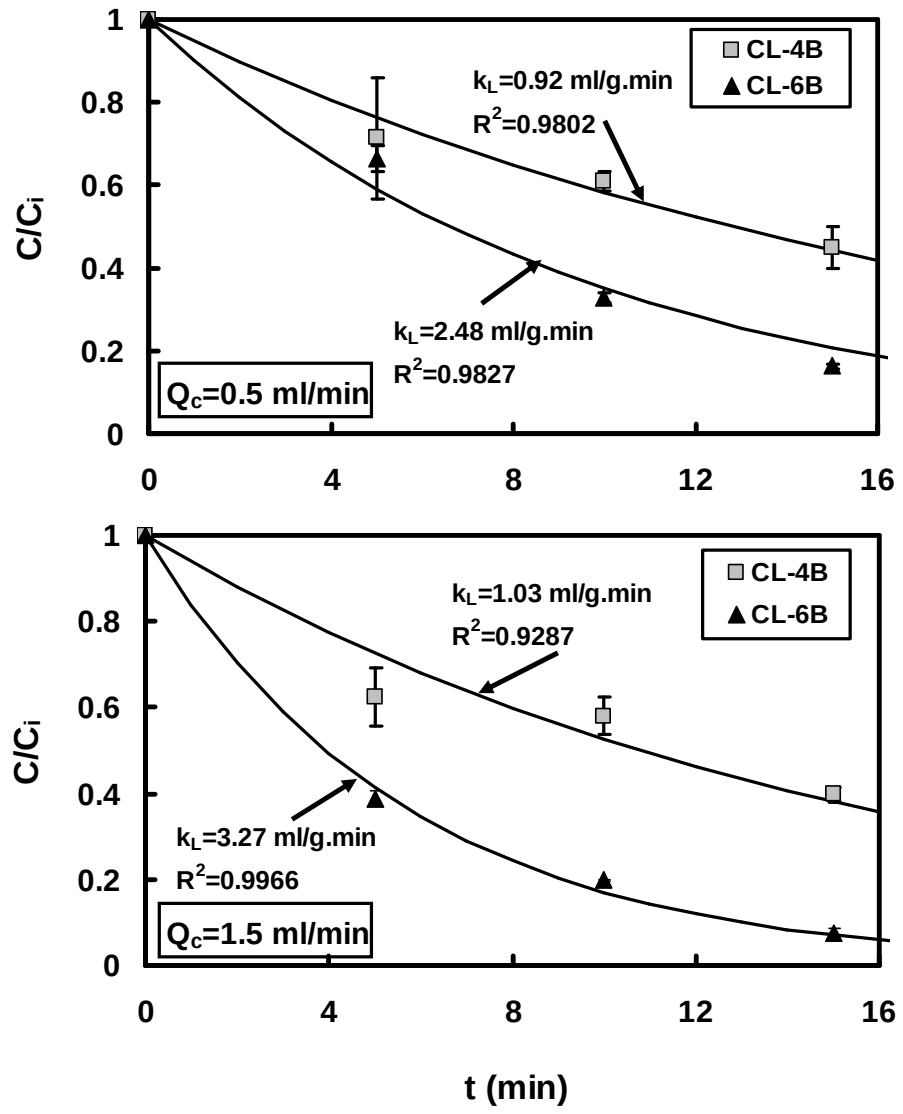

Figure 4-5: Measurement of first order rate constant, k_L , of modified CL-4B and CL-6B beads at two recirculation flow rates (Q_c) of 0.5 and 1.5 ml/min.

volume. Next, $k_L m_B / Q_s$ was kept at a constant value and the reservoir volume was increased to test the ability of our model to predict the decrease in removal rate associated with a decrease in the magnitude of starling flow rate relative to the reservoir volume (Q_s / V_R), see equation **(4-10)**.

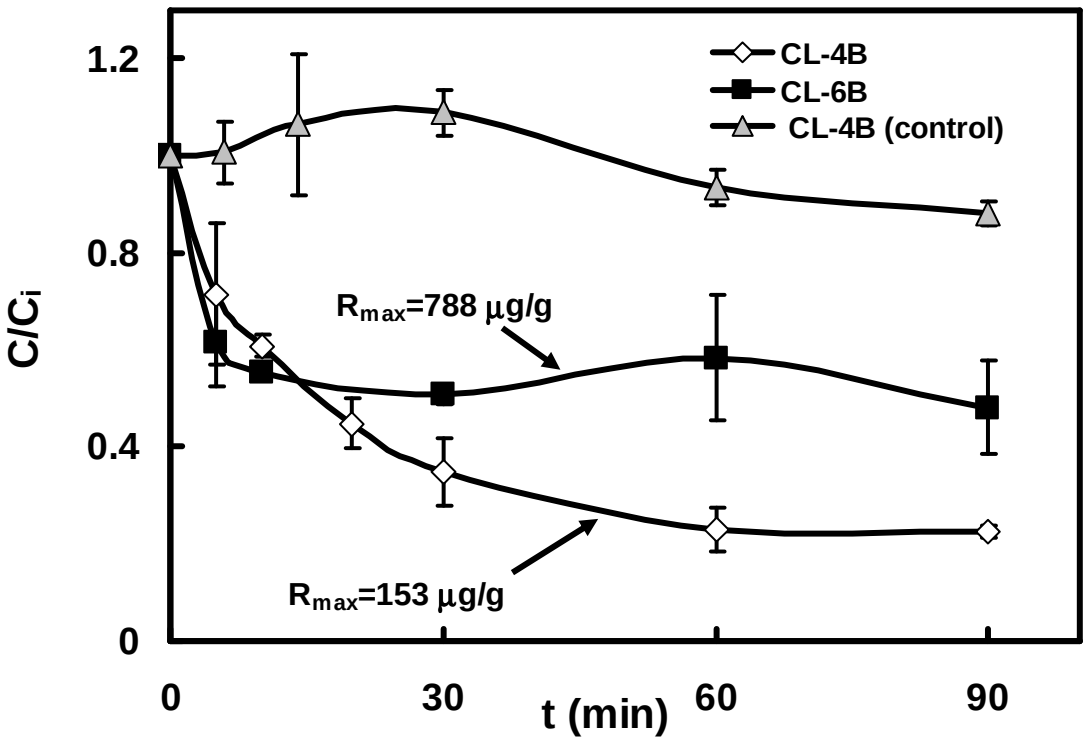

Figure 4-6: Measurement of antibody removal capacity of CL-4B and CL-6B beads, modified with A antigens. Control columns were loaded with CL-4B beads modified with B antigens. Antibody removal capacity per unit weight of beads is denoted by R_{max}.

The specific parameters that we varied in the model validation experiments and the corresponding values in each experiment are summarized in **Table 4-2**. The theoretical versus experimental values of θ and $t_{1/2}$ in our model validation experiments are summarized in **Table 4-3.** Each experiment is represented by the an identical Experiment number in both **Tables 4-2 and 4-3 .**

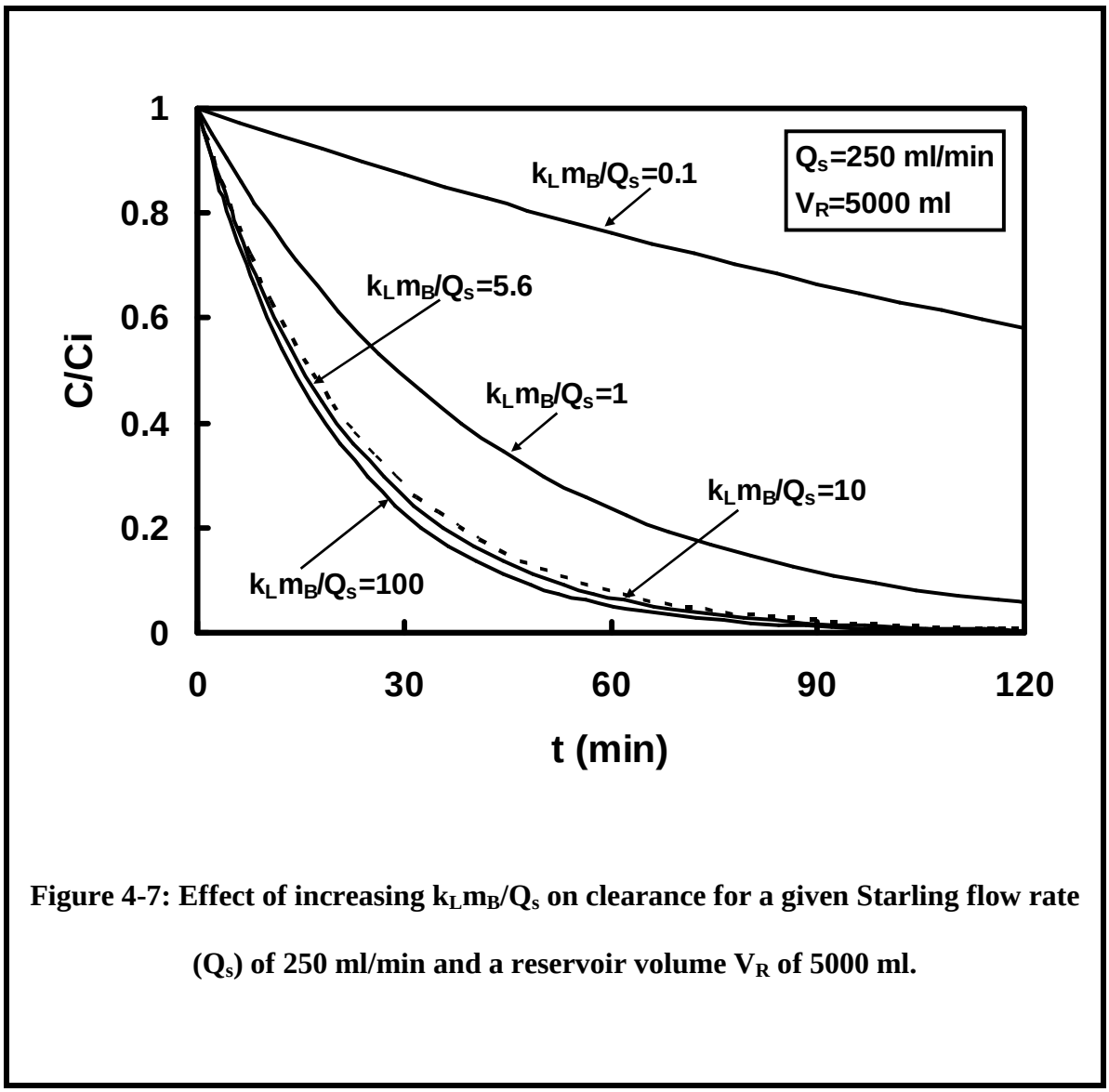

Figure 4-7: Effect of increasing $k_L m_B/Q_s$ on clearance for a given Starling flow rate (Q_s) of 250 ml/min and a reservoir volume V_R of 5000 ml.

Figure 4-10 compares antibody removal rates in two sets of BSAF devices packed with equal masses (1.5 g) of either CL-4B or CL-6B beads (different k_L values). Flow rate and reservoir volume were the same in both cases (2.2 ml/min and 12 ml). Antibody removal rate

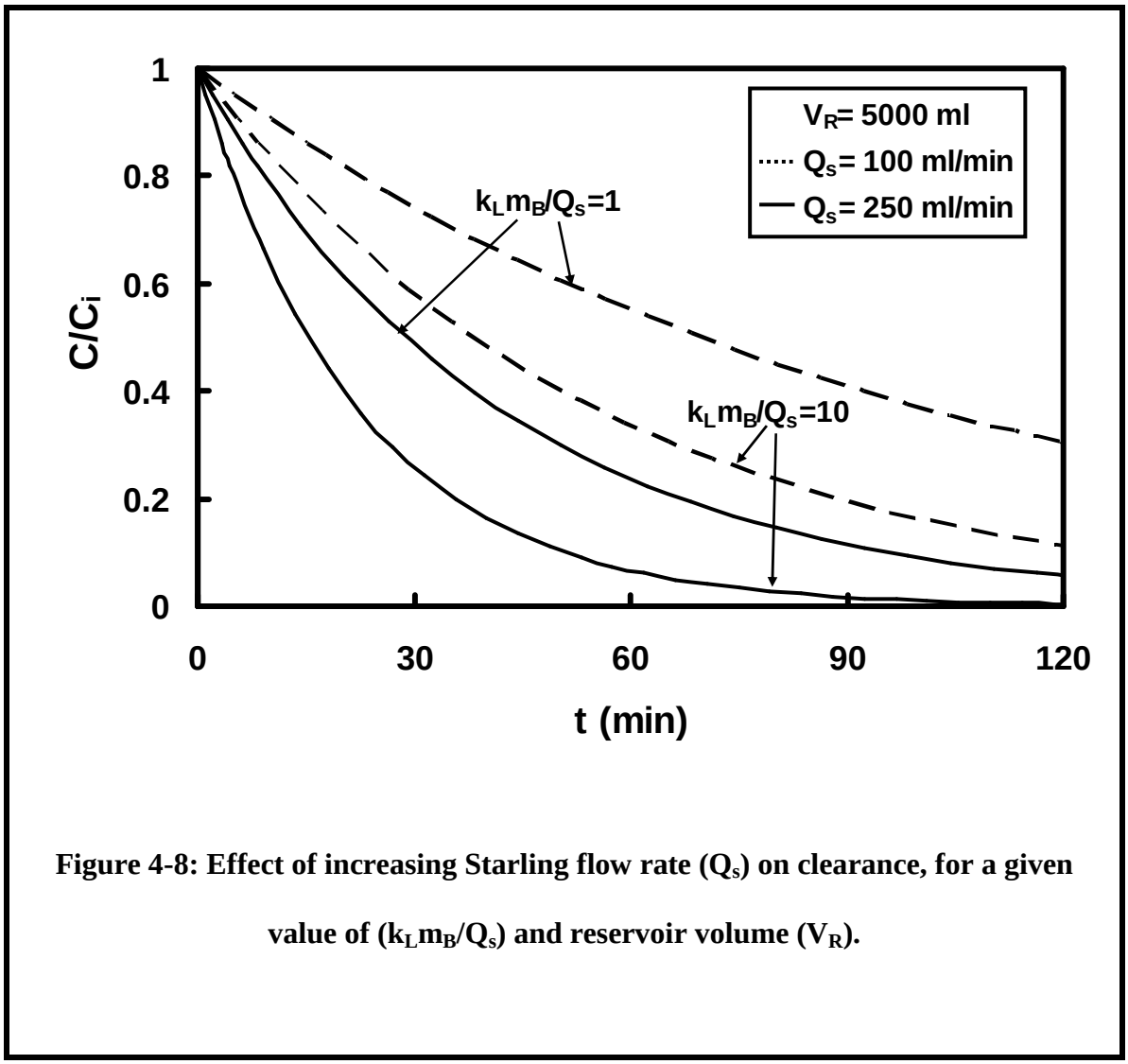

Figure 4-8: Effect of increasing Starling flow rate (Q_s) on clearance, for a given value of ($k_L m_B/Q_s$) and reservoir volume (V_R).

was predicted in the diffusion limited region for modules packed with CL-4B beads ($k_L m_B / Q_s = 0.9$) and in the intermediate regime for those modules packed with CL-6B beads ($k_L m_B / Q_s = 2.8$). Experimental data in both cases showed faster antibody removal

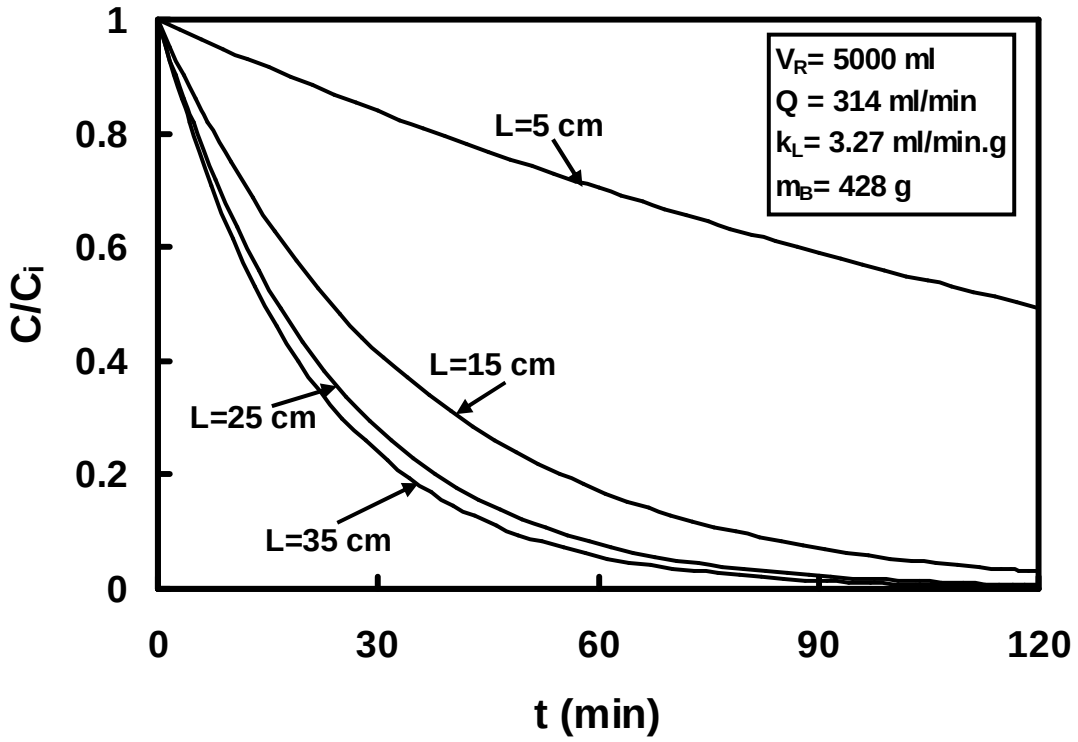

Figure 4-9: Effect of increasing module length (L) on clearance, for given values of reservoir volume (V_R), blood flow rate (Q), mass of beads (m_B) and first order rate constant of modified beads (k_L).

than the corresponding model predictions (the experimental $t_{1/2}$ values were 30% and 38% lower than the respective theoretical values in the modules packed with CL-4B and CL-6B beads, respectively).

Table 4-2: Description of the baseline values of various experimental parameters in the model validation experiments.

Experiment number	Bead type	k_L (ml/g.min)	m_B (g)	V_R (ml)
1	CL-4B	1.03	1.5	12
2	CL-4B	1.03	3.0	12
3	CL-6B	3.27	1.5	12
4	CL-6B	3.27	3.0	12
5	CL-6B	3.27	3.0	35

Table 4-3: Theoretical and experimental values of θ and $t_{1/2}$ in the model validation experiments.

Experiment number	θ Theoretical (ml/min)	θ Experimental (ml/min)	$t_{1/2}$ Theoretical (min)	$t_{1/2}$ Experimental (min)
1	0.82	1.17	10.11	7.12
2	1.12	0.68	7.42	12.22
3	1.30	2.11	6.42	3.95
4	1.49	1.42	5.57	5.84
5	1.49	2.39	16.26	10.15

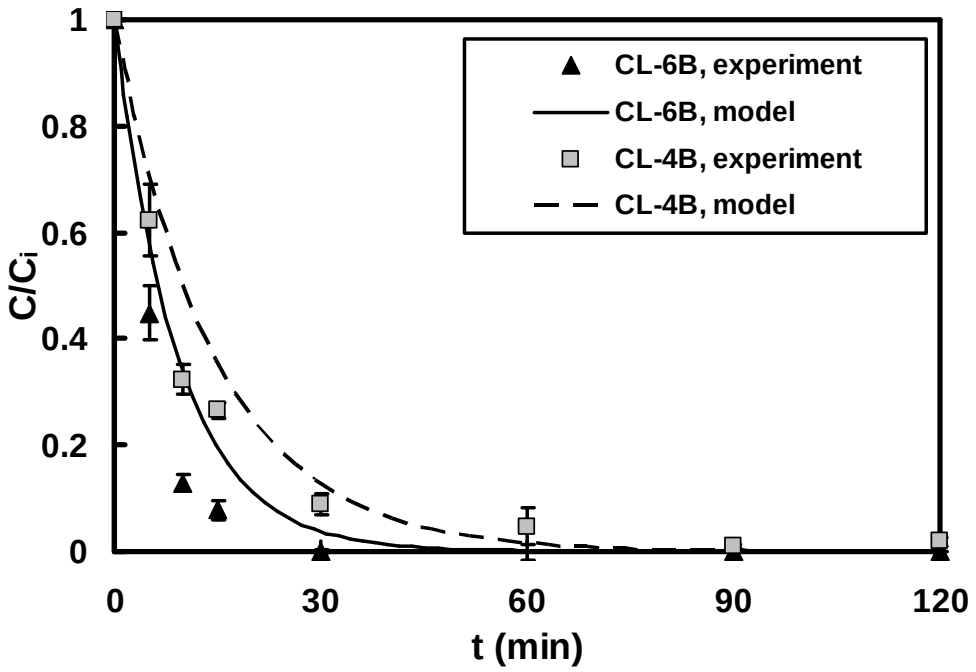

Figure 4-10: Effect of increasing $k_L m_B/Q_s$ on clearance. Two sets of BSAF devices were packed with equal mass (1.5 g) of CL-4B or CL-6B beads. Flow rate and reservoir volume were 2.2 ml/min and 12 ml, respectively.

Figures 4-11 and **4-12** compare antibody removal rates in BSAF devices packed with 1.5 g and 3 g of CL-4B and Cl-6B beads, respectively (constant k_L values in each case). Increasing the mass of beads from 1.5 g to 3.0 g resulted in 42% (CL-4B beads) and 32% (CL-6B beads) increase in the observed experimental $t_{1/2}$ values, whereas based on the mathematical model, we were expecting to observe 36% (CL-4B beads) and 15% (CL-6B beads) decrease in the $t_{1/2}$ values under the given experimental conditions.

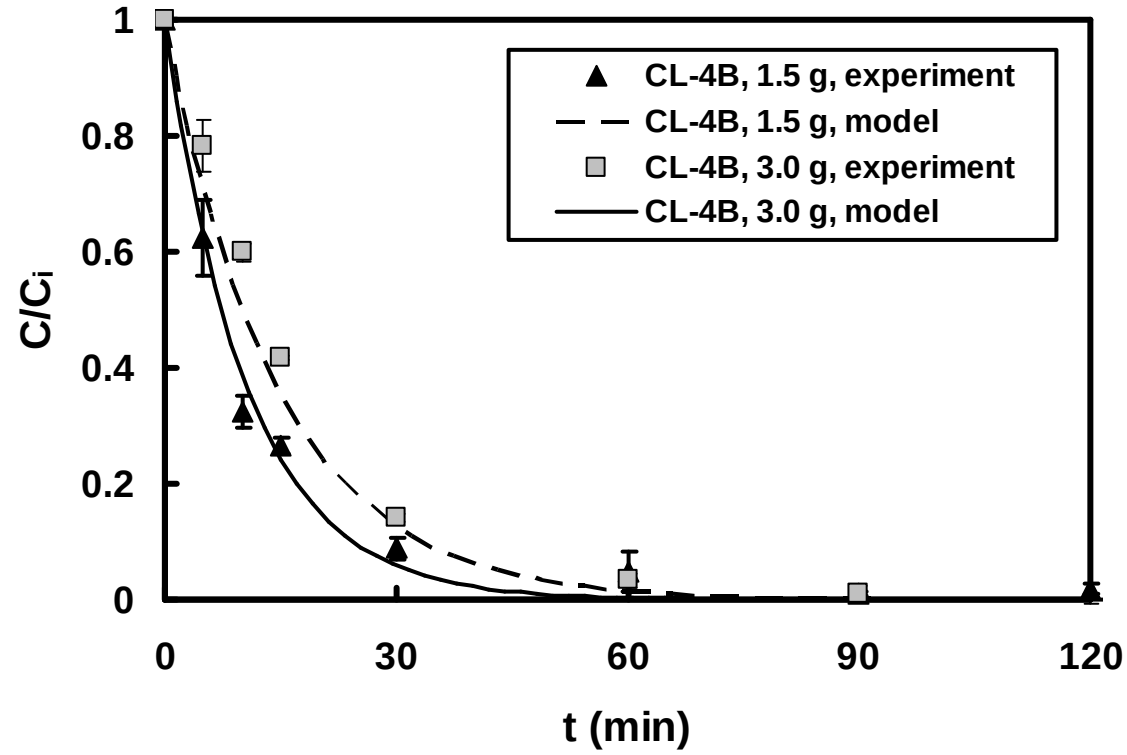

Figure 4-11: Effect of increasing mass of beads of a given k_L on clearance. Two sets of BSAF devices were packed with 1.5 g or 3.0 g of CL-4B beads. Flow rate and reservoir volume were 2.2 ml/min and 12 ml, respectively.

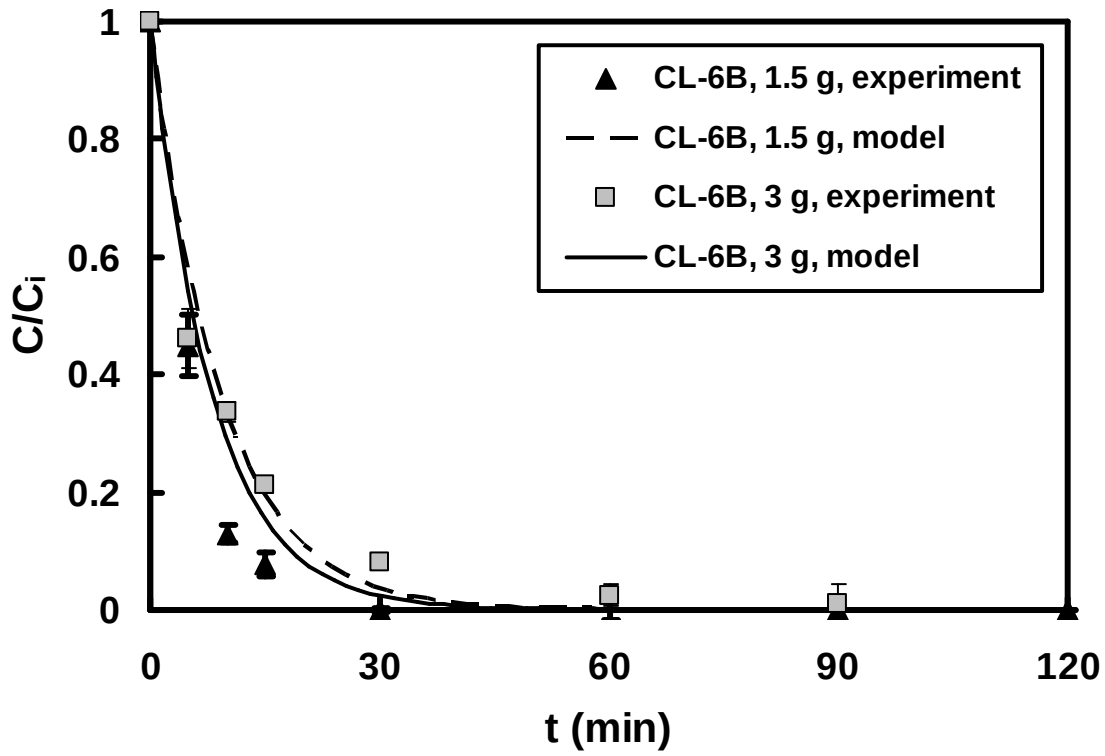

Figure 4-12: Effect of increasing mass of beads of a given k_L on clearance. Two sets of BSAF devices were packed with 1.5 g or 3.0 g of CL-6B beads. Flow rate and reservoir volume were 2.2 ml/min and 12 ml, respectively.

Figures 4-13 shows the change in rate of adsorption due to changes in the magnitude of Q_s / V_R. Both series of BSAF devices were packed with 3 g of CL-6B beads and the flow rate was maintained at 2.2 ml/min ($k_L m_B / Q_s = 5.6$ in both cases). The reservoir volume was increased from 12 ml to 35 ml. The model predicted 65% increase in $t_{1/2}$, whereas the experimental results showed 42% increase in this case.

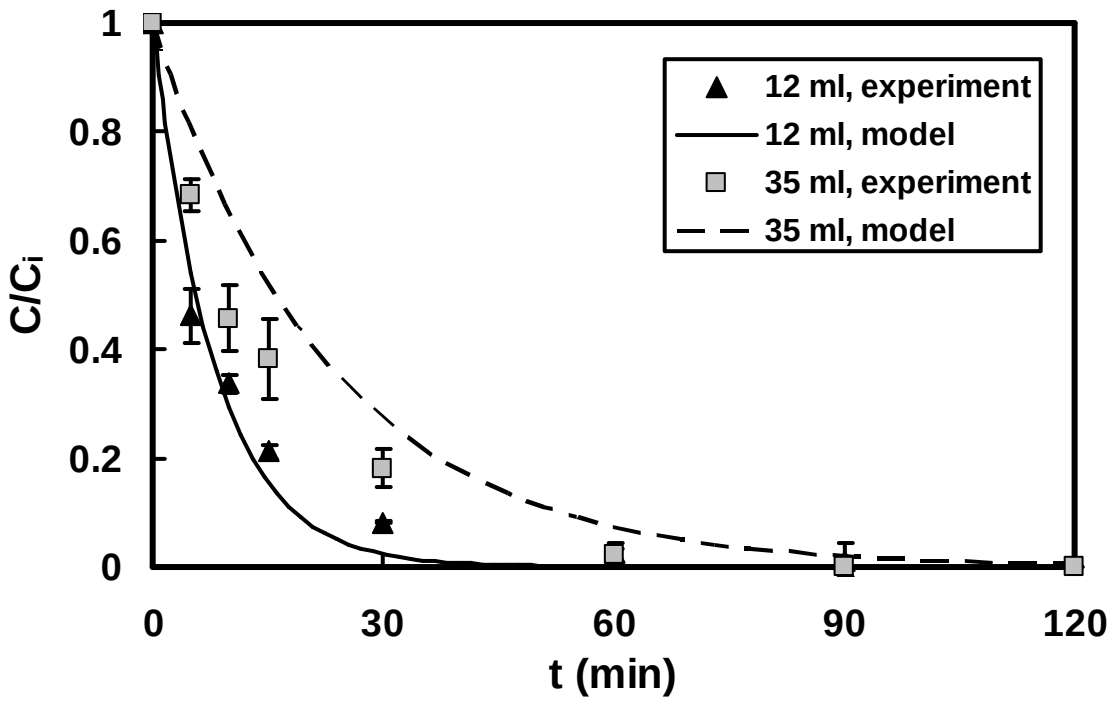

Figure 4-13: The effect of adsorption rate changes due to changes in the magnitude of Q_s/V_R. Two sets of BSAF devices were packed with 3.0 g of CL-6B beads. Flow rate was 2.2 ml/min. The reservoir volume was increased from 12 ml to 35 ml.

4.4 DISCUSSION

An ideal antibody filtering device selectively removes up to 100% of the target antibodies in a 2-4 hour time period and is biocompatible and simple to operate. To meet these design goals, we developed a new antibody filtration device containing microfiltration fibers with antibody capturing beads integrated within the interstitial fiber space (BSAF device). Our primary goal in this study was to identify the mechanisms underlying antibody capture in these novel BSAF devices. To do this we developed a simple mathematical model that predicts antibody removal rate in the BSAF as a function of key design and operational parameters, including the first order rate constant of antibody capturing beads, mass of the beads, Starling flow rate and the reservoir volume. The model was validated by measuring the time course of monoclonal anti-A antibody removal in BSAF devices packed with anti-A specific beads. Although we did not observe a perfect fit between experimental data and the respective model predictions in this study, we were able to show a reasonably good approximation of antibody removal data by the model in all cases.

In-vitro testing of monoclonal anti-A antibody removal in scaled-down prototypes of the clinical BSAF (as described in **Table 4-4**) resulted in 100% antibody removal within two hours (**Figure 4-13**). Gautam et al. previously showed that in-vitro capture of monoclonal anti-A antibody in scaled down SAF devices resulted in up to 35% reduction in the anti-A antibody concentration [136]. Thus, a significant improvement in anti-A antibody removal was achieved in our new BSAF modules. Both SAF and BSAF are immunoadsorbent devices which use low molecular weight (30 kDa) A-trisaccharide-polyacrylamide glycoconjugates for anti-A antibody adsorption. However, the vast bead surface area for antigen immobilization in BSAF devices represents a major advantage in BSAF modules.

BSAF devices are similar in principal to the microspheres-based detoxification system (MDS), being developed for blood detoxification in liver failure and sepsis [101-104]. The key difference between the two systems is the way in which the adsorbents are incorporated within the capture loop. The MDS combines the dialysate side of a standard plasma filter with a secondary extracorporeal flow loop in which adsorbent particles are suspended. The volume of this secondary loop is approximately 300 ml per 1 L of processed blood [104]. Conversely, BSAF modules have a shell side whose volume has been specifically calibrated to a size capable of housing both the fibers and the bead slurry within a single device. The module dimensions are approximately the same as in a standard plasma filter but contain fewer fibers and therefore allow more free shell volume to contain the bead slurry within the fiber interstitial space. Although the bead recirculation loop used in this study, seemingly appears similar to that used in microspheres-based detoxification system (MDS), fundamentally it only serves the purpose of keeping the beads in a continuously mixed and uniformly distributed state.

We used the model as a guide to design a BSAF device that would generate a clinically relevant rate of anti-A removal. Based on the model, the highest antibody removal rate for a given Starling flow rate and reservoir volume was predicted for the perfusion limited regime, when $k_L m_B / Q_s \to 10$. Therefore, a first rational step in optimization of design of BSAF devices was to maximize the value of $k_L m_B / Q_s$ in a given device until perfusion limited antibody removal was achieved. Antibody removal rate in the small scale BSAF devices, packed at their maximum loading capacity with 3 g of CL-6B beads, fell into the intermediate range with $k_L m_B / Q_s = 5.6$. When this removal rate was compared with the model prediction of antibody removal in an optimized state ($k_L m_B / Q_s$=10), we concluded that a further increase in $k_L m_B / Q_s$ was unwarranted, as antibody removal rate was already approaching the perfusion limited regime

(**Figure 4-7, dashed line**). The next step in BSAF design optimization was to maximize the magnitude of Q_s/V_R within a realistic range. In general, blood flow rate is determined based on the hemodynamic stability of a patient and usually ranges between 100 and 500 ml/min [83, 137-139] [27] , and since Q_s only represents a fraction of total blood flow rate, it may not exceed 250-300 ml/min. As shown in **Figure 4-8**, a Q_s of approximately 250 ml/min would be required to achieve 100% antibody removal in a clinical scale BSAF device ($V_R = 5000\,\text{ml}$), within two hours. Using the mathematical model (equation **4-5**) and assuming an average blood flow rate (Q) of 314 ml/min [83], we estimated that the length of the modules should be approximately 25 cm to achieve a Q_s of 250 ml/min. Subsequently, the minimum mass of CL-6B beads for a full scale BSAF device was calculated from our earlier optimization constraint: $k_L m_B / Q_s = 5.6$, assuming: Q_s=250 ml/min and $k_L = 3.27$ ml/g.min. A blood flow rate of 0.11 ml/min within each fiber [137-138] was used to calculate the total number of fibers in a clinical BSAF device. The BSAF inner shell diameter was calculated based on the minimum required volume to encompass the required number of fibers and beads in a device. The device dimensions and operating parameters for our envisioned clinical BSAF device are summarized in **Table 4-4**.

Although the BSAF is designed for direct hemoperfusion, we validated our model using a monoclonal antibody capture model instead of whole blood. This simplified system allowed us to understand the basic mechanisms underlying antibody capture in BSAF devices independent of the various complexities inherent to whole blood perfusion. For example, antibody concentrations and affinities for the immobilized A-trisaccharide epitopes naturally vary in different blood samples. Monoclonal antibodies are ideal for validation of a mathematical model since they provide uniform binding characteristics across multiple experiments. Upon testing the

BSAF with whole blood, the fiber hydraulic permeability, first order rate constant and viscosity must be re-evaluated and appropriate values must be used in the mathematical model. A simpler alternative would be to obtain time course of antibody removal in BSAF devices from various blood samples and fit our mathematical model to the averaged normalized concentrations over time. We could then estimate the model parameters from the best nonlinear regression fit. Using this method, we may be able to obtain average values for the three model parameters in whole blood. Nevertheless, the current model provides a basis to efficiently design and evaluate a BSAF device with a clinically relevant antibody removal rate. In Chapter 6.0, we will discuss applicability of our mathematical model to antibody capture in BSAF from whole blood.

Table 4-4: Design characteristics of a conceptual clinical scale and an appropriately scaled down BSAF device.

Module Characteristics	Clinical-scale	Small-Scale
Module length (cm)	25	25
Inner shell diameter (cm)	7.6	0.635
Number of fibers	2854	20
Mass of beads (g)	428	3
Blood flow rate (ml/min)	314	2.2
Blood volume (ml)	5000	35

5.0 TOWARDS DEVELOPMENT OF BSAF DEVICES WITH INTEGRATED BEAD MIXING MECHANISM

We summarized the many advantages of a sorbent suspension over a packed sorbent column in removal of target molecules from blood or plasma (see section 2.5.1). In BSAF devices a sorbent suspension in the fiber interstitial space particularly provides two main advantages; the beads in suspension are uniformly available for adsorption of the target antibodies, and more importantly, the flow resistance in the fiber interstitial space is negligible. Conversely, a tightly packed sorbent column within the fiber interstitial space causes significant pressure drop along the axial direction in the shell side. As a result, transmembrane pressure decreases and consequently Starling flow rate and the overall antibody removal rate in the device decrease as well. As we will show in this chapter, our experiments have demonstrated that, to maintain the bead slurry in suspension and uniformly distributed within the fiber interstitial space, a bead recirculation regimen is required. We observed that in the absence of a bead recirculation mechanism, Starling flow continuously pushed the beads toward one end of the device and hence compressed the beads into a packed sorbent column. This resulted in reduction of the overall antibody removal rate in the BSAF.

We are interested to maintain the bead recirculation pathway as an integrated unit within the device and our efforts are ongoing to design an integrated bead mixing mechanism to minimize the external tubing and simplify the device operation. In this chapter we will first

address the studies that highlighted the need for a bead recirculation mechanism in BSAF devices. We will then describe design, fabrication and testing of a new set of BSAF devices which incorporated an inner porous tube to internalize the bead recirculation pathway within the device. As we will describe further, these modules provided a simplified prototype of a more sophisticated device which will allow bead recirculation and antibody capture to occur simultaneously within a single unit. The efficiency of antibody removal directly from whole blood in our fabricated scaled down BSAF prototypes will be addressed in the following chapter.

5.1 MATERIALS AND METHODS

5.1.1 Preparation of Affinity Beads

Synthesized polyacrylamide glycoconjugates (Atri-pNPA[30]) containing 20 mol% of A-trisaccharides were covalently attached within the pores of cross linked Sepharose® CL-4B and CL-6B beads (Sigma-Aldrich, Louis, MO) according to the methods described before in section 4.2.1. To ensure consistency between the different batches of modified beads, we measured antibody removal capacity and first order rate constant of the modified beads according to the methods described in section 4.2.2.

5.1.2 Fabrication of the BSAF Modules

Small scale BSAF modules containing 20 fibers were fabricated as described in section 4.2.3. Additionally, another series of BSAF modules with incorporated inner porous tubes were fabricated as follows: Polycarbonate tubes (K-mac Plastics, Wyoming, MI) of 25 cm length and 1.25 cm inner diameter were used as the housing of our BSAF modules. In each case, a circular hole (0.5 mm) was drilled in the outer surface of the shell case at 1 cm from one end of the tube and a polycarbonate luer fitting (Value Plastics, Fort Collins, CO) was glued to the hole using UV light curing adhesive (DYMAX, Torrington, CT). A porous tube was fabricated by drilling circular holes of 1 cm diameter equally spaced at approximately 2 cm apart from one another in the peripheral area of a second cylindrical polycarbonate tube of 0.3 cm inner diameter and 25 cm length. Eighty matted polyethersulfone microfiltration hollow fiber membranes (MicroPES®, Membrana GmbH, Wuppertal, Germany) of 0.03 cm inner diameter and 0.01 cm wall thickness were wrapped around this tube. The tube was then placed in the center of the BSAF shell case in a manner which left approximately 3 cm of fibers protruding from each end of the housing and 2 cm of the inner tube protruding from only one end of the case. Both ends were filled with hot glue, and the excess glue was tomed with a razor blade once hardened. Polycarbonate caps with luer fittings were fabricated and attached to all three outlet ports of the device using UV light curing adhesive.

The design parameters of BSAF modules with inner porous tubes (including the module length, inner shell diameter, the number of fibers and the mass of beads) and the operational parameters (including reservoir volume and flow rate) were all appropriately scaled up in relation to the corresponding values of our small scale BSAF modules, which contained 20 fibers. Additionally, these values were appropriately scaled down in relation to the corresponding

values of our conceptual clinical scale BSAF devices. Therefore, hereupon we will refer to our fabricated BSAF modules with inner porous tubes as the intermediate scale devices and our fabricated small modules, containing 20 fibers, will be referred to as small scale devices. **Table 5-1** summarizes the device dimensions and operational parameters of our conceptual clinical scale BSAF devices, as well as the corresponding values of our scaled down (small scale and intermediate scale) modules.

5.1.3 In-Vitro Antibody Capture Experiments in Small Scale BSAF Devices

We performed a series of experiments to determine the effect of bead recirculation on antibody removal rate in BSAF devices. For measurement of antibody capture rate in BSAF devices in the absence of bead recirculation, the shell side of small scale BSAF devices was initially loaded with 3.0 g of modified CL-4B or CL-6B beads as described in section 4.2.5. Then, we connected the two shell ports of the modules with a short piece of Tygon® tubing, primed with PBS buffer. Subsequently, the tubing was connected to a Masterflex peristaltic pump and the flow rate was set at 6 ml/min. Bead recirculation was performed for 10 minutes before initiating antibody capture experiments which resulted in uniform bead distribution throughout the module length. Subsequently, bead recirculation was stopped and the two shell ports were capped and antibody capture experiments were performed as described in section 4.2.5.

Table 5-1: Device dimensions and operational parameters in our conceptual clinical scale, intermediate and small scale devices.

Module Characteristics	Clinical Scale	Intermediate Scale	Small Scale
Module length (cm)	25	25	25
Inner shell diameter (cm)	7.6	1.25	0.635
Inner porous tube diameter (cm)	1.82	0.3	N/A
Number of fibers	2854	80	20
Mass of beads (g)	428	11	3
Blood flow rate (ml/min)	314	8.8	2.2
Bead recirculation flow rate (ml/min)	642	18	6
Blood volume (ml)	5000	135	35

5.1.4 In-Vitro Antibody Capture Experiments in BSAF Modules with Inner Porous Tubes

Before initiating each antibody capture experiment, the shell compartment of a BSAF device with an inner porous tube was loaded with 11 g of modified CL-6B beads as follows: A beaker containing a 50% bead slurry in PBS (pH 7.4) buffer (Fisher Scientific, Pittsburgh, PA) was connected via a luer fitting to the shell of the BSAF using Tygon® tubing (Cole-Parmer, Vernon Hills, IL). A 1 ml polypropylene Rezorian cartridge (Supelco**,** St Louis**,** Mo) equipped with a polyethylene filter was connected to the central porous tube outlet port of the BSAF. The bead slurry was then pumped via a Masterflex peristaltic pump (Cole-Parmer, Vernon hills, IL) into the shell side at a flow rate of 10 ml/min, while excess liquid was filtered through the fiber and inner porous tube outlet ports. The Rezorian cartridge was then disconnected and the shell inlet port was connected to the central porous tube outlet port with a piece of Tygon® tubing, primed with PBS buffer. Subsequently, the tubing was connected to a Masterflex peristaltic pump and the flow rate was set at 18 ml/min.

The monoclonal antibody (mAb) solution was prepared as described in section 4.2.5. The fiber side inlet and outlet ports were connected to a reservoir containing 135 ml of mAb solution using Tygon® tubing. The antibody solution was recirculated through the BSAF module at a flow rate of 8.8 ml/min by a Masterflex pump attached to the inlet tubing. The reservoir solution was stirred throughout the experiment. Samples were taken from the reservoir at times 0, 5, 10, 15, 30, 60, 90 and 120 minutes and assayed for antibody concentration using enzyme linked immunosorbent assay (ELISA) as described before [116].

Antibody concentrations over time were normalized to an initial concentration of 10 μg/ml. An average normalized concentration value at each time point was calculated ($n = 2$). Antibody capture rates in the BSAF, as predicted by the model in equation **(4-10)**, were generated based on the parameter values summarized in **Table 5-2**. Each data set was compared to the model prediction of antibody capture rate by computing a coefficient of determination, R^2 [140], value : $R^2 = 1 - \frac{SS_{err}}{SS_{tot}}$, where SS_{err} is the sum of squared errors between the experimental values and the values predicted by the model for each time point and SS_{tot} is the total sum of squares of the experimental values.

5.2 RESULTS

5.2.1 Evaluation of the Effect of Bead Recirculation on Antibody Removal Rate in BSAF Devices

Figure 5-1 compares antibody capture rate in BSAF devices, packed with 3.0 g of modified CL-4B beads, in presence (+) or absence (-) of a bead recirculation regimen. Similarly, **Figure 5-2** shows the effect of bead recirculation on antibody capture rate in BSAF devices packed with 3.0 g of modified CL-6B beads. The R^2 values in the absence of bead recirculation were 0.3091 and 0.5333 in devices packed with CL-4B and CL-6B beads, respectably. Whereas, in presence of bead recirculation, there was better agreement between experimental clearance data and the model predictions (R^2 values were 0.9765 and 0.9793, for CL-4B and CL-6B, respectively). **Figure 5-3** shows the effect of bead recirculation on antibody removal rate in small scale BSAF

devices, in which all operational parameters were appropriately scaled down from a “clinical” BSAF device. Similar to the previous cases, antibody removal rate was lower in the absence of bead recirculation (R^2 values were 0.8528 and 0.9112 in the absence and presence of bead recirculation, respectively).

The bead slurry position within the BSAF modules, in presence and absence of bead recirculation, was visualized by staining the beads with a blue dye solution prior to loading the beads in the fiber interstitial space. **Figure 5-4** shows that the stained beads (blue) are uniformly distributed throughout the module when beads are continuously recirculated. **Figure 5-5** shows the same stained beads in a BSAF device in the absence of bead recirculation. The stained beads gradually moved toward one end of the device and formed a compressed sorbent bed throughout the module end (**Figure 5-5**).

5.2.2 In-Vitro Antibody Capture in BSAF Devices with Integrated Inner Porous Tubes

Figure 5-6 shows a schematic of the recirculation loop used in our in-vitro antibody capture in BSAF devices with integrated inner porous tubes. The mAb capture experiments were performed to evaluate the efficiency of our bead recirculation loop in maintaining uniformly mixed and well distributed bead slurry in the fiber interstitial space of BSAF devices. **Figure 5-7** shows the results of antibody clearance over time in two different antibody capture experiments (data points are shown as average of two experiments). As shown in **Figure 5-7,** there was good agreement between the model predictions and our experimental results $(R^2 = 0.9699)$; this indicated that a uniformly distributed bead slurry was maintained throughout the modules in the BSAF devices with inner porous tubes.

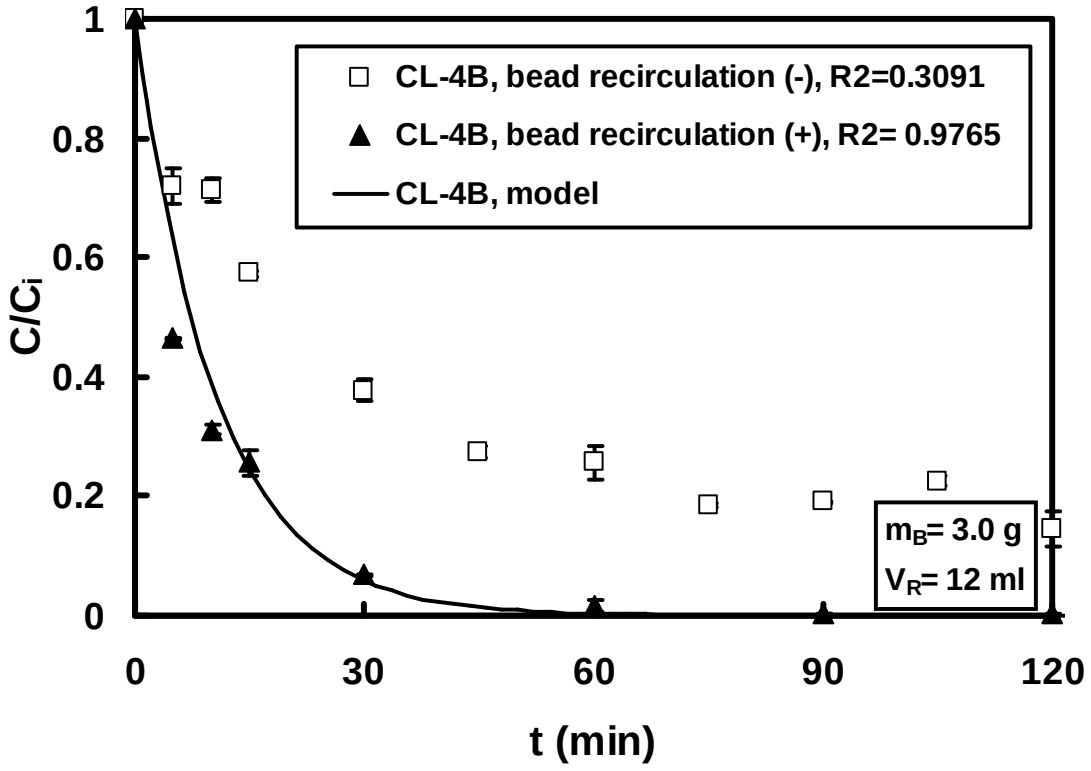

Figure 5-1: Effect of bead recirculation on clearance. Antibody clearance was measured in presence (+) or absence (-) of bead recirculation.

5.3 DISCUSSION

We demonstrated that to achieve an antibody removal rate in agreement with the model prediction, it was crucial to maintain a well mixed and uniformly distributed bead slurry in the interstitial fiber space. In the absence of a bead mixing mechanism, antibody removal rates

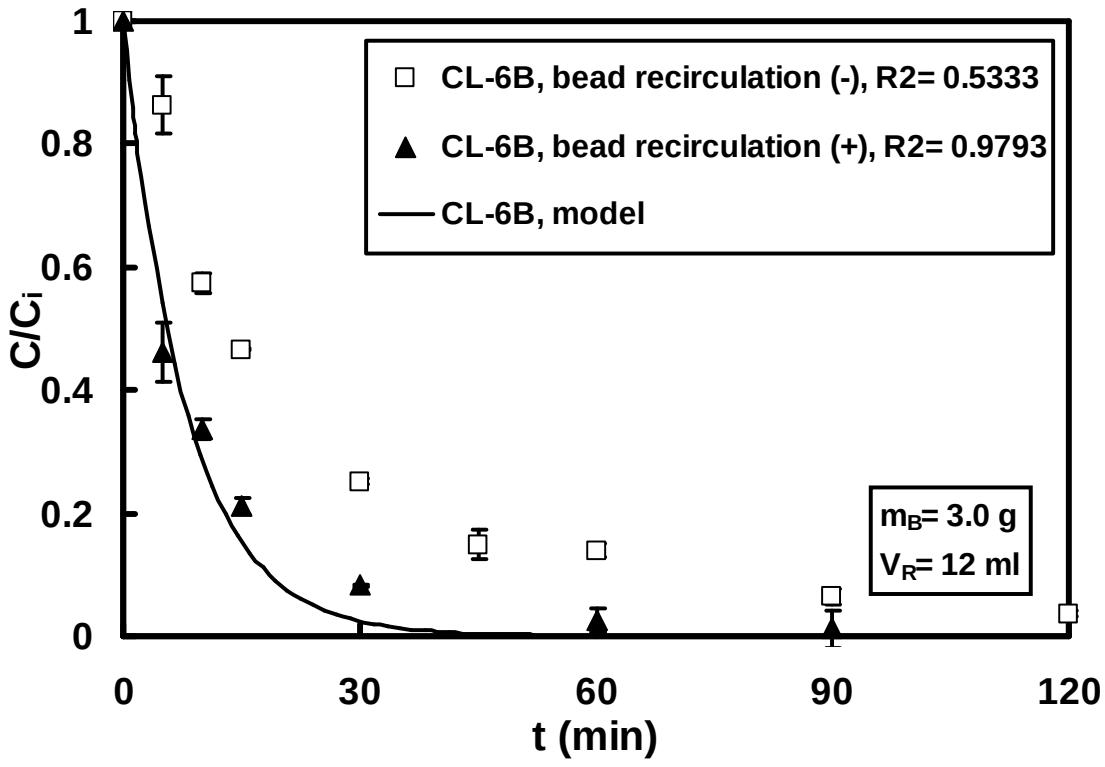

Figure 5-2: Effect of bead recirculation on clearance. Clearance was measured in presence (+) or absence (-) of bead recirculation.

were lower than predicted by our mathematical model due to the Starling flow continuously pushing the beads toward one end of the device. Incorporation of a simple bead recirculation loop, as shown in **Figure 5-4**, provided a mechanism to maintain uniformly distributed bead slurry throughout the module length. However, this simple bead recirculation system is not an

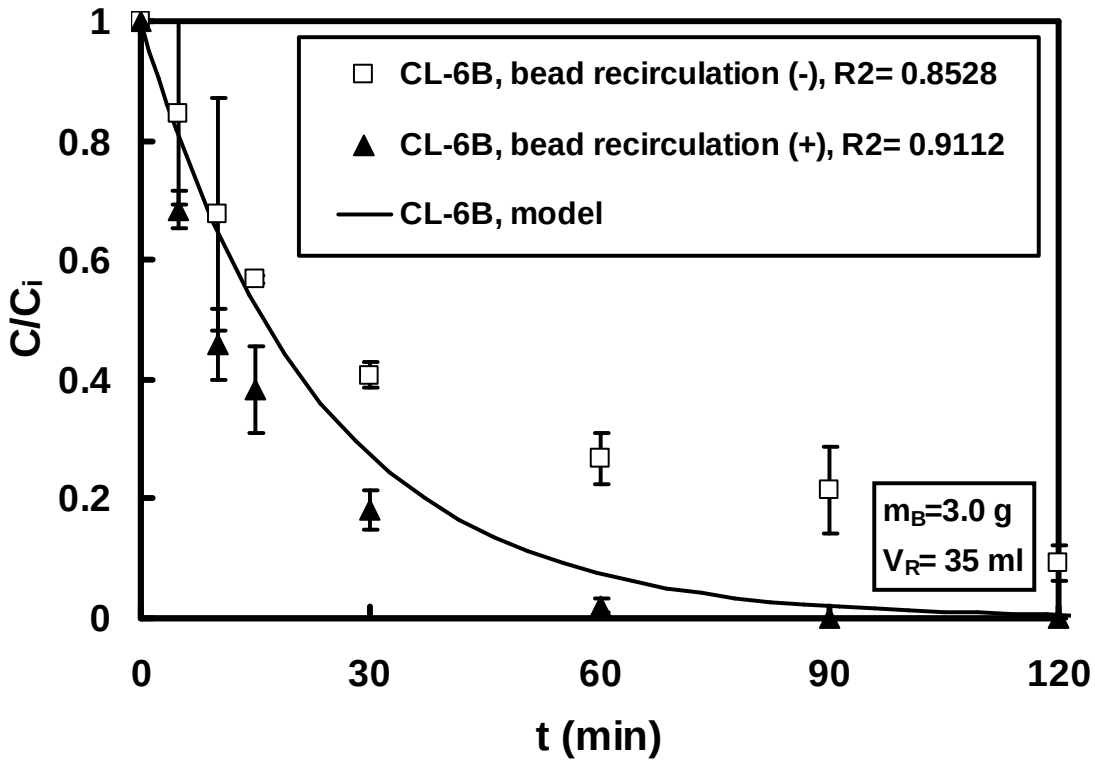

Figure 5-3: Effect of bead recirculation on clearance. Clearance was measured in presence (+) or absence (-) of bead recirculation.

ideal choice for a clinical full scale BSAF module, as our goal is to maintain the bead recirculation pathway as an integrated unit within the device, to minimize the external tubing and simplify device operation. This goal was achieved to some extent in this study by replacing the previous bead recirculation loop with a built-in porous tube which was connected to a neighboring shell port through a very short piece of tubing and a peristaltic pump **(Figure 5-6)**.

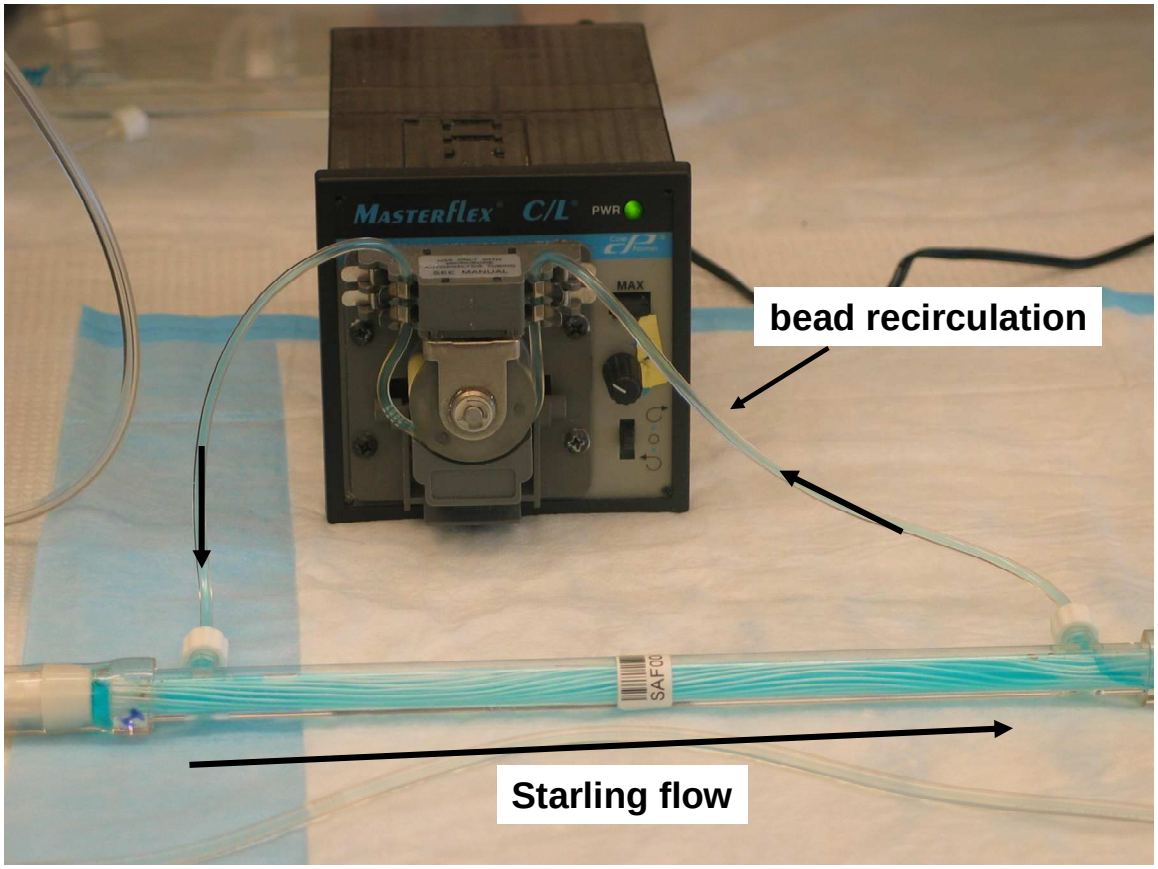

Figure 5-4: Visualization of the bead slurry position within a BSAF module, in presence of bead recirculation. The stained beads (blue) are uniformly distributed throughout the module, when beads are continuously recirculated.

Thus, the majority of the external tubing was eliminated in this design. Based on our in-vitro antibody capture data in the new BSAF modules with inner porous tubes, we concluded that a well distributed bead slurry was maintained throughout the module length.

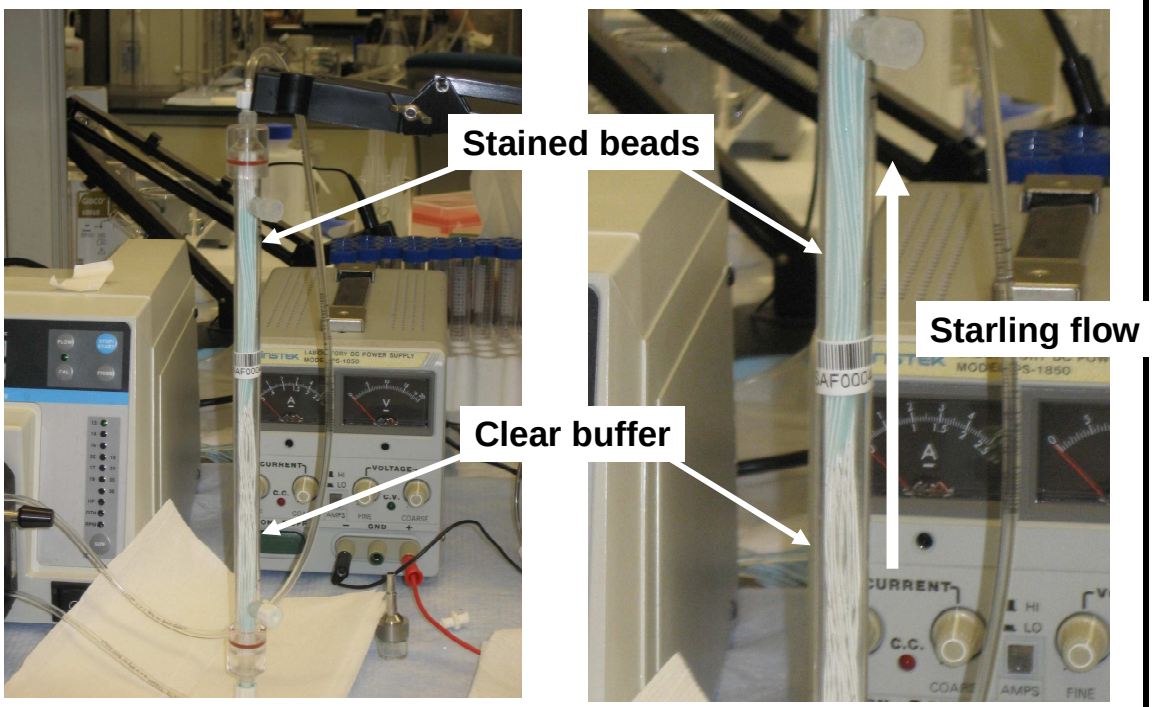

Figure 5-5: Visualization of the bead slurry position within a BSAF module, in the absence of bead recirculation. The stained beads gradually moved toward one end of the device and formed a compressed sorbent bed throughout the module end.

In addition to modification of the bead recirculation pathway, the BSAF modules with inner porous tubes in this study were appropriately scaled up from the small scale BSAF devices that we had tested in Chapter 4.0. The same antibody removal rate was observed in our fabricated small scale and intermediate scale modules. Thus we showed that we could use our mathematical model to scale up BSAF devices and accurately predict antibody capture rate in the clinical scale modules.

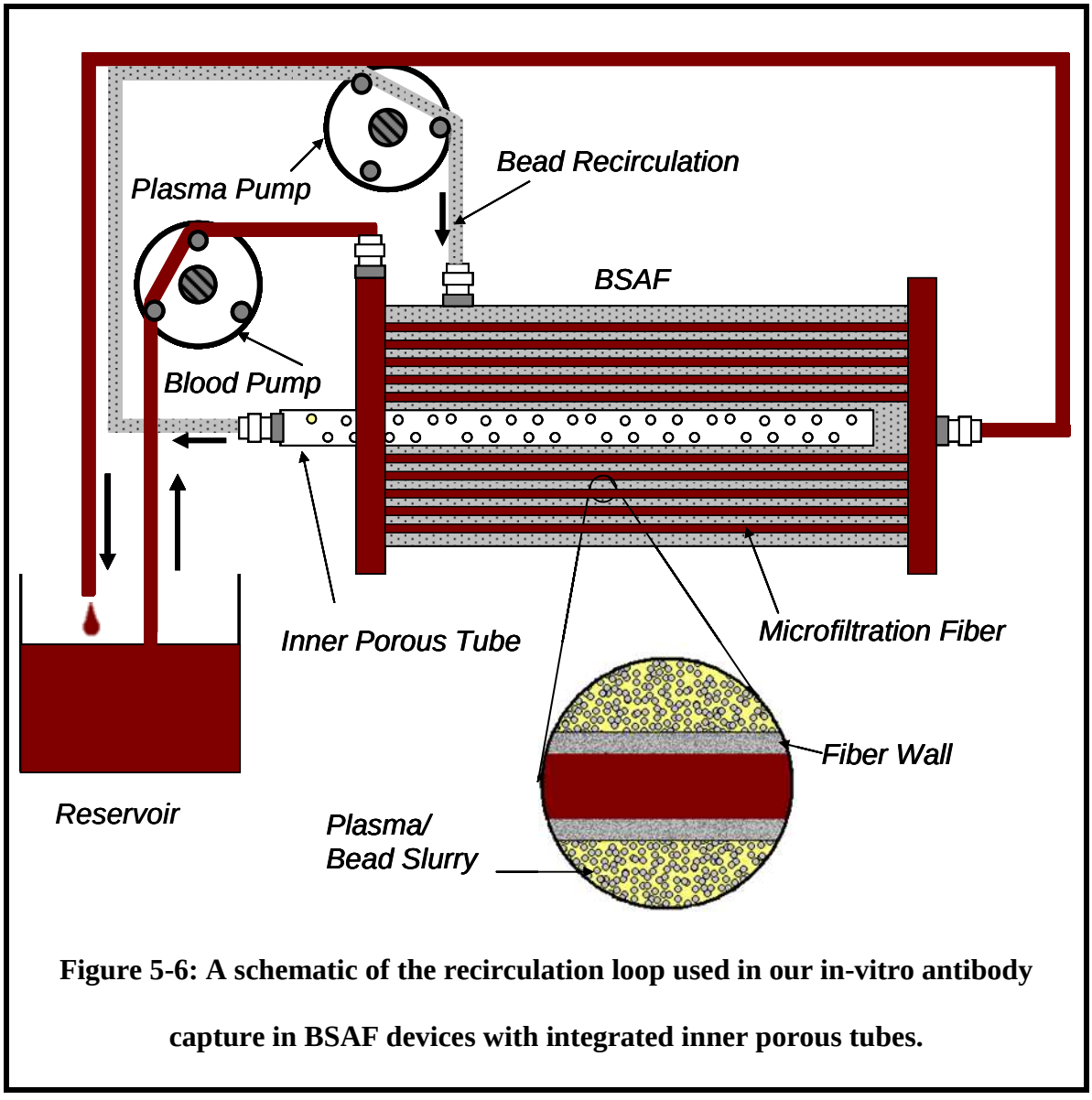

Figure 5-6: A schematic of the recirculation loop used in our in-vitro antibody capture in BSAF devices with integrated inner porous tubes.

We envision that the future generations of the BSAF devices would use the same principle to maintain efficient bead recirculation but in a more integrated fashion. **Figures 5-8 and 5-9** depict a conceptual integrated BSAF device which will allow bead recirculation and antibody capture to occur simultaneously within a single unit. The plasma pump and the external

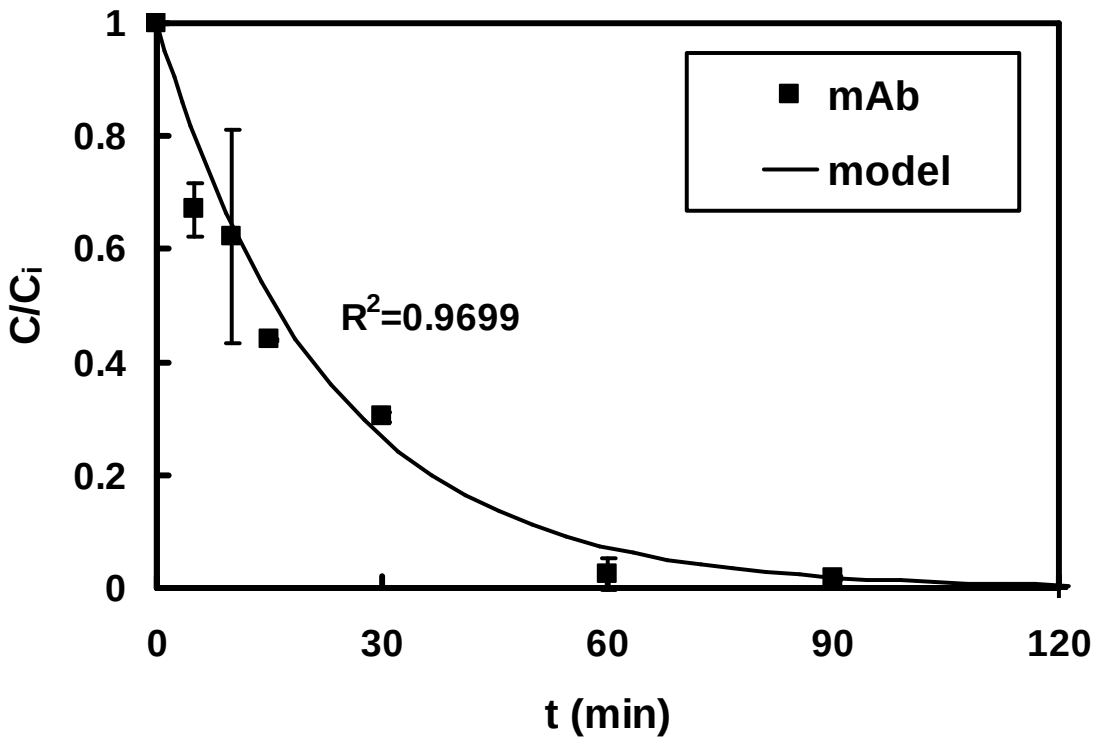

Figure 5-7: Monoclonal anti-A antibody (mAb) capture data and respective model prediction of time course of mAb removal in BSAF devices.

tubing, which were used for bead recirculation in this study, will be replaced with an integrated centrifugal pump. Through continuous rotation of an impeller, the centrifugal pump will provide

the energy to recirculate the bead slurry internally within the module. The centrifugal pump will be placed in a cavity at one end of the device (the cavity is not shown for simplicity). As the

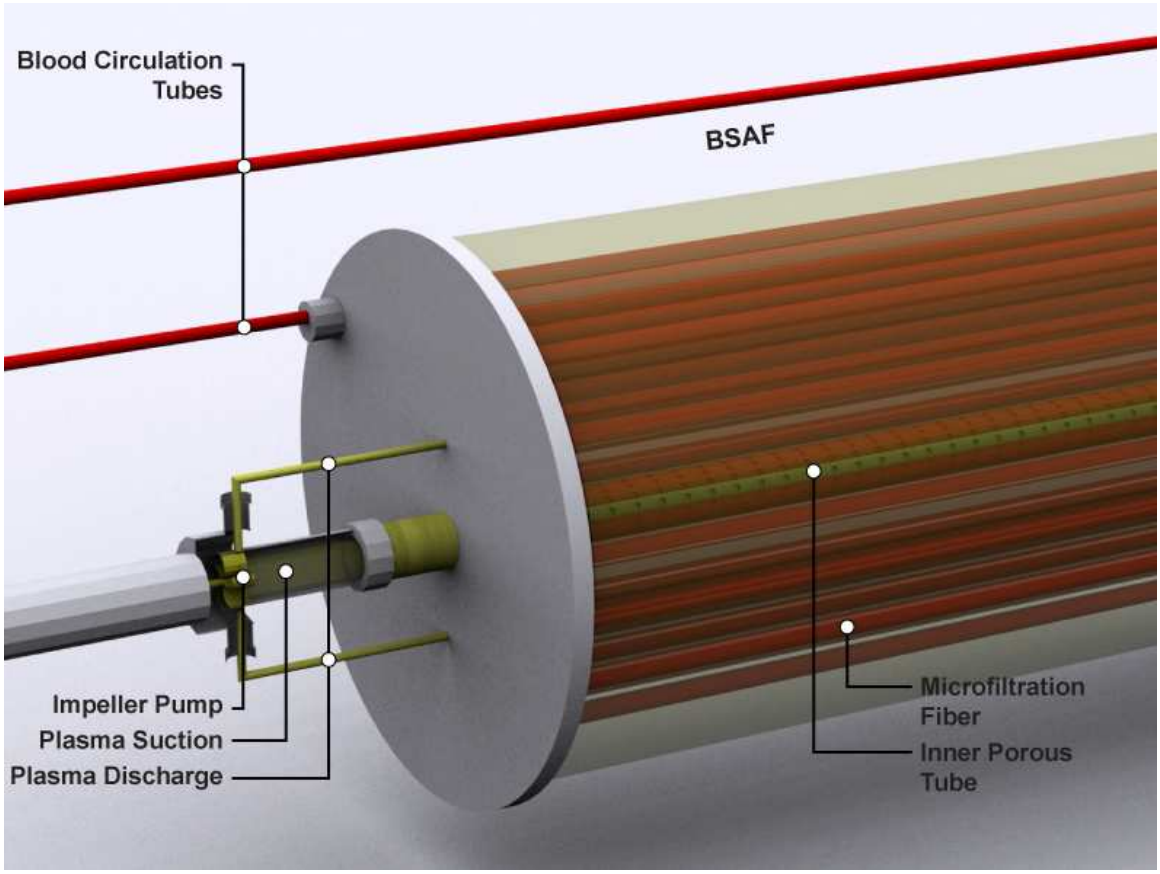

Figure 5-8: A schematic of the side view of a conceptual fully integrated BSAF device with an inner porous tube and an integrated centrifugal pump.

blades of the impeller rotate, the volume of the liquid between the blades expands and induces a sucking force to draw the bead slurry and plasma along the rotating axis through the outlet port of the inner porous tube. The rotating impeller radially accelerates the bead slurry outward and

expels the fluid into the downstream tubing, where it is pumped back into the shell **(Figure 5-9)**. Continuous rotation of the impeller provides a smooth, bead recirculation flow throughout the module length. Only one set of external pump/tubing will be required to recirculate blood through the BSAF modules.

A clinical BSAF device will be pre-packed with the bead slurry, and both inlet and outlet blood access lines will be compatible with normal hemodialysis tubing lines. Overall, the blood circuit during antibody removal in BSAF devices will be similar to a normal blood circuit set up during a hemodialysis session. Therefore antibody removal in BSAF devices could be performed in the clinical facilities which are already equipped with hemodialysis machinery. Antibody removal takes approximately two hours and one single BSAF device may be sufficient to remove antibodies from whole blood volume of an adult patient.

Antibody capture data in our fabricated BSAF prototypes with inner porous tubes have already provided us with a "proof of concept" that our envisioned integrated bead mixing mechanism will maintain the bead slurry in a uniformly distributed state. Future work should focus on experimental evaluation and characterization of the conceptualized integrated bead mixing mechanism for BSAF devices. In the following chapter, we will test antibody removal in our BSAF prototypes directly from whole blood.

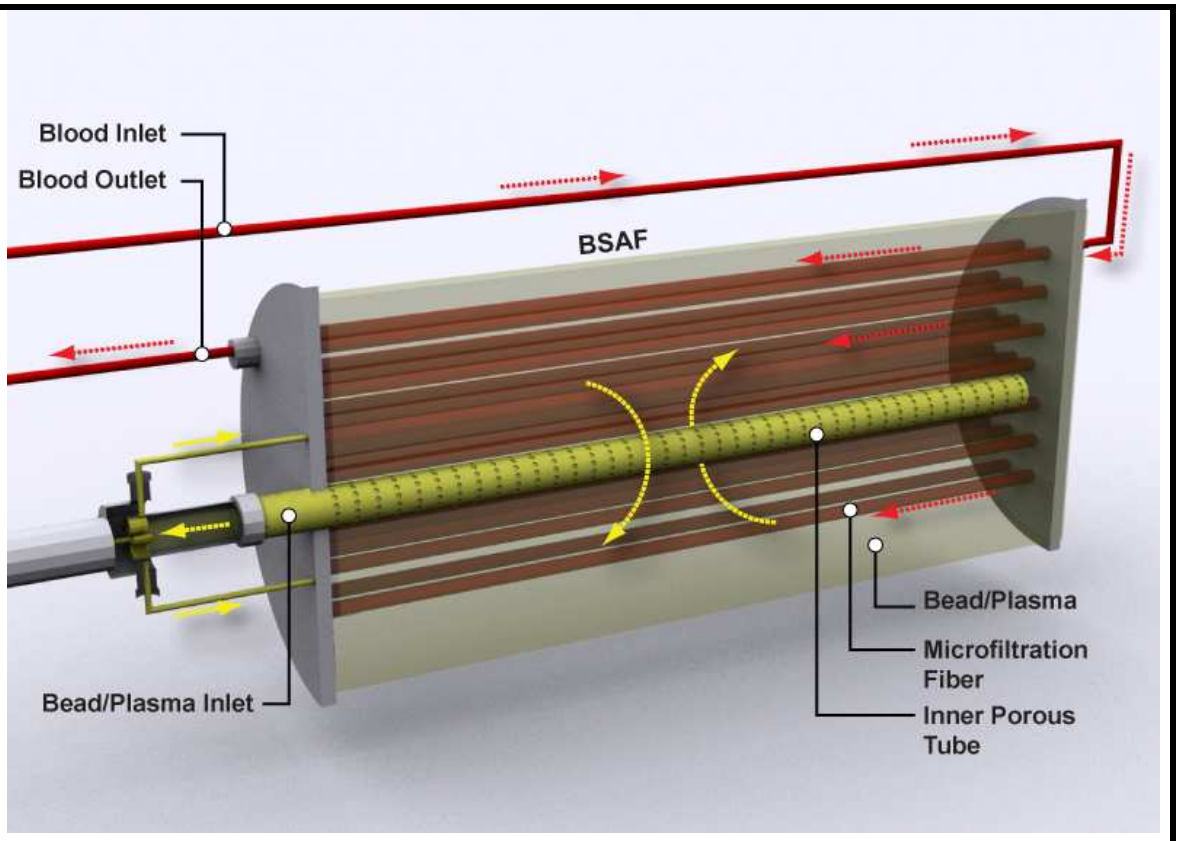

Figure 5-9: A schematic of the cross sectional side view of a conceptual fully integrated BSAF device with an inner porous tube and an integrated centrifugal pump.

Table 5-2: Description of the parameters of the mathematical model and the respective values, used to generate the model predictions of antibody capture rate in BSAF with inner porous tube.

Parameter name	Description	Baseline value
d_i	Fiber inner diameter	0.03
L	Module length	25
m_B	Mass of beads (g)	11
K	Fiber hydraulic permeability (cm/mm-Hg.min)	0.056
k_L	First order rate constant (ml/g.min)	3.27
μ	Viscosity (mm-Hg .min)	1.25×10^{-7}
Q	Volumetric flow rate (ml/min)	8.8
V_R	Reservoir volume (ml)	135

6.0 EVALUATION OF ANTI-A ANTIBODY CAPTURE FROM WHOLE HUMAN BLOOD IN INTEGRATED BEAD AND FIBER ANTIBODY FILTERS

In Chapter 4.0, we developed a simple mathematical model to predict antibody removal rate in BSAF modules based on key design and operational parameters. We used this model as a guide to design human patient-sized BSAF devices. We also fabricated scaled down prototypes of our conceptual clinical scale BSAF (small scale devices) and demonstrated that recirculation of monoclonal anti-A antibody in buffer solution through our scaled-down prototypes resulted in 100% antibody removal within two hours. In chapter 5.0, we scaled up from our small scale modules and fabricated intermediate scale devices (see **Table 5-1**) and modified the bead recirculation pathway to further integrate the bead mixing mechanism within the BSAF devices. The experimental work in Chapter 5.0 ensured both efficacy of our modified bead recirculation pathway and the capability of our mathematical model to scale up.

In this study, our goal was to evaluate the in-vitro anti-A antibody removal in our intermediate scale BSAF modules using direct hemoperfusion. We set up appropriately scaled down in-vitro blood recirculation loops, similar to that used in Chapter 5.0, and tested anti-A antibody capture in BSAF devices directly from whole human blood samples. We evaluated the capability of our BSAF devices to reduce IgM and IgG anti-A antibody titers in blood within two hours. Antibody capture specificity and dilution effects were evaluated by monitoring initial and final IgG and IgM anti-B antibody titers, total blood protein concentration and blood hematocrit.

Plasma free hemoglobin (PFHb) level was monitored throughout antibody capture experiments to detect possible device-induced hemolysis.

6.1 MATERIALS AND METHODS

6.1.1 In-Vitro Antibody Capture

Polyacrylamide glycoconjugates (Atri-pNPA^{30}) containing 20 mol% of A-trisaccharides were covalently attached within the pores of cross linked Sepharose® CL-6B beads (Sigma-Aldrich, Louis, MO) as described in section 4.2.1. BSAF modules with inner porous tubes were fabricated as described in section 5.1.2. The modules were loaded with 11 g of modified beads as described in section 5.1.4. The bead recirculation flow rate was set at 18 ml/min. Experiments were then performed to quantify antibody capture from fresh human blood samples in BSAF devices as follows: with the approval of the University of Pittsburgh Institutional Review Board (IRB), five blood samples (3 samples of type O and 2 samples of type B) were drawn from healthy, non-pregnant consenting donors over age 18. In each case, 135 ml of blood was drawn within 1 hour before initiation of an antibody capture experiment. Blood samples were individually collected in 150 ml dry blood collection bags (Jorgensen Laboratories Inc, Loveland Co), and 0.106 *M* sodium citrate anticoagulant solution (Fisher Scientific, Pittsburgh, PA) was added to each bag at a volumetric ratio of 1:10. During antibody capture experiments, the blood bags were placed in an Isotemp 202S water bath (Fisher Scientific, Pittsburgh, PA) to maintain blood temperature at 37 ^{o}C. The fiber side inlet and outlet ports were connected to the ports on the blood bags using Tygon® tubing. Blood was recirculated through the BSAF modules at a

flow rate of 8.8 ml/min by a Masterflex pump attached to the inlet tubing. Air was removed from the system while the capture loop was primed with blood. Blood samples were taken from a sampling port on the blood bags at time points 0, 15, 30, 75 and 120 minutes. Plasma was separated from blood cells by immediately spinning blood samples in a Fisher Scientific Centrific 228 centrifuge (Fisher Scientific, Pittsburgh, PA) for 30 minutes. All plasma samples were stored at -80^{o}C if not analyzed immediately. **Figure 6-1** shows the recirculation loop in antibody capture from whole blood. Blood inlet/outlet and bead/plasma inlet/outlet ports are shown in **Figure 6-2**.

6.1.2 Blood Analysis

Blood typing and measurement of anti-A/B antibody titers was performed according to standard blood bank procedures [117]. Briefly, plasma samples were serially diluted in 0.9% saline solution (Fisher Scientific, Pittsburgh, PA). All serial dilutions were given a consecutive titer step number. For example, a dilution of 1:1 corresponded to titer step 1, dilution of 1:2 corresponded to titer step 2, dilution of 1:4 corresponded to titer step 3 and so forth. One drop of A1 or B reference red blood cells (Immucore Inc., Norcross, GA) was added to each test tube and the tubes were spun for 1 minute at 3300 rpm. Tubes were then examined macroscopically for agglutination of A1 and B red blood cells, respectively. IgM anti-A and anti-B titers were recorded as the reciprocal of the largest dilutions that agglutinated A1 and B reference blood cells, respectively. Subsequently, IgG anti-A and anti-B titers were measured in the following manner: after addition of one drop of A1 or B reference red blood cells to serial dilutions of plasma, test tubes were incubated at 37^{o}C for one hour. Each test tube was then washed three times with 0.9% saline solution and after each washing step the supernatant was decanted. Two

drops of anti-IgG murine monoclonal antibody (Immucor-Gamma Biologicals Inc, Houston, TX) was added to the dry red blood cell pellet in each test tube and test tubes were centrifuged at 3300 rpm for 15 seconds. Hemagglutination was read macroscopically and IgG anti-A and anti-B titers were recorded as the reciprocal of the largest dilutions with positive agglutination of blood cells.

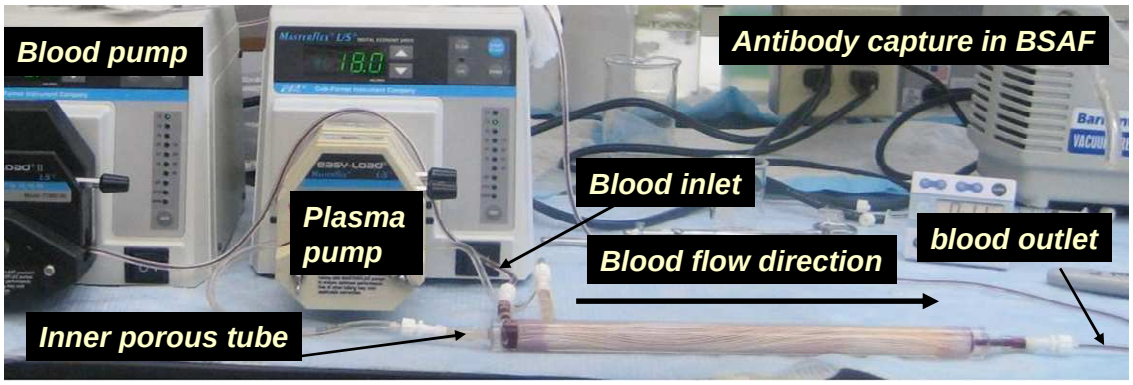

Figure 6-1: An actual experimental set up in blood recirculation through a BSAF device.

Hematocrit was measured in blood samples collected at time points 0 and 120 minutes, as described before [141]. Briefly, blood samples were collected in heparinized microcapillary tubes (Fisher Scientific, Pittsburgh, PA) and were spun in an IEC MB microhematocrit centrifuge (Damon IEC Division, Needham Heights, MA) for 5 minutes.

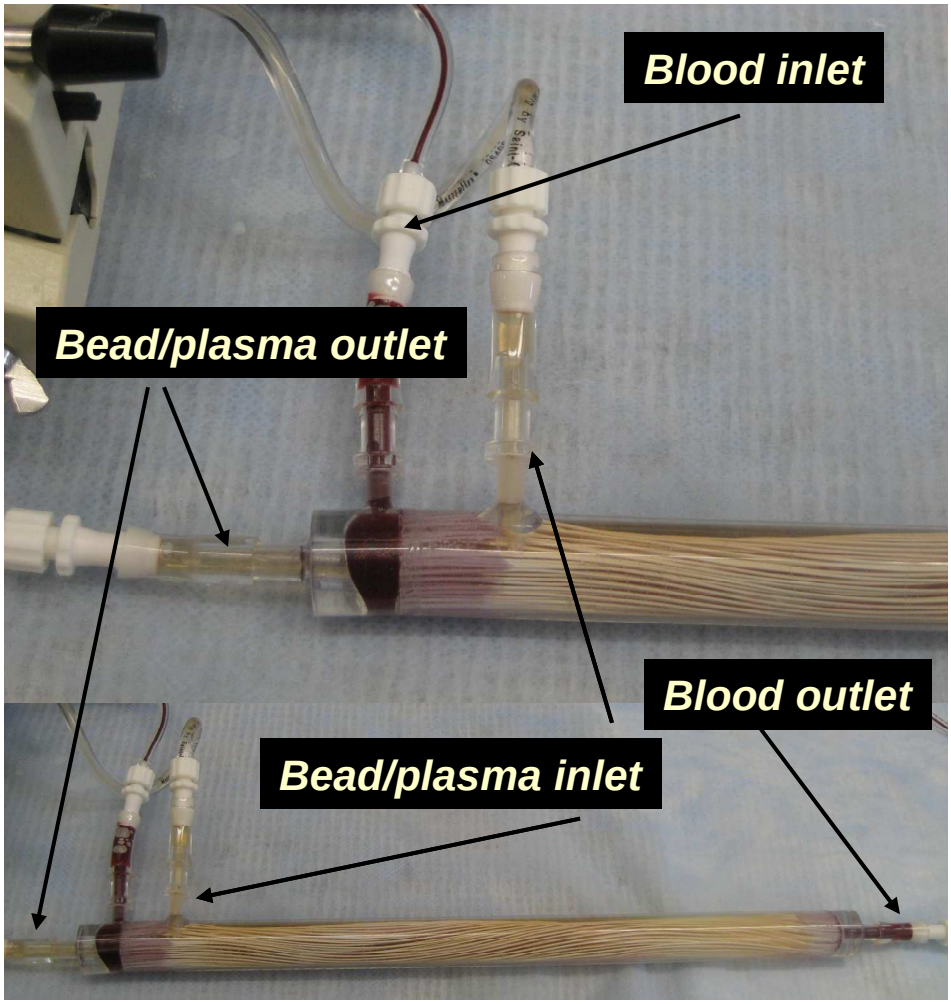

Figure 6-2: Blood inlet/outlet and bead/plasma inlet/outlet ports in blood recirculation through a BSAF device.

Hematocrit was reported as the ratio of the length of the packed erythrocytes to the total length of samples in the capillary tubes [141]. Total protein concentration was measured using Bradford protein assay (Pierce Protein Research Products, Rockford, IL). Plasma free hemoglobin (PFHb) level was measured as described elsewhere [142]. Briefly, plasma samples were spun at 10000 rpm in VWR Galaxy 7 microcentrifuge (VWR International, West Chester, PA) for 15 minutes. Light absorbance by supernatant was measured at 540 nm using a Genesys 5 UV spectrophotometer (Thermo Spectronic, Somerset, NJ). Light absorbance was converted to PFHb concentration, using reference values of known concentrations of bovine hemoglobin solution [143]. The normalized index of hemolysis (*NIH*) was calculated as previously described [144]: $NIH = \frac{\Delta Hb.V_R}{Q.t}.\frac{(100-Ht)}{100}$, where ΔHb is the change in PFHb level over time, t and V_R is the blood volume in the reservoir, Ht is blood hematocrit, and Q is the volumetric flow rate in a BSAF device.

6.1.3 Statistical Analysis

The values of IgM anti-A antibody titers over time were normalized to the corresponding initial titer in each experiment. An average normalized titer value at each time point was calculated between five blood experiments (n=5). A two-sample *t*-test was used to test the significance of the differences between the normalized IgM concentration values at times 15, 30 and 120 minutes in antibody capture from monoclonal antibody solution (n=2, data points were shown previously in **Figure 5-7**) and whole blood (n=5). A paired two-sample *t*- test was used to test the significance of differences between initial and final values of PFHb and total protein concentration, respectively (n=5). The null hypothesis in all cases was rejected for $p \leq 0.05$.

6.2 RESULTS

Antibody removal from whole blood was evaluated by measurement of changes in blood IgM and IgG anti-A antibody titers within two hours. We also evaluated antibody capture specificity and dilution effect by measurement of changes in anti-B antibody titers, total blood protein concentration and hematocrit. **Figure 6-3** shows the time course of IgM anti-A antibody capture in BSAF devices from blood and from monoclonal antibody solution (mAb). We did not observe a significant difference in antibody removal when we compared whole blood with the mAb solution ($p = 0.42$, 0.96 and 0.08 at times 15, 30 and 120 minutes, respectively). **Table 6-1** summarizes the results of blood analysis data from samples collected in five different experiments at times 0 and 120 minutes. Overall, we observed a significant reduction in IgM $(96 \pm 5\%, p < 0.001)$, and IgG $(81 \pm 18\%, p < 0.05)$ anti-A antibody titers. Blood concentration of IgM anti-A antibodies was reduced by 4.2±0.8 titer steps, dropping from an initial titer range of 8-32 to a final titer range of 0-2. Blood concentration of IgG anti-A antibodies was reduced at a slightly lower rate, by 2.8±1.1 titer steps, dropping from an initial titer range of 2-256 to a final range of 1-32. No change in IgG anti-B antibody titers was observed and nonspecific loss of IgM anti-B antibodies was not significant (reduced only by 0.7±0.6 titer steps, $p = 0.36$).

Figure 6-4 shows total plasma protein concentration in five different blood samples over time. A paired two-sample *t*- test was used to test the significance of differences between initial and final values of total protein concentration, in five different experiments (n=5). We did not observe a significant difference between the values of plasma protein concentration at time points 0 and 120 minutes ($n = 5, p = 0.22$). **Figure 6-5** shows PFHb concentration in five different blood samples over time. A paired two-sample *t*- test was used to test the significance

of differences between the initial and final values in five different experiments (n=5). No significant difference was observed between the PFHb levels at time points 0 and 120 minutes ($n = 5, p = 0.25$). The values of normalized index of hemolysis (*NIH*) for two hours of blood recirculation through BSAF devices, in five experiments, are summarized in **Table 6-1**. Blood hematocrit remained unchanged in each experiment.

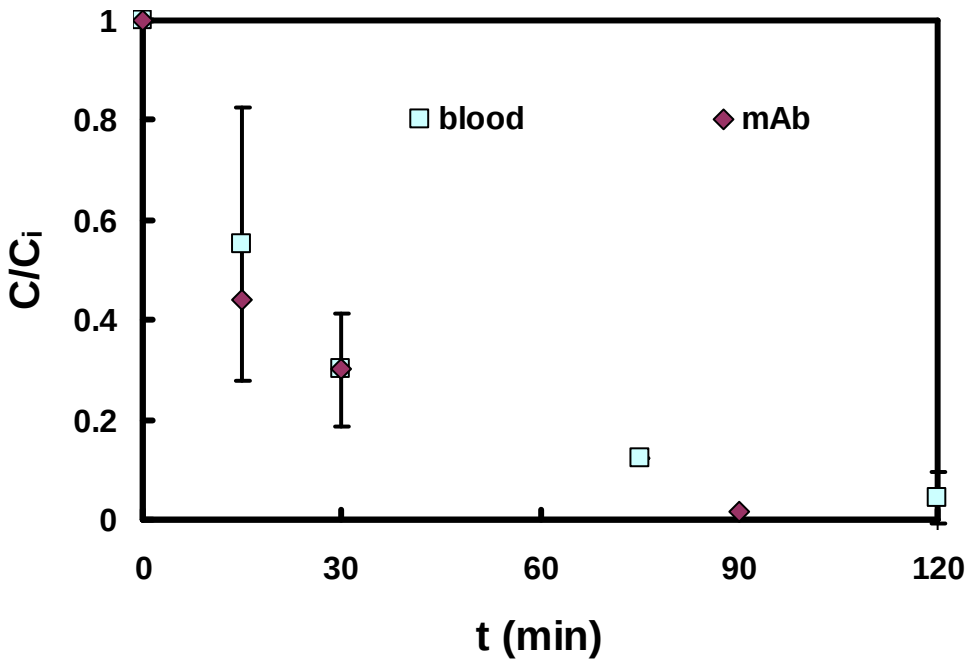

Figure 6-3: IgM anti-A antibody capture data from whole blood and from monoclonal antibody solution (mAb).

6.3 DISCUSSION

Removal of anti-A/B antibodies from blood in the peri-transplantation period significantly reduces the risk of humoral mediated rejection of an ABO-incompatible transplanted organ [3]. We are developing an extracorporeal antibody filter (BSAF) to specifically remove anti-A/B antibodies directly from whole blood. BSAF devices are cartridges containing microfiltration hollow fibers with antibody capturing beads continuously recirculating in the fiber interstitial spaces. We used our mathematical model of antibody removal in BSAF devices and in-vitro anti-A antibody capture from monoclonal antibody solution to design BSAF modules capable of depleting up to 100% of reservoir anti-A antibody concentration within two hours. However, since the model was primarily developed and validated for a simplified case of antibody removal from monoclonal antibody solution, further evaluation was necessary to show applicability of our BSAF devices in antibody removal directly from whole blood. In this study we set up in-vitro blood recirculation loops with parameters scaled down in equal proportions from typical clinical values and tested anti-A antibody removal rate. Our studies showed that IgM and IgG anti-A antibody titers in blood were specifically decreased by 96±5% and 81±18%, respectively, within two hours.

From a clinical standpoint, most centers target a pre-transplantation IgM anti-A/B antibody titer of 1:8 or below [20]. On the other hand, in some studies, IgG anti-A/B antibody titers of 1:32 or even higher did not adversely affect the result of ABO-incompatible transplantation [20, 84]. In our study, despite the wide range of initial antibody titers, we were able to reduce both IgM and IgG anti-A antibodies to 1:2 and 1:32 or below, respectively. Hence, our BSAF devices met our goal in achieving clinically acceptable pre-transplantation anti-A antibody titers. We understand that the final antibody titers and the duration of antibody capture

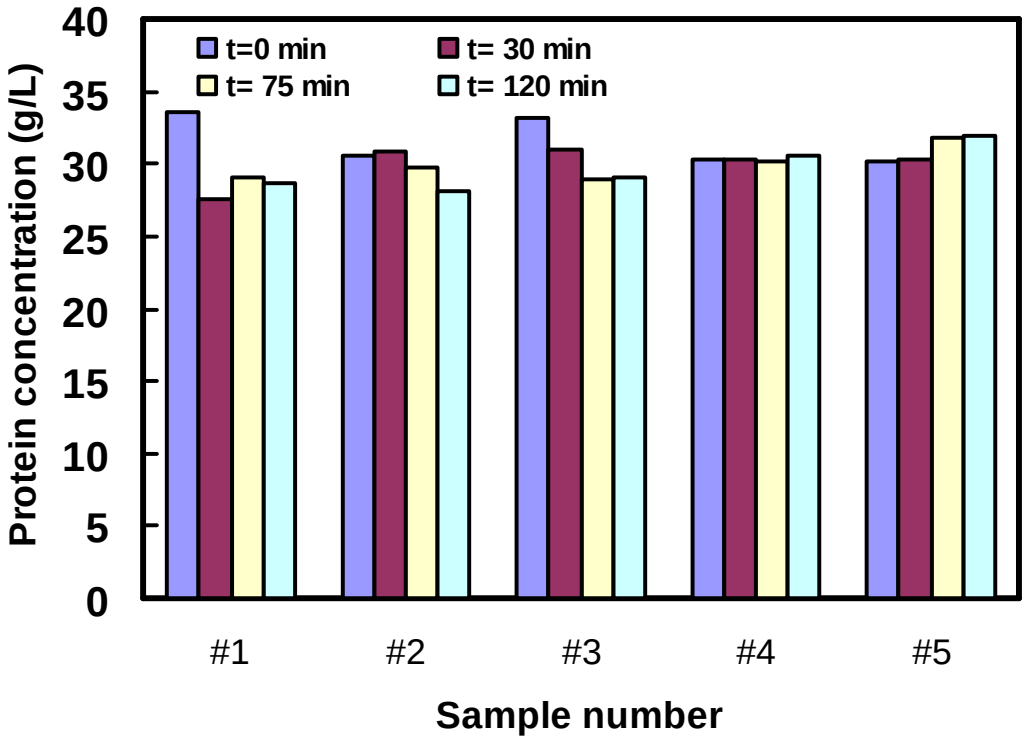

Figure 6-4: Total plasma protein concentration over time in 5 different blood samples.

may vary in an in-vivo setting. Patients with an initial antibody titer greater than 1:128 and a high titer rebound capability may require more than one session of antibody removal to meet the target antibody titer of 1:8 or below.

In this study, the concentration of IgM and IgG anti-A antibodies was reduced by an average of 4.2±0.8 and 2.8±1.1 titer steps, respectively. Thus, compared to other previously developed anti-A/B specific immunoadsorption devices, our BSAF modules showed comparable capability in reducing antibody titers. Rieben et al. reported an average of 4 titer step reduction in IgM anti-A antibodies in plasma recirculating through BioSorbent A and B columns [24]. Rydberg et al. showed 2 and 4 titer step reduction in IgM and IgG anti-A antibodies, respectively, during in-vitro plasma perfusion through Glycosorb® columns [25]. However, during each session of in-vivo plasma immunoadsorption through Glycosorb® devices, both IgG and IgM anti-A antibody titers were dropped by an average of 2 titer steps [93]. Additionally, similar to BioSorbent A [24] and Glycosorb® columns [25], our BSAF devices selectively removed anti-A antibodies and did not cause significant change in total plasma protein concentration. Previously, Rieben et al. showed negligible nonspecific adsorption of immunoglobulins on BioSorbent A and B columns [24]. In biocompatibility testing of Glycosorb® columns, Rydberg et al. reported no significant change in total serum albumin or total IgG, IgA, or IgM levels [25]. Although antibody removal capacity of the BSAF is comparable to these columns, the main advantage of the BSAF is its simplicity. Unlike conventional immunoadsorption columns, a separate plasmapheresis unit is not required prior to immunoadsorption. Eliminating the need for plasma separation simplifies extracorporeal perfusion and eliminates the hemodynamic instabilities that can be associated with plasmapheresis.

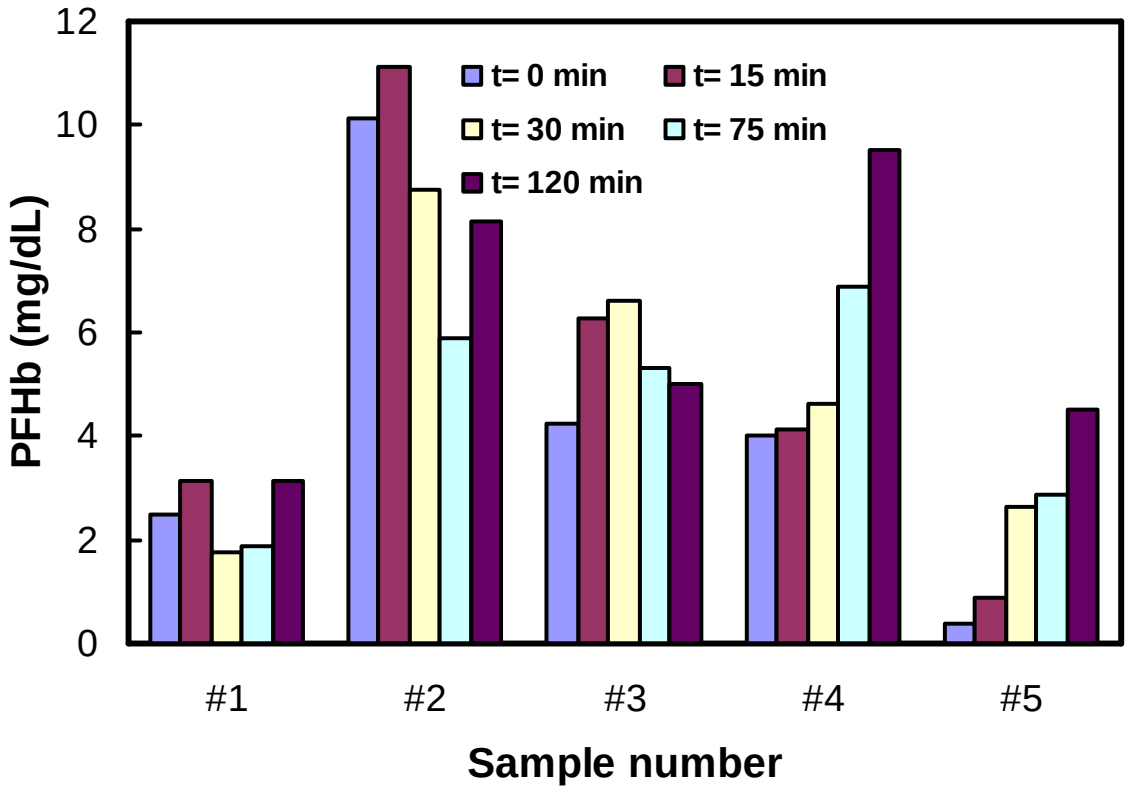

Figure 6-5: Plasma free hemoglobin (PFHb) concentration over time in 5 different blood samples.

We observed some inconsistencies between the numbers of titer steps reduced in different blood samples. For example, an initial anti-A antibody titer of 1:16 was reduced once by 5 titer steps and by only 3 titer steps in another blood sample. An initial antibody titer of 1:32 was reduced by 6 titer steps, whereas another blood sample with a lower initial antibody titer of 1:16 was reduced by 5 titer steps in another case. As all antibody capturing beads in this study were modified and prepared in one batch, variations in antibody binding capacity of the beads are not

Table 6-1: Analysis of initial (t=0) and final (t=120) blood samples in five different experiments.

Sample Number/ Blood Type	Anti-A (IgM) titer initial / final	Anti-A (IgG) titer initial / final	Anti-B (IgM) titer initial / final	Anti-B (IgG) titer initial / final	Hematocrit (%) initial / final	Plasma Free Hemoglobin (mg/dl) initial / final	Total Protein (g/dl) initial / final	Normalized Index of Hemolysis (NIH) (mg/dL)
1/B	1:8/0	1:2/1:1	N/A	N/A	25/25	2.5/3.1	3.4/ 2.9	0.06
2/B	1:16/0	1:16/1:1	N/A	N/A	37/37	10.1/8.1	3.1 / 2.8	-0.16
3/O	1:32/1:2	1:256/1:32	1:16/1:8	1:32/1:32	42/42	4.2/5.0	3.3 / 2.9	0.05
4/O	1:16/1:2	1:64/1:8	1:1/0	1:8/1:8	39/39	4.0/9.5	3.0 / 3.1	0.43
5/O	1:32/1:1	1:64/1:8	1:16/1:16	1:64/1:64	43/43	0.4/4.5	3.0/ 3.2	0.3

responsible for the observed inconsistencies in antibody removal patterns from various blood samples. Furthermore, the BSAF modules were designed to maintain an excess of anti-A antibody binding sites compared to the normal range of antibody concentrations in blood. One possible explanation is that the remaining anti-A antibody population in blood samples simply did not recognize or had low affinity for A-trisaccharide epitopes. Some previous studies have suggested that a small population of anti-A antibodies require a fourth sugar in the core

composition of A-tetrasaccharide epitopes for a high affinity binding interaction [145]. Complete removal of all anti-A antibodies from blood samples may therefore require use of a combination of A-trisaccharide and A-tetrasaccharide polyacrylamide glycoconjugates as the synthetic antigens in our device. Additionally, BSAF devices were more effective in removing IgM than IgG isotype. This difference could be attributed to the capability of IgM anti-A antibodies to form multivalent and hence more stable binding interactions with closely spaced immobilized Atrisaccharide-polyacrylamide antigens. IgM antibodies also form more stable complexes with C1 molecules (a prerequisite of complement activation) and are therefore considered the most potent antibody isotype in activation of the complement cascade [3].

Because the BSAF is perfused directly with whole blood, it was important to show that blood flow through our devices was not associated with a significant level of hemolysis. Although in our experiments the concentration of PFHb in different blood samples changed over time, a statistical analysis showed no significant change between initial and final values over all five blood experiments. The maximum increase in the PFHb concentration after two hours of blood recirculation through the BSAF devices was observed in blood sample #4, which showed a 5.5 mg/dL increase in PFHb concentration after two hours. Approximately 5 mg/dL/hr of PFHb can be removed by reticuloendothelial system in adult patients [146] and in humans a renal clearance of 12 mg/dL/hr is possible [146]. Therefore, the levels of increase in PFHb concentrations in this study were within the physiologically tolerable range [146]. Additionally the averaged normalized index of hemolysis (*NIH*) for two hours of blood recirculation through BSAF modules was 0.14 mg/dL (*NIH* values ranged between -0.16 and 0.43), which was comparable to the previously reported levels of *NIH* values for other blood contacting medical devices (typically <0.2 mg/dL) [144, 147]. In summary our study showed no significant evidence

of hemolysis or change in total plasma protein concentration. A more extensive evaluation of the biocompatibility of the BSAF, which will involve a larger number of blood samples (>10), needs to be performed in our future studies. Previously Rieben et al. [24] and Rydberg et al. [25] established the biocompatibility of plasma immunoadsorption in Biosorbent A and B and Glycosorb® columns, respectively. The BSAF is similar to these columns because only plasma comes into contact with the antibody adsorbing beads, which are the same materials found in both Biosorbent A and Glycosorb columns. Therefore, we would expect that BSAF devices show comparable biocompatibility data to these devices.

We observed close agreement between antibody capture data from whole blood and from mAb solution. This was contradictory to our approximation of 20-25% increase in Starling flow rate for blood flow through BSAF modules, compared to flow of mAb solution. One possible explanation is that fiber hydraulic permeability decreases during whole blood flow through the fibers, compared to flow of the monoclonal antibody solution. A decrease in fiber hydraulic permeability during whole blood flow has been linked to protein deposition and adherence of platelets and leukocytes on to the membranes [148]. As we did not observe a significant difference in total protein concentration in our studies, we do not believe that protein deposition would have been responsible for a decrease in fiber hydraulic permeability. Conversely, platelet adhesion to the fibers has been reported in blood flow through membranes when blood is not heparinized [148]. Scanning electron microscopy on the luminal surfaces of the fiber could detect adhered platelets and further confirm this theory. Additionally, direct measurement of model parameters (including fiber hydraulic permeability, first order rate constant and viscosity) in blood perfusion through BSAF devices could show the applicability of our developed mathematical model to a whole blood system.

In summary, we have developed a new antibody filtration device containing microfiltration fibers with antibody capturing beads integrated within the interstitial fiber space (BSAF device). The BSAF was capable of selectively removing clinically relevant levels of blood group antibodies from blood in a two hour time period and in a simple one step process. In our future studies we will establish the efficacy and biocompatibility of the BSAF in an in-vivo set up.

7.0 CONCLUSIONS

1. We conjugated blood group A-trisaccharide antigens to high (1000-2000 kDa) and low (30-50 kDa) molecular weight polyacrylamide spacers. The glycoconjugate interactions with anti-A antibodies were studied using surface plasmon resonance. The high molecular weight glycoconjugate (Atri-PAA^{1000}-biotin) enhanced antibody binding capacity by two to three fold compared to the low molecular weight conjugate (Atri-PAA^{30}-biotin), whereas varying the carbohydrate content in Atri-PAA^{1000}-biotin (20 mol% or 50 mol%) did not affect antibody binding capacity of the glycoconjugate. We concluded that with this estimated increase in capacity, a fiber based SAF device with a surface area of about 1.5 to 2 m^2 would provide sufficient capacity for 100% antibody capture from blood in a single device.
2. We introduced an antibody filtering device based on integrated microfiltration fibers with affinity beads distributed in the interstitial fiber space. We developed a simple mathematical model to guide the choice of key design and operational parameters for a clinical BSAF device. The model demonstrated that for a given flow rate and reservoir volume, antibody removal rate in a BSAF was dependent on the magnitude of a lumped parameter, $k_L m_B / Q_s$. This term characterizes the ratio of antibody uptake rate by the beads to the Starling flow rate in the device. Three distinct antibody removal regimes were observed with the following approximate boundaries: diffusion limited ($k_L m_B / Q_s \le 1$), intermediate ($1 < k_L m_B / Q_s < 10$) and perfusion limited ($k_L m_B / Q_s \ge 10$). In diffusion limited regime ($k_L m_B / Q_s \le 1$) antibody

removal rate primarily depends on antibody diffusion to the binding sites within the porous beads. Hence, antibody removal rate in the diffusion limited regime increases substantially as $k_L m_B / Q_s$ increases, but changes insignificantly in relation to an increase in Starling flow rate relative to the reservoir volume (Q_s / V_R). Antibody removal is perfusion limited when $k_L m_B / Q_s \geq 10$. In a perfusion limited regime antibody removal rate is solely dependent on the magnitude of Starling flow rate relative to the reservoir volume (Q_s / V_R). No significant increase in the antibody removal rate is expected by further increasing the magnitude of $k_L m_B / Q_s$ in a perfusion limited regime. An intermediate regime $(1 < k_L m_B / Q_s < 10)$ is distinguished in which antibody removal rate is affected by a combination of antibody diffusion and Starling flow rate in the device.

3. Key model predictions were in close agreement with experimental data obtained in in-vitro monoclonal anti-A antibody capture from buffer solution in BSAF devices. Additionally, the model provided a good approximation of antibody removal rate from whole blood.
4. We used the model to conceptually design a BSAF device capable of a clinically relevant rate of anti-A removal. Small and intermediate size BSAF devices (both appropriately scaled down from the "clinical" BSAF) were fabricated and tested in capture of anti-A from a buffer solution. Both sets of devices depleted 100% of reservoir anti-A antibody concentration within two hours.
5. We set up in-vitro blood recirculation loops with parameters scaled down from clinically relevant values and tested anti-A antibody removal from whole human blood in BSAF devices. A significant reduction in IgM $(96 \pm 5\%, p < 0.001)$, and IgG $(81 \pm 18\%, p < 0.05)$ anti-A antibody titers was observed within two hours. Overall, we observed a drop of 4.2±0.8 and 2.8±1.1 titer steps in IgM and IgG anti-A antibody titers, respectively. No significant

change in hematocrit, total plasma protein concentration, plasma free hemoglobin and anti-B antibody levels was observed. The normalized index of hemolysis (*NIH*) was 0.14±0.23 mg/dL. In conclusion, BSAF devices effectively, specifically and safely removed anti-A antibodies directly from whole blood.

6. We demonstrated that to achieve an antibody removal rate in agreement with the model prediction, it was crucial to maintain a well mixed and uniformly distributed bead slurry in the interstitial fiber space. In the absence of a bead mixing mechanism, antibody removal rates were slower than predicted by our mathematical model due to the Starling flow continuously pushing the beads toward one end of the device. We fabricated BSAF modules with integrated inner porous tubes and tested these modules in capture of anti-A antibodies. The BSAF modules with inner porous tubes were simplified prototypes of our envisioned integrated BSAF devices. Antibody capture data in these modules provided the "proof of concept" for our proposed BSAF devices with integrated bead mixing mechanism.
7. Future work should focus on experimental evaluation and characterization of the conceptualized integrated bead mixing mechanism for BSAF devices.
8. The work presented here may be easily applied to design blood purification devices for removal of other biomolecules from blood. Examples of such applications are in treatment of autoimmune diseases, hypercholesterolemia, liver failure and sepsis.

BLBLIOGRAPHY

1. Cohen D.J., et al., *Kidney and pancreas transplantation in the United States, 1995-2004.* Am. J. Transplant. , 2006. **6**(5 Pt 2): p.1153.
2. Tydén G., *The European Experience* . Transplantation. 2007. **84** (12 Suppl):S.2.
3. Platt J.L., *Antibodies in graft rejection.* Transplant Immunology., 1995. New York: Wiley-Liss. p.113.
4. Rydberg L., *ABO-incompatibility in solid organ transplantation.* Transfusion Medicine, 2001. **11**(4): p.325.
5. Watkins W.M., *The ABO blood group system: historical background.* Transfusion Medicine, 2001. **11**(4): p. 243.
6. Goldsby R.A., et al., *Immunology*. 5th ed. 2003, New York: W.H. Freeman and Company.
7. Stegall M., *ABO-incompatible liver transplant: is it justifiable?.* Liver Transpl. , 2003 **9**(1): p. 31.
8. Alexandre G. P., et al., *Human ABO-incompatible living donor renal homografts.* Neth. J. Med., 1985. **28**(6): p. 231.
9. Bannett A.D., et al., *Experiences with known ABO-mismatched renal transplants.* Transplant Proc., 1987. **19**(6): p. 4543.
10. Tanabe K. , et al., *Long-term results of ABO-incompatible living kidney transplantation: a single-center experience.* Transplantation, 1998. **65**(2): p. 224.
11. Squifflet J., et al., *Lessons learned from ABO-incompatible living donor kidney transplantation: 20 years later.* Exp. Clin. Transplant. , 2004 **2**(1): p. 208.
12. Toma H. , et al., *Long-term outcome of ABO-incompatible renal transplantation.* Urol. Clin. North. Am., 2001 **28**(4): p. 769.
13. Boberg K.M., et al., *ABO-incompatible deceased donor liver transplantation with the use of antigen-specific immunoadsorption and anti-CD20 monoclonal antibody.* Clin. Transplant., 2006. **20**(2): p. 265.
14. Donauer J., et al., *ABO-incompatible kidney transplantation using antigen-specific immunoadsorption and rituximab: a single center experience.* Xenotransplantation. 2006. **13**(2): p. 108.

15. Hanto D.W, et al, *ABO-incompatible liver transplantation with no immunological graft losses using total plasma exchange, splenectomy, and quadruple immunosuppression: evidence for accommodation.* Liver. Transpl. , 2003. **9**(1): p. 22.

16. Mor, E., et al., *Successful use of an enhanced immunosuppressive protocol with plasmapheresis for ABO-incompatible mismatched grafts in liver transplant recipients.* Transplantation, 1995. **59**(7): p. 986.

17. Norden, G. , et al., *ABO-incompatible live donor renal transplantation using blood group A/B carbohydrate antigen immunoadsorption and anti-CD20 antibody treatment.* Xenotransplantation, 2006. **13**(2): p. 148.

18. Skogsberg, U., et al., *Adult ABO-incompatible liver transplantation, using A and B donors.* Xenotransplantation, 2006. **13**(2): p. 154.

19. Troisi, R., et al., *ABO-mismatch adult living donor liver transplantation using antigen-specific immunoadsorption and quadruple immunosuppression without splenectomy.* Liver. Transpl. , 2006. **12**(9): p. 1412.

20. Beimler J. , et al., *ABO-incompatible transplantation--a safe way to perform renal transplantation?* Nephrol. Dial. Transplant. , 2007. **22**(1): p. 25.

21. Tanabe K., et al., *ABO-incompatible living kidney donor transplantation: results and immunological aspects.* Transplantation Proceedings, 1995. **27**(1): p. 1020.

22. Gloor J.M., et al., *ABO-incompatible kidney transplantation using both A2 and non-A2 living donors.* Transplantation, 2003 **75**(7): p. 971.

23. Ishida H., et al., *Anti-AB titer changes in patients with ABO incompatibility after living related kidney transplantations: survey of 101 cases to determine whether splenectomies are necessary for successful transplantation.* Transplantation, 2000. **70**(4): p. 681.

24. Rieben R., et al., *In vitro evaluation of the efficacy and biocompatibility of new, synthetic ABO immunoabsorbents.* Transplantation, 1995. **60**(5): p. 425.

25. Rydberg, L. et al., *In vitro assessment of a new ABO immunosorbent with synthetic carbohydrates attached to sepharose.* Transpl. Int., 2005. **17**(11): p. 666.

26. Bouget J., et al., *Plasma exchange morbidity in Guillain-Barre syndrome: results from the French prospective, randomized, multicenter study.* Crit. Care Med., 1993. **21**(5): p. 651.

27. Madore F., *Plasmapheresis. Technical aspects and indications.* Crit. Care Clin., 2002. **18**(2): p. 375.

28. Reimann P.M., et al., *Plasmapheresis: technique and complications.* Intensive Care Med. 1990. **16**(1): p. 3.

29. Ash S.R., et al., *Sorbent suspensions vs. sorbent columns for extracorporeal detoxification in hepatic failure.* Ther. Apher. Dial. , 2006. **10**(2): p. 145.

30. Xu Y., et al., *Removal of anti-porcine natural antibodies from human and nonhuman primate plasma in vitro and in vivo by a Galalpha1-3Galbeta1-4betaGlc-X immunoaffinity column.* Transplantation, 1998. **65**(2): p. 172.

31. Hout M.S., et al., *Specific removal of anti-A and anti-B antibodies by using modified dialysis filters.* ASAIO Journal, 2000. **46**(6): p. 702.

32. Gautam S., et al., *Monoclonal anti-A antibody removal by synthetic A antigen immobilized on specific antibody filters.* Biotechnology and Bioengineering, 2008. **99**: p. 876.

33. Hout M.S., et al., *Mathematical and experimental analyses of antibody transport in hollow-fiber-based specific antibody filters.* Biotechnology Progress, 2003. **19**(5): p. 1553.

34. Brandt S, et al., *Membrane based affinity technology for commercial scale purifications.* Bio/Technology, 1988. **6**: p. 779.

35. Springer G.F., et al., *Blood group isoantibody stimulation in man by feeding blood group-active bacteria.* J. Clin. Invest. , 1969. **48**(7): p. 1280.

36. Alberts B., et al., *Molecular Biology of The Cell*. 4th edition ed. 2002. New York: Garland Science.

37. Voet D., et al., *Fundamentals of Biochemistry*. Upgrade edition. 2002. John Wiley & Sons, Inc.

38. Platt J., *The immunological barriers to xenotransplantation.* Crit. Rev. Immunol. , 1996. **16**(4): p. 331.

39. Galili U., *Immune response, accommodation, and tolerance to transplantation carbohydrate antigens.* Transplantation, 2004. **78**(8): p. 1093.

40. Daniels, G., *The molecular genetics of blood group polymorphism.* Transpl Immunol. , 2005. **14**(3-4): p. 143.

41. Thorpe S.J., et al., *Expression of ABH blood group antigens in human heart tissue and its relevance to cardiac transplantation.* Transplantation , 1991. **51**(6): p. 1290.

42. Kaneko M., et al., *Molecular characterization of a human monoclonal antibody to B antigen in ABO blood type.* Immunol. Lett., 2003. **86**(1): p. 45.

43. Ratner B.D., et al., *Biomaterials Science: An Introduction to Materials in Medicine*. second edition ed. 2004. China: Elsevier Academic Press.

44. Platt J.L., *The barrier to xenotransplantation.* Transplantation, 1991. **52**(6): p. 937.

45. Cooper D., *Depletion of natural antibodies in non-human primates--a step towards successful discordant xenografting in humans.* Clin Transplant. , 1992 **6** (3 part 1): p. 178.

46. Cooper DK, et al., *Identification of alpha-galactosyl and other carbohydrate epitopes that are bound by human anti-pig antibodies: relevance to discordant xenografting in man.* Transpl Immunol. , 1993**. 1**(3): p. 198-205.

47. Lai L., et al., *Production of alpha-1,3-galactosyltransferase knockout pigs by nuclear transfer cloning.* Science , 2002. **295** (5557): p.1089.

48. Phelps C.J., et al., *Production of alpha 1,3-galactosyltransferase-deficient pigs.* Science., 2003. **299** (5605): p. 411.

49. Neethling F.A., et al., *Protection of pig kidney (PK15) cells from the cytotoxic effect of anti-pig antibodies by alpha-galactosyl oligosaccharides.* Transplantation , 1994. **57**(6): p. 959.

50. Ye Y., et al., *Evidence that intravenously administered alpha-galactosyl carbohydrates reduce baboon serum cytotoxicity to pig kidney cells (PK15) and transplanted pig hearts.* Transplantation , 1994. **58**(3): p. 330.

51. Taniguchi S., et al., *In vivo immunoadsorption of antipig antibodies in baboons using a specific Gal(alpha)1-3Gal column.* Transplantation, 1996. **62**(10): p. 1379.

52. Kozlowski T., et al., *Anti-Gal(alpha)1-3Gal antibody response to porcine bone marrow in unmodified baboons and baboons conditioned for tolerance induction.* Transplantation, 1998 **66**(2): p. 176.

53. Soares M.P., et al., *Accommodation.* Immunol Today. , 1999. **20** (10): p. 434.

54. Brouard S., et al., *Long-term survival of hamster-to-rat cardiac xenografts in the absence of a Th2 shift.* Transplantation , 1998. **65**(12): p. 1555.

55. Yuzawa Y., et al., *Interaction of antibody with Forssman antigen in guinea pigs. A mechanism of adaptation to antibody- and complement-mediated injury.* Am J Pathol. , 1995. **146**(5): p. 1260.

56. West L.J., et al., *ABO-incompatible heart transplantation in infants.* N. Engl. J. Med., 2001. **344**(11): p. 793.

57. Alexandre G.P., et al., *Human ABO-incompatible living donor renal homografts.* Neth. J. Med., 1985. **28**(6): p. 231.

58. Bannett A.D., et al., *Experiences with known ABO-mismatched renal transplants.* Transplant. Proc. , 1987. **19**(6): p. 4543.

59. Ross C.N., et al., *Renal transplantation following immunoadsorption in highly sensitized recipients.* Transplantation , 1993. **55**(4): p. 785.

60. Sonnenday C.J., et al., *Preemptive therapy with plasmapheresis/intravenous immunoglobulin allows successful live donor renal transplantation in patients with a positive cross-match.* Transplant. Proc. , 2002. **34**(5): p. 1614.

61. Porter K., *The effects of antibodies on human renal allografts.* Transplant Proc. , 1976. **8**(2): p. 189.

62. Economidou J., et al., *Quantitative measurements concerning A and B antigen sites.* Vox Sang. , 1967. **12**(5): p. 321.

63. Rydberg L., et al., *Blood group ABO-incompatible (A2 to O) kidney transplantation in human subjects: a clinical, serologic, and biochemical approach.* Transplant Proc. , 1987. **19**(6): p. 4528.

64. Nelson P.W., et al., *Ten-year experience in transplantation of A2 kidneys into B and O recipients.* Transplantation. , 1998. **65**(2): p. 256.

65. Alkhunaizi A.M., et al., *Renal transplantation across the ABO barrier using A2 kidneys.* Transplantation. , 1999 . **67**(10): p. 1319.

66. Gordon R.D., et al., *Liver transplantation across ABO blood groups.* Surgery, 1986. **100:**(2): p. 342.

67. Sanchez-Urdazpal L., et al., *Increased bile duct complications in ABO incompatible liver transplant recipients.* Transplant Proc. , 1991. **23** (1 Pt 2): p. 1440.

68. Tanaka A., et al.,, *Living related liver transplantation across ABO blood groups.* Transplantation. , 1994. **58**(5): p. 548.

69. Varela-Fascinetto G., et al., *Long-term results in pediatric ABO-incompatible liver transplantation.* Transplant Proc. , 1999. **31** (1-2): p. 467.

70. Pierson R.N. 3rd, et al., *Successful management of an ABO-mismatched lung allograft using antigen-specific immunoadsorption, complement inhibition, and immunomodulatory therapy.* Transplantation , 2002. **74**(1): p. 79.

71. Strüber M., et al., *Intentional ABO-incompatible lung transplantation.* Am. J. Transplant. , 2008 **8**(11): p. 2476.

72. Galili U., et al., *A unique natural human IgG antibody with anti-alpha-galactosyl specificity.* J. Exp. Med. , 1984 **160** (5) p. 1519.

73. Good A.H., et al., *Identification of carbohydrate structures that bind human antiporcine antibodies: implications for discordant xenografting in humans.* Transplant. Proc., 1992. **24**(2): p. 559.

74. Oriol R., et al., *Carbohydrate antigens of pig tissues reacting with human natural antibodies as potential targets for hyperacute vascular rejection in pig-to-man organ xenotransplantation.* Transplantation , 1993. **56**(6): p. 1433.

75. Yang Y.G., et al., *Xenotransplantation: current status and a perspective on the future.* Nat. Rev. Immunol. , 2007 **7**(7): p. 519.

76. Watts A., et al., *Plasma perfusion by apheresis through a Gal immunoaffinity column successfully depletes anti-Gal antibody: experience with 320 aphereses in baboons.* Xenotransplantation , 2000 **7**(3): p. 181.

77. Alwayn I.P., et al., *The problem of anti-pig antibodies in pig-to-primate xenografting: current and novel methods of depletion and/or suppression of production of anti-pig antibodies.* Xenotransplantation , 1999. **6**(3): p. 157.

78. Gerber B., et al., *Differences between synthetic oligosaccharide immunoabsorbents in depletion capacity for xenoreactive anti-Galalpha1-3Gal antibodies from human serum.* Xenotransplantation, 2001. **8**(2): p. 106.

79. Qureshi A.I., et al., *Plasma exchange versus intravenous immunoglobulin treatment in myasthenic crisis.* Neurology , 1999. **52**(3): p. 629.

80. Benny W.B., et al., *Clinical evaluation of a staphylococcal protein A immunoadsorption system in the treatment of myasthenia gravis patients.* Transfusion, 1999. **39**(7): p. 682.

81. Levy J.B., et al., *Long-term outcome of anti-glomerular basement membrane antibody disease treated with plasma exchange and immunosuppression.* Ann. Intern. Med. , 2001. **134**(11): p. 1033.

82. Freiburghaus C., et al., *Tolerance induction using the Malmö treatment model 1982-1995.* Haemophilia, 1999. **5**(1): p. 32.

83. Daugirdas J.T., et al., Handbook of dialysis. Third edition, 2001. Philadelphia: Lippincott Williams& Wilkins.

84. Usui M., et al., *Experiences and problems pre-operative anti-CD20 monoclonal antibody infusion therapy with splenectomy and plasma exchange for ABO-incompatible living-donor liver transplantation.* Clin Transplant., 2007. **21**(1): p. 24.

85. Fischel R.J., et al., *Safe and effective plasma exchange to remove antibodies prior to xenogeneic heart transplantation in small primates.* ASAIO Trans., 1991. **37**(3): p. M498.

86. Burgstaler E.A., et al., *Therapeutic plasma exchange: a paired comparison of Fresenius AS104 vs. COBE Spectra.* J. Clin. Apher., 2001. **16**(2): p. 61.

87. Agishi T., et al., *Double filtration plasmapheresis.* Ther. Apher., 2000. **4**(1): p. 29.

88. Felson D.T., et al., *The Prosorba column for treatment of refractory rheumatoid arthritis: a randomized, double-blind, sham-controlled trial.* Arthritis. Rheum., 1999. **42**(10): p. 2153.

89. Bensinger W., et al., *Engraftment and transfusion requirements after allogeneic marrow transplantation for patients with acute non-lymphocytic leukemia in first complete remission* . Bone Marrow Transplant. 1989. **4**: p. 409.

90. Mazid M.A., et al., *An improved affinity support and immunoadsorbent with a synthetic blood group oligosaccharide and polymer coating for hemoperfusion.* J. Appl. Biomater., 1992. **3**(1): p. 9.

91. Tyden G., et al., *ABO incompatible kidney transplantations without splenectomy, using antigen-specific immunoadsorption and rituximab.* Am. J. Transplant. 2005. **5** (1): p. 145.

92. Ahlenstiel T., et al., *ABO-incompatible kidney transplantation of an 8-yr-old girl with donor/recipient-constellation A1B/B.* Xenotransplantation, 2006. **13**(2): p. 141.

93. Kumlien G., et al., *Clinical experience with a new apheresis filter that specifically depletes ABO blood group antibodies.* Transfusion Medicine, 2006. **46**(9): p. 1568.

94. Tydén G., *Cost effectiveness of ABO-incompatible kidney transplantations.* Transplantation, 2006. **82**(2): p. 166.

95. Tydén G., et al., *Successful ABO-incompatible kidney transplantations without splenectomy using antigen-specific immunoadsorption and rituximab.* Transplantation, 2003. **76**(4): p. 730.

96. Tydén G., et al., *Implementation of a Protocol for ABO-incompatible kidney transplantation--a three-center experience with 60 consecutive transplantations.* Transplantation , 2007. **83**(9): p. 1153.

97. Wilpert J., et al., *ABO-incompatible kidney transplantation-proposal of an intensified apheresis strategy for patients with high initial isoagglutinine titers.* J. Clin. Apher., 2007. **22**(6): p. 314.

98. Karoor S, et al., *Immunoaffinity removal of xenoreactive antibodies using modified dialysis or microfiltration membranes.* Biotechnol Bioeng. , 2003. **81**(2): p. 134.

99. Charcosset C., et al., *Protein A immunoaffinity hollow fiber membranes for immunoglobulin G purification: experimental characterization.* Biotechnol Bioeng., 1995. **48**(4): p. 415.

100. Alikhani A., et al., *High molecular weight blood group A trisaccharide-polyacrylamide glycoconjugates as synthetic blood group A antigens for anti-A antibody removal devices.* Journal of Biomedical Materials Research Part B: Applied Biomaterials, 2009. **91**(2): p. 845.

101. Falkenhagen D., et al., *Fluidized bed adsorbent systems for extracorporeal liver support.* Ther. Apher. Dial., 2006. **10**(2): p. 154.

102. Ettenauer M., et al., *Magnetic fluorescent microparticles as markers for particle transfer in extracorporeal blood purification.* Biomacromolecules, 2007. **12**: p. 3693.

103. Weber C., et al., *Extracorporeal removal of proinflammatory cytokines by specific absorption onto microspheres.* ASAIO J. , 1996. **42**(5): p. M908.

104. Weber V., et al., *Efficient adsorption of tumor necrosis factor with an in vitro set-up of the microspheres-based detoxification system.* Blood Purif., 2007. **25**(2): p. 169.

105. Falkenhagen D., et al., *Patient safety technology for microadsorbent systems in extracorporeal blood purification.* Artif. Organs., 2002. **26**(2): p. 84.

106. Brandl M., et al., *New methods for hemoglobin detection in a microparticle-plasma suspension.* Int. J. Artif Organs. , 2006. **29**(11): p. 1092.

107. Weber V., et al., *Development of specific adsorbents for human tumor necrosis factor-alpha: influence of antibody immobilization on performance and biocompatibility.* Biomacromolecules , 2005. **6**(4): p. 1864.

108. Weber C., et al., *The Microspheres based Detoxification System (MDS). A new extracorporeal blood purification technology based on recirculated microspherical adsorbent particles.* Int. J. Artif. Organs. , 1994. **17**(11): p. 595.

109. Thomas Bosch T.W., *State of the Art of Low-density Lipoprotein Apheresis in the Year 2003.* Therapeutic Apheresis and Dialysis, 2004. (2): p. 76.

110. Ullrich H., et al., *Improved treatment of sudden hearing loss by specific fibrinogen aphaeresis.* Journal of Clinical Apheresis, 2004. **19**(2): p. 71.

111. Fagerstam L.,*Surface plasmon resonance detection in affinity technologies.* In Kline T., Handbook of Affinity Chromatography, 1993. New York: Marcel Dekker, Inc.

112. Harrison B.A., et al., *A kinetics approach to the characterization of an IgM specific for the glycolipid asialo-GM1*. J. Immunol. Methods., 1998. **212**(1): p. 29.

113. Otamiri M., et al., *Analysis of human serum antibody-carbohydrate interaction using biosensor based on surface plasmon resonance.* Int. J. Biol. Macromol. 1999. **26**(4): p. 263.

114. Thomas R., et al., *Structure of an anti-blood group A Fv and improvement of its binding affinity without loss of specificity.* J. Biol. Chem. 2002. **277**(3): p. 2059.

115. Sigmundsson K., et al., *Determination of Active Concentrations and Association and Dissociation Rate Constants of Interacting Biomolecules: An Analytical Solution to the Theory for Kinetic and Mass Transport Limitations in Biosensor Technology and Its Experimental Verification.* Biochemistry, 2002. **41**(26): p. 8263.

116. Solovan J.C., et al., *Synthetic blood group antigens for anti-A removal device and their interaction with monoclonal anti-A IgM.* Transplant Immunology, 2006. **16**(3-4): p. 245.

117. Walker R., *American association of blood banks. Technical manual.* 11th ed. 1993. Bethesda: American association of blood banks.

118. Brenac V., et al., *Capture of a monoclonal antibody and prediction of separation conditions using a synthetic multimodal ligand attached on chips and beads.* Journal of Chromatography B, 2005. **818**(1): p. 61.

119. Korchagina E.Y., et al., *Synthesis of spacered trisaccharides with blood group A and B specificities and fragments and structural analogues of them.* Soviet Journal of Bioorganic Chemistry, 1992. **18**: p. 153.

120. Bovin N.V., et al., *Synthesis of polymeric neoglycoconjugates based on N-substituted polyacrylamides.* Glycoconj. Journal., 1993. **10**(2): p. 142.

121. Shilova N.V., et al., *High molecular weight neoglycoconjugates for solid phase assays.* Glycoconj. J. 2005. **22**(1-2): p. 43.

122. Yarmush M.L., et al., *An analysis of transport resistances in the operation of BIAcore; implications for kinetic studies of biospecific interactions.* Mol. Immunol., 1996. **33**(15): p. 1203.

123. Morton T.A., et al., *Interpreting Complex Binding Kinetics from Optical Biosensors: A Comparison of Analysis by Linearization, the Integrated Rate Equation, and Numerical Integration.* Analytical Biochemistry, 1995. **227**(1): p. 176.

124. Thomas R., et al., *Structure of an anti-blood group A Fv and improvement of its binding affinity without loss of specificity.* J. Biol. Chem., 2002. **277**(3): p. 2059.

125. Schier R., et al., *Isolation of picomolar affinity anti-c-erbB-2 single-chain Fv by molecular evolution of the complementarity determining regions in the center of the antibody binding site.* J . Mol. Biol. 1996. **263**(4): p. 551.

126. Yang W.P., et al., *CDR walking mutagenesis for the affinity maturation of a potent human anti-HIV-1 antibody into the picomolar range.* J. Mol. Biol. 1995. **254**(3): p. 392.

127. Karlsson R., et al., *Direct and competitive kinetic analysis of the interaction between human IgG1 and a one domain analogue of protein A.* J. Immunol. Methods., 1995. **183**(1): p. 43.

128. Drake A.W.M., et al., *Characterizing high-affinity antigen/antibody complexes by kinetic- and equilibrium-based methods.* Analytical Biochemistry, 2004. **328**(1): p. 35.

129. Kortt A.A., et al., *Influence of mass transfer and surface ligand heterogeneity on quantitative BIAcore binding data. Analysis of the interaction of NC10 Fab with an anti-idiotype Fab'.* J. Mol. Recognit., 1997. **10**(3): p. 148.

130. Glaser R.W., et al., *Antigen-antibody binding and mass transport by convection and diffusion to a surface: a two-dimensional computer model of binding and dissociation kinetics.* Anal. Biochem., 1993. **213**(1): p. 152.

131. Christensen L.L.H., *Theoretical Analysis of Protein Concentration Determination Using Biosensor Technology under Conditions of Partial Mass Transport Limitation.* Analytical Biochemistry, 1997. **249**(2): p. 153.

132. Starling E.H., *On the absorption of fluid from the convecfive tissue space.* J. Physiol. , 1896. **19**: p. 312.

133. Apelblat A., et al., *A mathematical analysis of capillary-tissue fluid exchange.* Biorheology. , 1974. **11**(1): p. 1.

134. Bird R.B., et al., Transport Phenomena., Second edition, 2002. New York: John Wiley and Sons,Inc.

135. Hermanson G.T., et al., Immobilized Affinity Ligand Techniques. 1992. San Diego: Academic Press Inc.

136. Gautam S., et al., *Monoclonal anti-A antibody removal by synthetic A antigen immobilized on specific antibody filters.* Biotechnology and Bioengineering, 2008. **99**: p. 876.

137. Fukunaga K., et al., *Preliminary evaluation study of a prototype hollow fiber membrane for the continuous membrane autotransfusion system.* Ther. Apher., 1999. **3**(1): p. 63.

138. Unger J.K., et al., *Maximal flow rates and sieving coefficients in different plasmafilters: effects of increased membrane surfaces and effective length under standardized in vitro conditions.* J. Clin. Apher., 2002. **17**(4): p. 190.

139. Krisper P., et al., *In vivo quantification of liver dialysis: comparison of albumin dialysis and fractionated plasma separation.* J. Hepatol., 2005. **43**(3): p. 451.

140. Rosner, B., *Fundamentals Of Biostatistics.* Fifth edition, 2005. Duxbury Pr.

141. Han V, S.K., Devine DV., *A comparative study of common techniques used to measure haemolysis in stored red cell concentrates.* Vox Sang. , 2010. **98** (2):p. 116

142. Yazer M.H., et al., *A comparison of hemolysis and red cell mechanical fragility in blood collected with different cell salvage suction devices.* Transfusion Medicine, 2008. **48**(6): p. 1188.

143. Lee C. J., et al., *The Purification and Comparative Analysis of Hemoglobin from Animal Bloods.* Artificial Cells, Blood Substitutes and Biotechnology, 1992. **20**(2-4): p. 477.

144. Kim N.J., et al., *Parametric study of blade tip clearance, flow rate, and impeller speed on blood damage in rotary blood pump.* Artif. Organs, 2009. **33**(6): p. 468.

145. Rieben R., et al., *Specificity of monoclonal antibodies against ABH and related structures tested by ELISA with synthetic glycoconjugates.* Transfus. Clin. Biol., 1997. **4**(1): p. 47.

146. Baskurt O.K., et al., *Handbook of Hemorheology and Hemodynamics* - Volume 69 Biomedical and Health Research, 2007. Amsterdam: IOS press.

147. Kameneva M.V., et al., *In vitro evaluation of hemolysis and sublethal blood trauma in a novel subcutaneous vascular access system for hemodialysis.* ASAIO J., 2002. **48**(1): p. 34.

148. Chanard J., et al., *New insights in dialysis membrane biocompatibility: relevance of adsorption properties and heparin binding.* Nephrol. Dial. Transplant. , 2003. **18**(2): p. 252.